Università degli Studi di Ferrara

UNIVERSIDAD NACIONAL de CHILECITO

DOCTORAL COURSE IN

PHYSICS

co-supervised thesis with

Universidad Nacional de Chilecito

CYCLE XXXI

DIRECTOR Prof. V. Guidi

Measuring Complex Sound Intensity from Wave Impedance

Scientific/Disciplinary Sector (SDS) FIS/01

Co-Supervisor
Università di Ferrara
Prof. Stanzial, Domenico

Candidate

Dott. Graffigna, Carlos E.

Co-Supervisor
Universidad de Chilecito
Prof. Barcelo, Gabriel

Acknowledgments

This thesis work has been conceived within a general deal among the University of Ferrara (UniFE), the National Research Council of Italy (CNR) and the National University of Chilecito (UNdeC), and has been supported on the basis of special agreements between the Department of Physics and Earth Sciences (UniFE), the Institute of Acoustics and Sensors "Orso Mario Corbino" (IDASC-CNR) and the Institute for Microelectronics and Microsystems (IMM-CNR). The theoretical and experimental work has been carried out at the joint Acoustics Laboratory of the IMM-CNR Bologna Unit and the UniFE Physics Department, under the supervision of Dr. Domenico Stanzial.

ABSTRACT

The definition of sound intensity as a complex quantity, where the real part coincides with the active intensity vector known from classic textbooks and the imaginary part is related to local oscillatory transport of energy, is still a controversial problem.

To overcome this impasse, this work exposes a solid physical foundation to the concept of complex sound intensity and proposes a device for measuring the complex sound intensity in 3-D from the wave impedance.

Furthermore, the concepts and methods have been validated by simulation results and measurements in real environments, and their application in the field of clinical audiometry has been addressed.

ABSTRACT

La definizione dell'intensità acustica come una grandezza complessa avente la parte reale coincidente con il vettore di intensità attiva già noto in letteratura e la parte immaginaria legata alle oscillazioni locali dell'energia, è ancora un problema controverso.

Per superare questo problema, il presente lavoro fornisce una solida base fisica al concetto di intensità acustica complessa e propone lo schema di un dispositivo per la misura dell'intensità complessa in tre dimensioni a partire dagli spettri dell'impedenza acustica.

Inoltre, i concetti e i metodi qui formulati sono stati convalidati per mezzo di simulazioni analitiche e numeriche, e, sperimentalmente, con misure in ambienti reali e applicazioni nel campo dell'audiometria clinica.

ABSTRACT

La definición de intensidad acústica como una cantidad compleja, donde la parte real coincide con el vector de intensidad activa ya conocido en literatura, y la parte imaginaria está relacionada con las oscilaciones locales de energía, es todavía un problema controversial.

Para superar este impasse, el presente trabajo brinda una solida base física al concepto de intensidad acústica compleja y propone el esquema de un dispositivo para la medición de la intensidad compleja en tres dimensiones a partir de la impedancia acústica.

Además, los conceptos y métodos formulados aquí han sido convalidados a través de simulaciones analíticas y numéricas, y experimentalmente verificados por medio de mediciones en ambientes reales y aplicaciones en el campo de la audiometría clínica.

Table of Contents

List of Figures

List of Tables

INTRODUCTION

The definition of sound intensity as a complex quantity, where the real part coincides with the active intensity vector known from classic textbooks [4],[5] and the imaginary part (the so called reactive intensity) is related to local oscillatory transport of energy, is still a controversial problem.

In a recent publication, [6] two definitions of complex intensity have been reviewed and compared by both numerical simulations and experimental measurements. The authors concluded that "the potential application of complex intensity as a diagnostic tool is limited by difficulties in measuring reactive intensity in complex sound fields."

To overcome this impasse, this work will show a solid physical foundation to the concept of complex sound intensity from the impedance calculation as considered by other branches of study such as electronics, where the intensity concepts are clearer due to the variables are one-dimensional. In this regard, the connection between the complex sound intensity and the impedance of sound waves is established through an equation named the acoustic energy-mass equation, according to the physical dimensions of its connected quantities. A similar approach was faced in [7] for one dimension.

A device for measuring the complex sound intensity from the wave impedance will be developed in order to give an experimental support by applying these new definitions and concepts in real environments. The measuring process will be completely described, starting from the acoustic theoretical fundamentals, and verified with symbolic and numerical simulation. The measuring hardware available will be examined by focusing on two intensimetric probes which have a different operating principle. Special attention has been given to the probe calibration process which will be described, and two calibration methodologies and a measuring algorithm will be proposed. Some measurements will be taken in different acoustic fields, in order to verify the whole measuring process.

Finally, a real medical application will be shown, where the new measuring methodology is used in an audiometric clinical investigation.

OUTLINE OF THE REPORT

The research has been organized in six chapters and one reference. The framework of the report is as follows:

Chapter 1 gives the theoretical bases and acoustic fundamentals of the research, and a new definition of the complex sound intensity is presented which is connected with the wave impedance from the energy-mass equation.

Chapter 2 discusses how numerical and symbolic simulation is used for three canonical case-studies.

Chapter 3 describes the operation principle of the intensimetric probes and the calibration methods.

Chapter 4 explains the measuring algorithm proposed and some measurements are shown.

Chapter 5 shows a real application for an audiometric clinical investigation.

Chapter 6 presents some of the conclusions drawn.

Appendix shows a prototype to measure the complex sound intensity.

Chapter 1

BASIC LINEAR ACOUSTICS AND THE RELATIONSHIP BETWEEN WAVE IMPEDANCE AND COMPLEX SOUND INTENSITY

In this chapter the theoretical bases and acoustic fundamentals of the research will be exposed [8][4], and a new definition of the complex sound intensity connected with the wave impedance from the energy-mass equation is presented.

1.1 Sound Propagation and Linear Acoustics

The study of acoustics is the study of vibrations [9] and the wave propagation in a medium, which can be solid, liquid or gas. In this work, we will study mainly waves traveling in a gaseous medium. However, the theory here presented can be applied in any linear acoustic field.

A sound wave involves space and time variations of three main parameters in the medium: density ρ, pressure p and particle velocity $\boldsymbol{v}$ [8]. These parameters can be written as in Eq. 1.1, where the first terms ρ_{-}, p_{-}, and $\boldsymbol{v}_{-}$are constants and their values correspond to the parameters in stationary state (when there is not any sound wave present). The second terms are the variable sound-field quantities density $\rho_{\sim}$, sound pressure $p_{\sim}$, and particle velocity $\boldsymbol{v}_{\sim}$. Thus, a sound field can be described by two of these sound field quantity functions: $p(\boldsymbol{x}, t)$ and particle velocity vector $\boldsymbol{v}(\boldsymbol{x}, t)$. These functions describe the position and time dependence of the pressure and the particle velocity respectively.

$$\begin{aligned} \rho &= \rho_{-} + \rho_{\sim} \\ p &= p_{-} + p_{\sim} \\ \boldsymbol{v} &= \boldsymbol{v}_{-} + \boldsymbol{v}_{\sim} \end{aligned} \tag{1.1}$$

Notice that two velocities can be considered in a sound field: the velocity of the particles of the medium and the propagation speed of the sound wave. For this reason, $\boldsymbol{v}_{\sim}$ is called the particle velocity.

In this regard, the acoustic particle does not have a strict size, it must be a volume so small that pressure, velocity and density can be consider constant within it. So, we consider a cubical element of the medium $d\boldsymbol{x} = [dx, dy, dz]$ with these properties that we called acoustic particle.

Let us start by the equations of hydrodynamics 1.4 and 1.6, and the equation of state of the medium Eq.1.8.

The variation of the acoustic particle velocity and its acceleration are given by Eq. 1.2 and 1.3.

$$d\boldsymbol{v}(\boldsymbol{x},t) = \frac{\partial \boldsymbol{v}(\boldsymbol{x},t)}{\partial t}dt + d\boldsymbol{x}\cdot\nabla\boldsymbol{v}(\boldsymbol{x},t) \tag{1.2}$$

The first term in Eq. 1.2 represents the fact that the velocity field varies with time, while the second term expresses the fact that the position of the acoustic particle changes due of its motion.

The acoustic particle acceleration is given by the quotient of the velocity change and the time increment as it is shown in Eq. 1.3

$$\frac{d\boldsymbol{v}(\boldsymbol{x},t)}{dt} = \frac{\partial \boldsymbol{v}(\boldsymbol{x},t)}{\partial t} + \boldsymbol{v}(\boldsymbol{x},t)\cdot\nabla\boldsymbol{v}(\boldsymbol{x},t) \tag{1.3}$$

The acceleration of the mass contained in the volume of the acoustic particle is produced by a force that is proportional to the difference between the pressures acting on the boundary surfaces of this acoustic particle. Applying the Newton's equation of motion, we can write the first fundamental equation of hydrodynamics as follows:

$$\rho(\boldsymbol{x},t)\left[\frac{\partial \boldsymbol{v}(\boldsymbol{x},t)}{\partial t} + \boldsymbol{v}(\boldsymbol{x},t)\cdot\nabla\boldsymbol{v}(\boldsymbol{x},t)\right] = -\nabla p(\boldsymbol{x},t) \tag{1.4}$$

On the other hand, the second fundamental equation of the hydrodynamics comes from the law of conservation of mass, where a mass flowing out of volume V through the surface A in time interval dt is equal to the decrease of the mass contained in volume V. When transforming the surface integral by means of the divergence theorem into a volume integral, the Eq. 1.5 can be written as

$$\oint_A \rho(\boldsymbol{x},t)\boldsymbol{v}(\boldsymbol{x},t)\cdot dA = -\frac{\partial}{\partial t}\int_V \rho(\boldsymbol{x},t)\cdot dV = \int_V \nabla\cdot(\rho(\boldsymbol{x},t)\boldsymbol{v}(\boldsymbol{x},t))\cdot dV \tag{1.5}$$

Since Eq. 1.5 is valid for arbitrary elements, the integrands are equal:

$$\nabla\cdot(\rho(\boldsymbol{x},t)\boldsymbol{v}(\boldsymbol{x},t)) = -\frac{\partial\rho(\boldsymbol{x},t)}{\partial t} \tag{1.6}$$

Now, in order to find a relationship between pressure p and density ρ, the equation of the state of the medium is invoked.

In a sound wave, the changes of state normally happen so rapidly that there is no time for the temperature to equalize with the surrounding medium, so the changes of state are not isothermal but adiabatic.

Thus, the Eq.1.7 represents the adiabatic law for gases, where γ is the adiabatic index equal to the ratio of the specific heats, p and V are the pressure and the Volume respectively.

$$pV^{\gamma} = const. \tag{1.7}$$

For small amplitudes, where $p_{\sim}(\boldsymbol{x}, t) \ll p_{-}$, the Eq. 1.7 can be written as in Eq. 1.8, where c is the speed of sound and can be calculated as $c^2 = \frac{\gamma p_{-}}{\rho_{-}}$.

$$p_{\sim}(\boldsymbol{x}, t) = c^2 \rho_{\sim}(\boldsymbol{x}, t) \tag{1.8}$$

In "linear" acoustics, the alternating quantities can be considered small in comparison with the static quantities, so the basic hydrodynamic equations 1.4 and 1.6 can be simplified.

The density ρ is set equal to the static density ρ_{-}. The spatial variation of the velocity, is given by $\boldsymbol{v}(\boldsymbol{x}, t) \cdot \nabla \boldsymbol{v}(\boldsymbol{x}, t)$, so the equation 1.3 can be written directly as:

$$\frac{d\boldsymbol{v}(\boldsymbol{x}, t)}{dt} \cong \frac{\partial \boldsymbol{v}(\boldsymbol{x}, t)}{\partial t} \tag{1.9}$$

1.2 Wave Equation for a Plane Wave

The plane wave is the most important canonical case and the simplest wave field, whose model is given by a source placed at minus infinite and the waves are traveling to plus infinite along the propagation direction. Therefore the sound field quantities are functions of only one position coordinate, for example x. In this way, the velocity vector has only one component $\boldsymbol{v}_{\sim} = [v_{\sim x}, 0, 0]$ or $v_{\sim} = v_{\sim x}$, and the Eq. 1.4 and 1.6 can be written like a system of partial differential equations by the Eq.1.10 and 1.11 respectively with the Eq.1.8.

$$\rho \frac{\partial v_{\sim}(x, t)}{\partial t} = -\frac{\partial p_{\sim}(x, t)}{\partial x} \tag{1.10}$$

$$\rho \frac{\partial v_{\sim}(x, t)}{\partial x} = -\frac{\partial \rho_{\sim}(x, t)}{\partial t} = -\frac{1}{c^2} \frac{\partial p_{\sim}(x, t)}{\partial t} \tag{1.11}$$

In order to solve the system of partial differential equations, the particle velocity quantity can be eliminated by taking the partial derivative of Eq. 1.10 with respect to x and taking the partial derivative of Eq. 1.11 with respect to time.

The result is the wave equation for the sound pressure $p_{\sim}$in the plane wave case:

$$\frac{\partial^2 p_{\sim}(x, t)}{\partial x^2} = \frac{1}{c^2} \frac{\partial^2 p_{\sim}(x, t)}{\partial t^2} \tag{1.12}$$

In general, the wave equation is

$$\nabla^2 p_\sim (x,t) = \frac{\partial^2 p_\sim (\boldsymbol{x},t)}{\partial x^2} + \frac{\partial^2 p_\sim (\boldsymbol{x},t)}{\partial y^2} + \frac{\partial^2 p_\sim (\boldsymbol{x},t)}{\partial z^2} = \frac{1}{c^2}\frac{\partial^2 p_\sim (\boldsymbol{x},t)}{\partial t^2} \tag{1.13}$$

The wave equation can be written in terms of the so-called velocity potential function $\Phi(\boldsymbol{x},t)$ instead of one of the sound field quantities, which the sound pressure $p_\sim(\boldsymbol{x},t)$ and the particle velocity vector $\boldsymbol{v}_\sim(\boldsymbol{x},t)$ can be obtained as follows:

$$p_\sim (\boldsymbol{x},t) = \rho \cdot \frac{\partial \Phi(\boldsymbol{x},t)}{\partial t} \tag{1.14}$$

$$\boldsymbol{v}_\sim (\boldsymbol{x},t) = -\nabla \Phi(\boldsymbol{x},t) \tag{1.15}$$

A solution of the wave equation is a plane wave traveling in the positive x-direction:

$$p_\sim (\boldsymbol{x},t) = p_0 f\left(t - \frac{x}{c}\right) \tag{1.16}$$

where p_0 is a constant pressure and $f(u)$ is an arbitrary function whose second derivative respect to the argument u exists. The spatial distribution is given by the function $f\left(t - \frac{x}{c}\right)$, while the pressure distribution moves with the time parallel to the positive x-axis.

The particle velocity $v_\sim(\boldsymbol{x},t)$ can be obtained by substitution Eq.1.16 in the Eq.1.10, resulting in:

$$v_\sim (\boldsymbol{x},t) = \frac{p_0}{\rho c} f\left(t - \frac{x}{c}\right) = v_0 f\left(t - \frac{x}{c}\right) \tag{1.17}$$

where v_0 is a constant velocity.

Looking at equations 1.16 and 1.17, sound pressure and particle velocity have the same time distribution at a fixed point x and the same spatial distribution at a particular instant of time t. Therefore, in a plane wave, sound pressure and particle velocity are always in phase.

In order to simplify the notation of the sound field quantity functions, variable sound pressure and variable particle velocity vector will be directly called $p(\boldsymbol{x},t)$ and $\boldsymbol{v}(\boldsymbol{x},t)$ respectively.

1.2.1 The Characteristic and Specific Acoustic Impedance

Continuing with the solution of the wave equation, a particular solution is a sinusoidal wave:

$$p(\boldsymbol{x},t) = p_0 sin\left(\omega\left(t - \frac{x}{c}\right) + \phi\right) \tag{1.18}$$

where p_0 is a constant pressure equal to the peak value of the pressure signal, ω is the angular frequency, and ϕ is the phase of the wave. Using the Eq. 1.10 once more, the particle velocity for a sinusoidal wave is:

$$v\left(\boldsymbol{x},t\right)=\frac{p_0}{\rho c}sin\left(\omega\left(t-\frac{x}{c}\right)+\phi\right) \tag{1.19}$$

The acoustic field quantities $p\left(\boldsymbol{x},t\right)$ and $v\left(\boldsymbol{x},t\right)$ can be written in a complex representation as follows:

$$\hat{p}\left(\boldsymbol{x},t\right)=p_0e^{i\omega t}e^{-i\frac{\omega x}{c}}e^{i\phi};\ p=\Re\left\{\hat{p}\left(\boldsymbol{x},t\right)\right\} \tag{1.20}$$

$$\hat{v}\left(\boldsymbol{x},t\right)=v_0e^{i\omega t}e^{-i\frac{\omega x}{c}}e^{i\phi}=\frac{p_0}{\rho c}e^{i\omega t}e^{-i\frac{\omega x}{c}}e^{i\phi};\ v=\Re\left\{\hat{v}\left(\boldsymbol{x},t\right)\right\} \tag{1.21}$$

If the quotient of the complex sound pressure Eq.1.20 and the complex particle velocity Eq.1.21 is taken, the result is a constant equal to ρc, i.e.:

$$Z_0=\frac{\hat{p}\left(\boldsymbol{x},t\right)}{\hat{v}\left(\boldsymbol{x},t\right)}=\rho c \tag{1.22}$$

which is called the acoustic characteristic impedance, or the wave impedance of the medium.

In fact, the characteristic impedance is a special case of the specific acoustic impedance Z_s, which is defined for each component frequency $f=\omega/(2\pi)$ of any general plane wave by the time independent quotient of the complex sound pressure and complex particle velocity.

$$Z_s:=\frac{\hat{p}}{\hat{v}} \tag{1.23}$$

The units of the specific impedance in the SI base units are the $rayl_{MKS}$ and the $rayl_{CGS}$, which are equal to:

$$1\,rayl_{MKS}=1\,\frac{Kg}{m^2s};\ 1\,rayl_{CGS}=1\,\frac{g}{cm^2s}; \tag{1.24}$$

1.2.2 Instantaneous Sound Intensity, Energy Density and Continuity Equation

If a particle of matter is considered where a force F acts upon it and the particle moves in space from point A to B following the trajectory $\boldsymbol{s}$, the work done on the particle is:

$$W=\int_A^B\boldsymbol{F}\cdot d\boldsymbol{s} \tag{1.25}$$

$$W(t) = m\int_A^B \frac{\boldsymbol{v}(t)}{dt}\cdot d\boldsymbol{s}(t) = m\int_A^B \boldsymbol{v}(t)\cdot d\boldsymbol{v}(t) = \frac{1}{2}m\boldsymbol{v}^2(t) \tag{1.26}$$

Notice that the scalar product between $\boldsymbol{F}$ and $d\boldsymbol{s}$ in Eq.1.25 gives the work done only by the component of the force in the direction of the particle displacement.

The substitution of Newton's Law of Motion in Eq.1.25 shows that in Eq.1.26 the work done on a particle is equal to the change in a quantity defined to be the "kinetic energy" of the particle. If the mass m is replaced for the volumetric mass density ρ, we can write the Eq.1.27 which is the "kinetic energy density."

$$w_k(t) = \frac{1}{2}\rho\boldsymbol{v}^2(t) \tag{1.27}$$

On the other hand, forces which act on and within material media without energy lost by friction produce negative work, which can be interpreted as "stored" energy that can be recoverable by reversal of the work path. Negative work done by an internal conservative force is defined as "potential energy". The most common examples of this kind of force are those due to gravity, and the linear elastic forces produced by material strain. In acoustics, the potential energy is associated with volumetric strain of an elemental fluid volume that is equal to the negative work done by the internal fluid pressure, acting on the surface of the elemental volume during strain. Therefore the potential energy per unit volume is given by:

$$dw_k(t) = -p(t)\left(\frac{dV(t)}{V(t)}\right) \tag{1.28}$$

By the statement of conservation of mass, the expression dV/V can be substituted by $-d\rho/\rho$, and by using Eq. 1.8, Eq.1.28 can be written as follows:

$$dw_k(t) = p(t)\frac{dp(t)}{\rho c^2} \tag{1.29}$$

Hence, the potential energy density w_p is obtained by integration of Eq.1.29:

$$w_p(t) = \frac{p^2(t)}{2\rho c^2} \tag{1.30}$$

The total energy density associated with an acoustic disturbance is:

$$w(t) = w_p(t) + w_x(t) = \frac{1}{2}\rho\boldsymbol{v}^2(t) + \frac{p^2(t)}{2\rho c^2} \tag{1.31}$$

The work rate per unit area may be written as

$$\frac{dW/dt}{dS} = p\left(t\right) \cdot v_n\left(t\right) \tag{1.32}$$

where $v_n = \boldsymbol{v} \cdot \boldsymbol{n}$ is the component of particle velocity normal to a surface S.
As a result, we define the instantaneous sound intensity in the following vector quantity:

$$\boldsymbol{j}(t) = p\left(t\right) \cdot \boldsymbol{v}\left(t\right) \tag{1.33}$$

which represents the instantaneous work rate per unit area in the direction of v.

1.2.3 Time-average Operator and its Application to Energetic Quantities

Now, let us start by defining the stationary time-average operator Eq.1.34, which will be used in the time independent analysis of the acoustic energetic quantities

$$\langle \cdot \rangle := \lim_{T \to \infty} \frac{1}{2T} \int_{-T}^{+T} (\cdot)\ dt \tag{1.34}$$

where T is the period of the signal $(\cdot)$, which is in a general case $T \to \infty$.
The active sound intensity $I\left(\boldsymbol{x}\right)$ is obtained by definition [4] using the time-average operator with the instantaneous sound intensity vector $\boldsymbol{j}\left(\boldsymbol{x}, t\right)$ (Eq.1.33:

$$\boldsymbol{I}\left(\boldsymbol{x}\right) = \left\langle p\left(\boldsymbol{x}, t\right) \cdot \boldsymbol{v}\left(\boldsymbol{x}, t\right) \right\rangle \tag{1.35}$$

The time-average can also be used also to find the mean of the kinetic, potential and total energy densities:

$$W_k\left(\boldsymbol{x}\right) = \left\langle w_k\left(\boldsymbol{x}, t\right) \right\rangle = \frac{1}{2} \rho \left\langle \boldsymbol{v}^2\left(\boldsymbol{x}, t\right) \right\rangle \tag{1.36}$$

$$W_p\left(\boldsymbol{x}\right) = \left\langle w_p\left(\boldsymbol{x}, t\right) \right\rangle = \frac{\left\langle p^2\left(\boldsymbol{x}, t\right) \right\rangle}{2\rho c^2} \tag{1.37}$$

$$W\left(\boldsymbol{x}\right) = \left\langle w_k\left(\boldsymbol{x}, t\right) \right\rangle + \left\langle w_p\left(\boldsymbol{x}, t\right) \right\rangle = W_k\left(\boldsymbol{x}\right) + W_p\left(\boldsymbol{x}\right) \tag{1.38}$$

In the same way, as the continuity equation was used in section 1.2 in the law of conservation of mass to find the wave equation, we can also use it here in terms of the flow of sound energy:

$$\nabla \cdot \boldsymbol{j}(\boldsymbol{x}, t) = -\frac{\partial w(\boldsymbol{x}, t)}{\partial t} \tag{1.39}$$

Using the time-average operator in Eq.1.39 the following result is obtained:

$$\nabla \cdot \boldsymbol{I}(\boldsymbol{x}) = 0 \tag{1.40}$$

The physical meaning of Eq.1.40 is that in a volume where there are no sources or sinks, all the energy that goes into the volume gets out of it. Furthermore, this condition implies that the energy streamlines never cross each other.

1.3 In-phase and Quadrature-Phase Decomposition of Air Particle Velocity

As it was explained in subsection 1.1, an acoustic sound field can be described by two sound field quantity functions: sound pressure $p(\boldsymbol{x}, t)$ which is a scalar quantity, and particle velocity vector $\boldsymbol{v}(\boldsymbol{x}, t)$.

Following the theory explained in [10], the particle velocity vector can be decomposed in the time domain as the sum of two mutually orthogonal vectors $\boldsymbol{v}_p(\boldsymbol{x}, t)$ and $\boldsymbol{v}_q(\boldsymbol{x}, t)$ in the Hilbert space where the scalar product $< .|. >$ is defined by the time-average operator Eq.1.41.

$$\langle \boldsymbol{v}_p(\boldsymbol{x}, t) \cdot \boldsymbol{v}_q(\boldsymbol{x}, t) \rangle = 0 \tag{1.41}$$

The first component vector $\boldsymbol{v}_p$ is defined, at each point $\boldsymbol{x}$ of any general sound field, as a very special projection of the instantaneous particle velocity $\boldsymbol{v}(\boldsymbol{x}, t)$ along the spatial direction of the active intensity $\boldsymbol{I}(\boldsymbol{x}) = \langle p(\boldsymbol{x}, t)\boldsymbol{v}(\boldsymbol{x}, t) \rangle$, i.e.

$$\boldsymbol{v}_p(\boldsymbol{x}, t) \coloneqq \frac{\boldsymbol{I}(\boldsymbol{x})}{\langle p^2(\boldsymbol{x}, t) \rangle} p(\boldsymbol{x}, t) \ . \tag{1.42}$$

To complete the definition of the vector $\boldsymbol{v}_p$, in addition to its time-independent direction at $\boldsymbol{x}$, its instantaneous phase and amplitude have to be specified. According to equation 1.42, these are respectively given in terms of the pressure $p(\boldsymbol{x}, t)$ and of its normalization factor $\langle p^2(\boldsymbol{x}, t) \rangle / I(\boldsymbol{x})$, in such a way that $|\boldsymbol{v}_p|$ becomes a signal with the same phase spectrum of $p(t)$, but, with an amplitude spectrum re-scaled by the time-independent quantity $M(\boldsymbol{x}) = I / \langle p^2 \rangle$. Of course $\boldsymbol{v}_p$ is a very special vector, it has the same direction of $\boldsymbol{I}(\boldsymbol{x})$ and components $[v_p(x, t)\ ,\ v_p(y, t)\ ,\ v_p(z, t)]$, each of which has the same phase spectrum of $p(t)$ but with different normalization factors given respectively by $\langle p^2 \rangle / I_i$.[1]

We can say that this strange vector $\boldsymbol{v}_p(\boldsymbol{x}, t)$ gathers its space-directional information from past and future through the $\langle \cdot \rangle(\boldsymbol{x})$ operator while getting its instantaneous properties from the pressure signal at $\boldsymbol{x}$. In this regard it can be called a "syntropic" quantity.

The quantity $p\boldsymbol{v}_p$ should be called *radiating intensity* and for that reason the identity $\langle p\boldsymbol{v}_p \rangle \equiv \langle p\boldsymbol{v} \rangle$ always holds by definition.

[1] It is worth to note here that the normalization factor $\langle p^2 \rangle / I$ of the modulus $|\boldsymbol{v}_p|$ is known, from classic textbooks, as the pressure-intensity index (Ref.[4]).

Once determined $\boldsymbol{v}_p$ as in equation 1.42, the second component vector $\boldsymbol{v}_q$ is simply defined as the complementary vector:

$$\boldsymbol{v}_q\left(\boldsymbol{x},t\right) \coloneqq \boldsymbol{v} - \boldsymbol{v}_p \tag{1.43}$$

that is the instantaneous difference between the particle velocity $\boldsymbol{v}$ and $\boldsymbol{v}_p$ itself. This definition of $\boldsymbol{v}_q$ gives rise to a second syntropic quantity which now has an important property: each of its component signals are always in phase quadrature with the pressure so that $\langle p\boldsymbol{v}_q\rangle \equiv \boldsymbol{0}$. This property will be explained in more detailed in the following subsection, where the concept of "reactivity" arising from the *oscillating intensity* $p\boldsymbol{v}_q$ will be also illustrated.

To conclude, it can be said that at any point $\boldsymbol{x}$ of any general (monochromatic and non-monochromatic) field, the particle velocity can always be decomposed as the sum of two syntropic component vectors, the first one always being in phase and the second one always in quadrature phase with the pressure. These vectors are respectively defined in equations 1.42 and 1.43 and their sum results in the instantaneous particle velocity vector:

$$\boldsymbol{v}\left(\boldsymbol{x},t\right) = \boldsymbol{v}_p\left(\boldsymbol{x},t\right) + \boldsymbol{v}_q\left(\boldsymbol{x},t\right) \tag{1.44}$$

1.4 Active and Reactive Intensity

Let us start with the usual definition of active sound intensity:

$$I\left(\boldsymbol{x}\right) = \left\langle p\left(\boldsymbol{x},t\right)\boldsymbol{v}(\boldsymbol{x},t)\right\rangle \tag{1.45}$$

that is a time-independent 3D spatial vector, whose components are the time-average products of the pressure signal with the three particle velocity components.

As it was explained in the previous subsection, the particle velocity vector can be decomposed as the sum in the time-domain of two components $\boldsymbol{v}_p$ and $\boldsymbol{v}_q$ as it is shown in Eq. 1.44. Therefore, the Eq. 1.45 can be written using the new definition of $\boldsymbol{v}$ as follows:

$$I\left(\boldsymbol{x}\right) = \left\langle p\left(\boldsymbol{x},t\right)\boldsymbol{v}_p(\boldsymbol{x},t)\right\rangle + \left\langle p\left(\boldsymbol{x},t\right)\boldsymbol{v}_q(\boldsymbol{x},t)\right\rangle \tag{1.46}$$

In Eq. 1.46, we can see that the second term is identically equal to zero. This is because $\boldsymbol{v}_q$ was defined orthogonal to p in the Hilbert's space of signals. Hence, in practice, the active intensity is equal to the time average of the product between the pressure and the particle velocity component which is in phase with the pressure.

So now the question is, what can we say about the phase-quadrature part?

In this sense, the phase-quadrature part is related with the reactive intensity which represents energy locally oscillating into the acoustic system. Since its average always vanishes, the only way to calculate it is going to the second order statistical analysis. As a result, the square of the particle velocity vector can be written as in Eq.1.47, where the term $\langle 2\cdot\boldsymbol{v}_p\cdot\boldsymbol{v}_q\rangle$ is not present because it is identically equal to zero due to orthogonality in the Hilbert space of signals.

$$\left\langle \boldsymbol{v}^2(\boldsymbol{x},t)\right\rangle = \left\langle \boldsymbol{v}_p^2(\boldsymbol{x},t)\right\rangle + \left\langle \boldsymbol{v}_q^2(\boldsymbol{x},t)\right\rangle \tag{1.47}$$

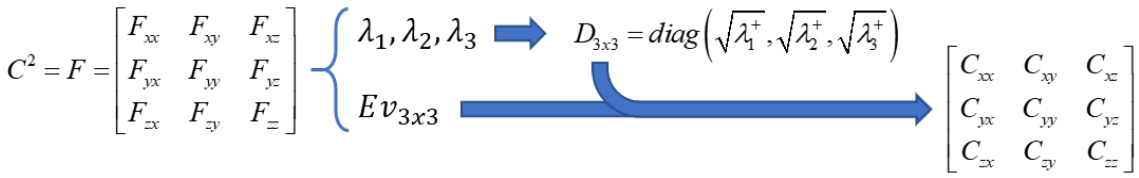

Figure 1.1: Square Root Process in Matrix

If the Eq. 1.47 is multiplied by $\langle p^2(\boldsymbol{x},t)\rangle$ the following equations can be written as:

$$S^2(\boldsymbol{x}) = \left\langle p^2(\boldsymbol{x},t)\right\rangle \langle \boldsymbol{v}(\boldsymbol{x},t)\cdot\boldsymbol{v}(\boldsymbol{x},t)\rangle = \left\langle p^2(\boldsymbol{x},t)\right\rangle (\langle \boldsymbol{v}_p(\boldsymbol{x},t)\cdot\boldsymbol{v}_p(\boldsymbol{x},t)\rangle + \langle \boldsymbol{v}_q(\boldsymbol{x},t)\cdot\boldsymbol{v}_q(\boldsymbol{x},t)\rangle) \tag{1.48}$$

$$I^2(\boldsymbol{x}) = \left\langle p^2(\boldsymbol{x},t)\right\rangle \langle \boldsymbol{v}_p(\boldsymbol{x},t)\cdot\boldsymbol{v}_p(\boldsymbol{x},t)\rangle \tag{1.49}$$

$$Q^2(\boldsymbol{x}) = \left\langle p^2(\boldsymbol{x},t)\right\rangle \langle \boldsymbol{v}_q(\boldsymbol{x},t)\cdot\boldsymbol{v}_q(\boldsymbol{x},t)\rangle \tag{1.50}$$

where $S(\boldsymbol{x})$ and $I(\boldsymbol{x})$ are the apparent and active intensity modulus, and $Q(\boldsymbol{x})$ is the reactivity.

Using the equations 1.36 and 1.37, the apparent intensity modulus can also be written in terms of the kinetic and potential energy densities as follows:

$$S(\boldsymbol{x}) = 2c\sqrt{W_k(\boldsymbol{x})\,W_p(\boldsymbol{x})} \tag{1.51}$$

Comparing the Eq.1.47 with the equations 1.48, 1.49 and 1.50, the following expression can be written as:

$$S^2(\boldsymbol{x}) = I^2(\boldsymbol{x}) + Q^2(\boldsymbol{x}) \tag{1.52}$$

In practice, active and apparent intensity can be easily calculated from the usual definition Eq. 1.45, and the Eq.1.48 respectively, while the total reactivity can be found using the Eq.1.52 as:

$$Q(\boldsymbol{x}) = \sqrt{S^2(\boldsymbol{x}) - I^2(\boldsymbol{x})} \tag{1.53}$$

1.4.1 Definition of the Reactivity Tensor

The mathematical real nature of the reactivity is that of a tensorial quantity [10], in this way the Eq. 1.50 can be formulated as follows:

$$\mathbb{Q}\left(\boldsymbol{x}\right)=\sqrt{\left\langle p^{2}\left(\boldsymbol{x},t\right)\right\rangle \left\langle \boldsymbol{v}_{q}(\boldsymbol{x},t)\otimes\boldsymbol{v}_{q}(\boldsymbol{x},t)\right\rangle }=\sqrt{\left\langle p^{2}\left(\boldsymbol{x},t\right)\right\rangle }\cdot\sqrt{\begin{bmatrix}\left\langle \boldsymbol{v}_{q_{xx}}\right\rangle & \left\langle \boldsymbol{v}_{q_{xy}}\right\rangle & \left\langle \boldsymbol{v}_{q_{xz}}\right\rangle \\ \left\langle \boldsymbol{v}_{q_{yx}}\right\rangle & \left\langle \boldsymbol{v}_{q_{yy}}\right\rangle & \left\langle \boldsymbol{v}_{q_{yz}}\right\rangle \\ \left\langle \boldsymbol{v}_{q_{zx}}\right\rangle & \left\langle \boldsymbol{v}_{q_{zy}}\right\rangle & \left\langle \boldsymbol{v}_{q_{zz}}\right\rangle \end{bmatrix}}$$

where $\mathbb{Q}\left(\boldsymbol{x}\right)$ is the reactivity tensor, obtained as the product between the root mean square of p and the square root of the mean of the matrix obtained from the tensorial product of the particle velocity in phase quadrature with the pressure, whose elements are represented by $\boldsymbol{v}_{q_{ij}}$. Subscripts i and j represent the spatial dimensions x, y, and z.

Notice that the square root is not a trivial operation when it is applied to a matrix [11]. A singular case where the square root operation in matrix is simpler happens in diagonal matrices, where the square root is directly applied to each (positive) element of the diagonal.

Therefore, we can implement the algorithm schematized in Fig.1.1, where F represents the squared matrix of C whose elements are F_{ij} and C_{ij} respectively, λ_i are the eigenvalues of the matrix F, E_{3x3} is a matrix whose columns are the corresponding eigenvectors of F, and D is a diagonal matrix whose trace is formed by the square root of the positive eigenvalues (the negative eigenvalues are replaced by zero).

As a result, the square root of matrix C is obtained by calculating the eigenvalues and eigenvectors, building the diagonal matrix from the square root of the positive eigenvalues, and finally calculating the matrix C using the following equation:

$$C_{3x3}=E_{3x3}\cdot D_{3x3}\cdot E_{3x3}^{-1}$$

1.4.2 Definition of the Complex Sound Intensity

Next, we will see how complex sound intensity can be defined.

Looking at the usual definition of the active intensity Eq. 1.45, which is a time independent spatial vector, complex sound intensity can be accordingly defined as a complex spatial vector, where the real part is the active intensity vector and the imaginary part is a vector that we call the reactive intensity vector, defined as a time-independent real vector field $\boldsymbol{Q_T}\left(\boldsymbol{x}\right)$ which results from the application of the reactivity tensor $\mathbb{Q}\left(\boldsymbol{x}\right)$ to the unit vector $\boldsymbol{T}\left(\boldsymbol{x}\right):=\boldsymbol{I}I^{-1}$ tangent to any power streamline in general sound fields.

This reactive intensity vector represents the local action of the reactivity tensor on the active intensity due to average oscillating intensity across an oriented surface element $\boldsymbol{T}dS$ normal to the active intensity.

Hence, the reactive and complex sound intensity vectors, $\bar{\boldsymbol{S}}\left(\boldsymbol{x}\right)$ and $\boldsymbol{Q_T}\left(\boldsymbol{x}\right)$ can be defined as:

$$\boldsymbol{Q_T}\left(\boldsymbol{x}\right):=\mathbb{Q}\left(\boldsymbol{x}\right)\cdot\boldsymbol{T};\quad\boldsymbol{T}=\frac{\boldsymbol{I}\left(\boldsymbol{x}\right)}{\left|\boldsymbol{I}\left(\boldsymbol{x}\right)\right|}\tag{1.54}$$

$$\hat{\boldsymbol{S}}\left(\boldsymbol{x}\right) := \boldsymbol{I}\left(\boldsymbol{x}\right) + i\,\boldsymbol{Q_T}\left(\boldsymbol{x}\right)\,. \tag{1.55}$$

1.5 Relationship Between Wave Impedance and Complex Sound Intensity

In order to shed light on physical connection between the stationary time average definition given in the previous subsection and the spectral analysis of the complex sound intensity, an approach based on some energetic indicators is proposed in this work [12]. In this way, the natural and general relationship between wave impedance and complex intensity will be also formulated.

Let us start by writing down the formula for the c-normalized speed of the energy particle, $\eta(\boldsymbol{x})$, as it can be easily inferred from the general definition given in Eq.5, p. 932 of Ref.[13]:

$$\eta(\boldsymbol{x}) := \frac{I(\boldsymbol{x})}{c \cdot W(\boldsymbol{x})} = \frac{I(\boldsymbol{x})}{c \cdot (W_p(\boldsymbol{x}) + W_k(\boldsymbol{x}))} \tag{1.56}$$

where $I(\boldsymbol{x})$ is the active intensity modulus, c is the sound speed, and $W(\boldsymbol{x})$ is the time-stationary energy density given by the sum of potential and kinetic energy densities, $W_p(\boldsymbol{x})$ and $W_k(\boldsymbol{x})$ respectively, given by the next Eq.:

$$W_p(\boldsymbol{x}) = \left\langle \frac{p^2(\boldsymbol{x},t)}{2 \cdot \rho \cdot c^2} \right\rangle \tag{1.57}$$

$$W_k(\boldsymbol{x}) = \left\langle \frac{1}{2} \cdot \rho \cdot \boldsymbol{v}^2(\boldsymbol{x},t) \right\rangle \tag{1.58}$$

As shown in Ref.[10], the Eq.1.56, once multiplied by the characteristic impedance ρc, can be also interpreted as the energy conductance of any general sound field with complex intensity as in Eq.1.55. In the same way, energy susceptance μ and energy admittance σ can be defined as follows:

$$\mu(\boldsymbol{x}) := \frac{Q_T(\boldsymbol{x})}{c \cdot W(\boldsymbol{x})} = \frac{Q_T(\boldsymbol{x})}{c \cdot (W_p(\boldsymbol{x}) + W_k(\boldsymbol{x}))}$$

$$\sigma(\boldsymbol{x}) := \frac{S(\boldsymbol{x})}{c \cdot W(\boldsymbol{x})} = \frac{S(\boldsymbol{x})}{c \cdot (W_p(\boldsymbol{x}) + W_k(\boldsymbol{x}))}$$

where $Q_T(\boldsymbol{x})$ and $S(\boldsymbol{x})$ are the modules of the reactive and complex intensity vectors respectively.

Now, the question is: how this new vision of sound intensity theory can be linked to the concept of wave impedance as usually modeled and calculated in classical literature?

The answer to this question can be obtained simply by analyzing the behavior of the energetic indicators graphically regarding Wk and Wp separately:

$$\eta_p(\boldsymbol{x}) = \frac{I(\boldsymbol{x})}{c \cdot W_p(\boldsymbol{x})}; \quad \eta_k(\boldsymbol{x}) = \frac{I(\boldsymbol{x})}{c \cdot W_k(\boldsymbol{x})}$$

$$\mu_p(\boldsymbol{x}) = \frac{Q_T(\boldsymbol{x})}{c \cdot W_p(\boldsymbol{x})}; \quad \mu_k(\boldsymbol{x}) = \frac{Q_T(\boldsymbol{x})}{c \cdot W_k(\boldsymbol{x})}$$

$$\sigma_p(\boldsymbol{x}) = \frac{S(\boldsymbol{x})}{c \cdot W_p(\boldsymbol{x})}; \quad \sigma_k(\boldsymbol{x}) = \frac{S(\boldsymbol{x})}{c \cdot W_k(\boldsymbol{x})}$$

This analysis will be carried out in chapter 2, where all versions of the energetic indicators and the wave impedance are plotted together for two canonical model fields: divergent spherical wave (DSW) and quasi stationary wave in one dimension (QSW-1D).

The results show that in the monochromatic cases, only those indicators related with the kinetic energy density are directly connected with the wave impedance (Eq.1.59)[14].

$$\hat{Z}(\mathbf{x},\omega) \coloneqq R(\mathbf{x},\omega) + iX(\mathbf{x},\omega) = (\eta_k(\boldsymbol{x}) + i\mu_k(\boldsymbol{x}))\,\rho c = \left(\frac{I(\boldsymbol{x})}{2cW_k(\boldsymbol{x})} + i\frac{Q(\boldsymbol{x})}{2cW_k(\boldsymbol{x})}\right)\rho c \tag{1.59}$$

In general, the wave impedance can be evaluated along the i-th axis as usual, from the complex ratio of Fourier transforms of pressure and the corresponding velocity signal:

$$\hat{Z}_i(\boldsymbol{x},\omega) := \frac{\mathscr{F}[p(\boldsymbol{x},t)]}{\mathscr{F}[v_i(\boldsymbol{x},t)]} \equiv \frac{\hat{P}(\boldsymbol{x},\omega)}{\hat{V}_i(\boldsymbol{x},\omega)} = R_i(\boldsymbol{x},\omega) + i\,X_i(\boldsymbol{x},\omega) \tag{1.60}$$

where $R_i(\boldsymbol{x},\omega) = \Re\left(\hat{Z}_i\right)$ is the resistance, $X_i(\boldsymbol{x},\omega) = \Im\left(\hat{Z}_i\right)$ is the reactance of the sound energy current along the i-th axis at $\boldsymbol{x}$, and $i = \sqrt{-1}$.

So, the Eq. 1.59 links the wave impedance to the frequency distribution of the complex sound intensity defined in Eq. 1.55 by the following spectral equation:

$$\hat{S}_i(\boldsymbol{x},\omega) = \hat{Z}_i(\boldsymbol{x},\omega)\,|V_i(\boldsymbol{x},\omega)|^2 \tag{1.61}$$

The same analysis can be made in a more handling form in terms of the *wave admittance vector [15].* In this way, admittance can be defined directly as a complex vector quantity as follows:

$$\hat{\boldsymbol{Y}}(\boldsymbol{x},\omega) \coloneqq \frac{\mathscr{F}[\boldsymbol{v}(\boldsymbol{x},t)]}{\mathscr{F}[p(\boldsymbol{x},t)]} \equiv \frac{\hat{\boldsymbol{V}}(\boldsymbol{x},\omega)}{\hat{P}(\boldsymbol{x},\omega)} = \boldsymbol{G}(\boldsymbol{x},\omega) + i\,\boldsymbol{B}(\boldsymbol{x},\omega) \tag{1.62}$$

The energy-mass equation then becomes:

$$\hat{\boldsymbol{S}}(\boldsymbol{x},\omega) \coloneqq \boldsymbol{I}(\boldsymbol{x},\omega) + i\,\boldsymbol{Q_T}(\boldsymbol{x},\omega) = \hat{\boldsymbol{Y}}(\boldsymbol{x},\omega)\left|\hat{P}(\boldsymbol{x},\omega)\right|^2 \tag{1.63}$$

In fact, Eq. 1.63 is valid when the impedance is calculated in the bases where the tensor $\mathbb{Q}(\boldsymbol{x},\omega)$ is a diagonal matrix. Otherwise, a general solution is found by using the Eq.1.54, where the reactivity spectral tensor is obtained from the admittance as follows:

$$\mathbb{Q}(\boldsymbol{x},\omega) = \left|\hat{P}(\boldsymbol{x},\omega)\right|^2 \cdot \sqrt{\begin{bmatrix} B_xB_x & B_xB_y & B_xB_z \\ B_yB_x & B_yB_y & B_yB_z \\ B_zB_x & B_zB_y & B_zB_z \end{bmatrix}} \tag{1.64}$$

The Eq. 1.63 is a general and powerful relationship giving the spectral components of both active and reactive intensities $\boldsymbol{I}$ and $\boldsymbol{Q_T}$, and can be used as the practical tools for measuring the complex intensity.

In fact:

1. It allows to recover the active intensity vector $\boldsymbol{I}(\boldsymbol{x}) = \langle p\boldsymbol{v}\rangle = \langle p\boldsymbol{v}_p\rangle = \sqrt{\langle p^2\rangle\left\langle \boldsymbol{v}_p^2\right\rangle}\boldsymbol{T}(\boldsymbol{x})$ from the overall value of the frequency distribution of active intensity components $I_i(\boldsymbol{x},\omega)$ defined as the real part of equation 1.63 i.e.

$$\mathbf{I}(\boldsymbol{x},\omega) \coloneqq \Re\left(\hat{\boldsymbol{Y}}(\boldsymbol{x},\omega)\right)\left|\hat{P}(\boldsymbol{x},\omega)\right|^2 = \boldsymbol{G}(\boldsymbol{x},\omega)\left|\hat{P}(\boldsymbol{x},\omega)\right|^2 \tag{1.65}$$

$$\boldsymbol{I}(\boldsymbol{x}) = \left[I_x(\boldsymbol{x}),\, I_y(\boldsymbol{x}),\, I_z(\boldsymbol{x})\right], \qquad I_i(\boldsymbol{x}) = \sum_{\omega} I_i(\boldsymbol{x},\omega)\,; \tag{1.66}$$

2. It allows to calculate the frequency distribution of reactive intensity vector $\boldsymbol{Q_T}(\boldsymbol{x},\omega)$ by applying the spectral reactivity tensor $\mathbb{Q}(\boldsymbol{x},\omega)$ to the tangent vector $\boldsymbol{T}(\boldsymbol{x},\omega) = \boldsymbol{I}(\boldsymbol{x},\omega)\cdot\boldsymbol{I}^{-1}(\boldsymbol{x},\omega)$:

$$\boldsymbol{Q_T}(\boldsymbol{x},\omega) = \mathbb{Q}(\boldsymbol{x},\omega)\cdot\boldsymbol{T}(\boldsymbol{x},\omega) \tag{1.67}$$

It must be emphasized here that unlike Eq. 1.66 which gives de facto an alternative complete measure of the active intensity, the frequency-overall vector quantity coming from the components 1.67 it is not coincident with the time-independent reactive intensity defined in 1.54, that is $Q_{i\boldsymbol{T}}(\boldsymbol{x}) \neq \left[\sum_{\omega} Q_{i\boldsymbol{T}}(\boldsymbol{x},\omega)\right]_{i=x,y,z}$. The reactive intensity can be measured from 1.67 only in monochromatic fields of fixed frequency ω_0, that is $\boldsymbol{Q_T}(\boldsymbol{x}) = \left[Q_{i\boldsymbol{T}}(\boldsymbol{x},\omega_0)\right]_{i=x,y,z}$. This means that, while the spectral components of active intensity add-on like vectorial quantities in space, the reactive intensity components do not.

A final remark takes into consideration the frequency distribution of the norm $Q(\boldsymbol{x}) = \|\mathsf{Q}\|$. According to Eq. 1.53, it can be shown that:

$$Q(\boldsymbol{x},\omega) = \sqrt{\sum_{i=x,y,z}\left(\left|P(\boldsymbol{x},\omega)\right|^2\left|V_i(\boldsymbol{x},\omega)\right|^2 - I_i(\boldsymbol{x},\omega)^2\right)} \tag{1.68}$$

However only when the correct frequency-overall procedure is applied, the norm $Q(\boldsymbol{x})$ can be recovered as:

$$Q(\boldsymbol{x}) = \sqrt{\langle p^2 \rangle \langle \boldsymbol{v}^2 \rangle - I^2} = \sqrt{\sum_{i=x,y,z} \left[\sum_{\omega} |P(\boldsymbol{x},\omega)|^2 \cdot \sum_{\omega} |V_i(\boldsymbol{x},\omega)|^2 - \left(\sum_{\omega} I_i(\boldsymbol{x},\omega) \right)^2 \right]}. \tag{1.69}$$

To conclude, the Eq. 1.63 establishes a fundamental relationship between the energy and the mass flows in any general sound field, and should be called the *acoustic energy-mass equation* in agreement with the physical dimensions of its left and right side respectively.

Graphic evidence that the energy-mass equation is verified both in monochromatic and non-monochromatic fields is shown in the next section, where the magnitudes of active and reactive intensity have been explicitly calculated from their constitutive averaging process in time-domain (i.e. $|\langle p\boldsymbol{v} \rangle|$and $|\mathbb{Q}(\boldsymbol{x})\boldsymbol{T}(\boldsymbol{x})|$), and from their respective frequency distributions given by $\hat{S}_i(\boldsymbol{x},\omega)$, and rendered on the same plot for easy comparison. Simulations informed in the next section regard quasi-stationary plane-waves fields in 1-D and 2-D, and divergent spherical waves as a model of a 3-D field.

1.6 Recovering the Sign of Susceptance

In the previous section, the connection between the wave impedance and the spectral complex sound intensity was exposed. Now, we will examine a methodology developed in order to keep all information from the susceptance.

When observing Eq. 1.64, where the spectral reactivity tensor $\mathbb{Q}(\boldsymbol{x},\omega)$ is obtained from the power spectrum of pressure and the square root of the tensorial product of the susceptance vector, the sign of the suceptance is lost.

The solution is to find the spectral reactivity tensor by avoiding the square and square root operations. This is possible only when the impedance is calculated in the bases where the reactivity tensor is a diagonal matrix.

Therefore, the algorithm is shown in Fig.1.2 and can be written as follows:

1. Calculate the reactivity tensor from admittance in the basis x, y, z using the Eq.1.64: $\mathbb{Q}_{xyz}(\boldsymbol{x},\omega)$
2. Calculate the eigenvectors E_{3x3} of the $\mathbb{Q}_{xyz}(\boldsymbol{x},\omega)$ in order to know the new basis a, b, c where the reactivity tensor is represented in diagonal form.
3. Transform the particle velocity spectrum to basis a, b, c obtaining $\hat{\boldsymbol{V}}_{abc}(\boldsymbol{x},\omega)$
4. Calculate the admittance in the basis a, b, c as $\hat{\boldsymbol{Y}}_{abc}(\boldsymbol{x},\omega) = \frac{\hat{\boldsymbol{V}}_{abc}(\boldsymbol{x},\omega)}{\hat{P}(\boldsymbol{x},\omega)}$
5. Calculate the spectral reactivity tensor directly from the susceptance vector in the basis a, b, c as: $\mathbb{Q}_{abc}(\boldsymbol{x},\omega) = \left|\hat{P}(\boldsymbol{x},\omega)\right|^2 \cdot diag(B_a, B_b, B_c)$
6. Transform the reactivity tensor $\mathbb{Q}_{abc}(\boldsymbol{x},\omega)$ to the original basis x, y, z using the eigenvectors as: $\mathbb{Q}_{xyz}(\boldsymbol{x},\omega) = Ev_{3x3} \cdot \mathbb{Q}_{xyz}(\boldsymbol{x},\omega) \cdot Ev_{3x3}^{-1}$

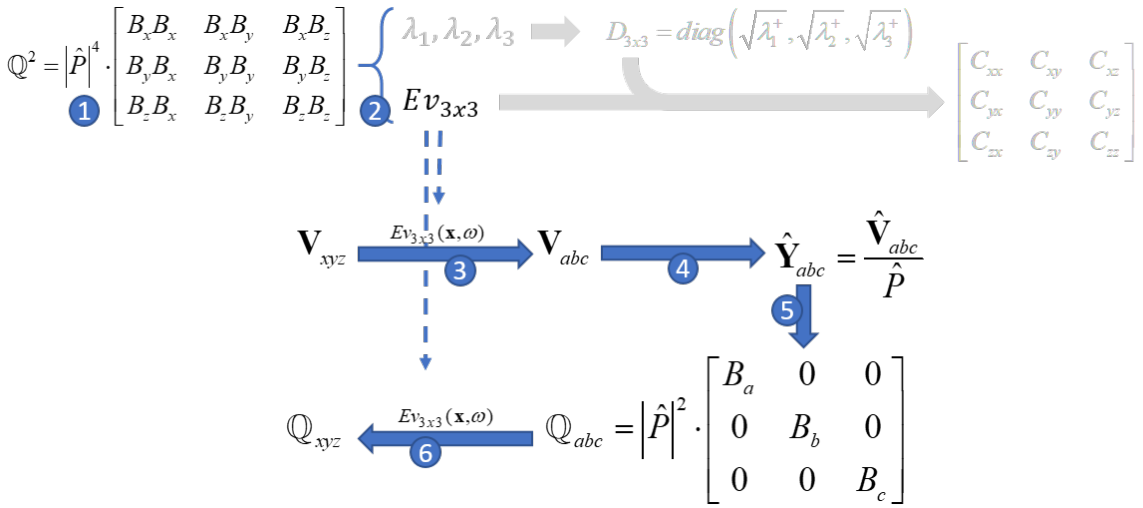

Figure 1.2: Alternative Square Root Process to Obtain The Spectral Reactivity Tensor without Lost of Signum

7. Finally, the reactive intensity can be obtained through the Eq.1.67 using the spectral reactivity tensor obtained in 6.

Notice that this process has to be made for each frequency component.

To conclude, the frequency distribution of each reactive intensity component $Q_{i\boldsymbol{T}}(\boldsymbol{x},\omega)$ represented in the basis x, y, z provides new information about its origin: whether it comes from mass or compliant reactance, depending on the conventional signum $(X_i(\boldsymbol{x},\omega))$ as Beranek already addressed in Ref. [16].

Chapter 2

SYMBOLIC AND NUMERICAL SIMULATION

In this chapter, three canonical case-studies are described in order to analyze and visualize the sound fields in different situations.

In this way, the new definitions and concepts shown in chapter 1 will be used in each simulation case to verify them and to clarify the theoretical fundamentals.

The case-studies reviewed here are the divergent spherical wave in 3-D and the quasi-stationary wave in 1-D and 2-D.

The symbolic computation engine, provided by the Maple(TM) software, is used for the quasi-stationary wave in one dimension and the divergent spherical wave cases, while for the quasi-stationary wave model in two dimensions, numerical simulation is used in order to decrease the running time.

2.1 Divergent Spherical Wave (3-D)

The model chosen for the divergent spherical wave field is the pulsating sphere with less radius than the wavelength $a_0 \ll \lambda$(Fig.2.1). All the relevant quantities used for the graphical demonstration of Eq.1.59 in this case-study are reported below.

2.1.1 Model

The free field velocity potential $\phi(r,t)$ for a sphere centered at $r = 0$, whose radius a varies like a sinusoid of circular frequency ω from the equilibrium position a_0, can be written as:

$$\phi(r,t) = \frac{\hat{A}\mathrm{e}^{i(\omega t - kr)}}{r}; \quad \hat{A} = \frac{a_0^2 b\omega \mathrm{e}^{ika_0}}{1 + ika_0}; \tag{2.1}$$

where the complex amplitude $\hat{A}$ depends on the amplitude of the vibration $b \ll a_0$, and $k = \omega/c$ is the propagation constant in radians per meter. Clearly, the field has a spherical symmetry and our analysis will be focused only on $r > a_0$ to disregard the singularity at $r = 0$.

The observable quantities (i.e. the pressure and velocity perturbation fields) are derived from ϕ as:

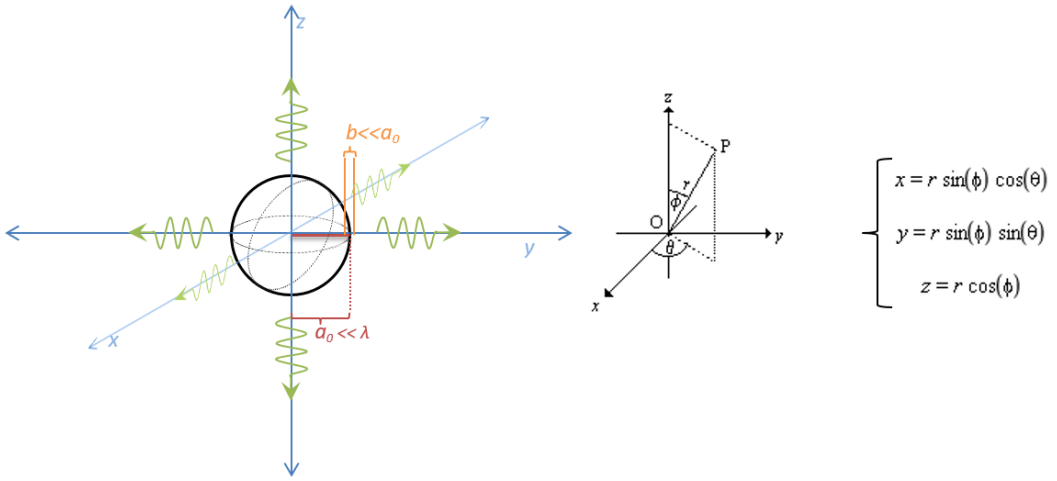

Figure 2.1: Divergent Spherical Wave Model. Spherical coordinates are used in order to reduce to one only spatial variable “r”.

$$\hat{p}\,(r,t) = -\rho\frac{\partial\phi(r,t)}{\partial t} = -\frac{i\rho a_0^2 b\omega^2 \mathrm{e}^{i(ka_0+\omega t-kr)}}{(1+ika_0)\,r}; \quad p\,(r,t) := \Re\left\{\hat{p}\,(r,t)\right\}; \tag{2.2}$$

$$\hat{v}\,(r,t) = \frac{\partial\phi(r,t)}{\partial r} = -\frac{a_0^2 b\omega \mathrm{e}^{i(ka_0+\omega t-kr)}\,(ikr+1)}{(1+ika_0)\,r^2}; \quad v\,(r,t) := \Re\left\{\hat{v}(r,t)\right\}; \tag{2.3}$$

where of course the direction of the air particle velocity (2.3) is always coincident with the radial direction [17]. In this situation, the rank of the reactivity tensor is degraded to one, thus the reactivity Q coincides with the modulus of the reactive intensity vector Q_T , which has the same direction of the active intensity vector I.

2.1.2 Impedance Calculation

The wave impedance is a time-independent complex quantity obtained from the relationship between the complex pressure and the complex particle velocity amplitudes to obtain:

$$\hat{Z}(r,\omega) := \frac{\hat{p}}{\hat{v}} = \frac{i\rho c\omega r}{c+i\omega r} \tag{2.4}$$

$$\begin{gathered} R := \Re\left\{\hat{Z}(r,\omega)\right\} = \frac{\rho c^2\omega r^2 k}{c^2+\omega^2 r^2}; \qquad X := \Im\left\{\widehat{Z}(r,\omega)\right\} = \frac{\rho c^2\omega r}{c^2+\omega^2 r^2}; \\ \delta := \arctan\left(\frac{X(r,\omega)}{R(r,\omega)}\right) = \arctan\left(\frac{c}{\omega r}\right) \end{gathered} \tag{2.5}$$

where R is the acoustic resistance, X is the reactance and δ is the phase difference between

pressure and velocity for any circular frequency ω.

2.1.3 Calculation of Energetic Quantities and Indicators

The energetic quantities are calculated directly from Eqs. 2.2 and 2.3 using the stationary time-average functional $\langle\cdot\rangle := \lim_{T\to\infty} \frac{1}{2T}\int_{-T}^{+T}(\cdot)\,dt$. In this way the following results can be obtained as a function of r :

$$I := \langle pv \rangle = \frac{1}{2}\frac{k^4 a_0^4 b^2 \rho c^3}{r^2\left(1+k^2a_0^2\right)}; \tag{2.6}$$

$$\begin{gathered} Wk := \frac{1}{2}\rho\left\langle v^2\right\rangle = \frac{1}{4}\frac{(kc)^2 a_0^4 b^2 \rho\left(1+k^2r^2\right)}{\left(1+k^2a_0^2\right)r^4}\,; \qquad Wp := \frac{1}{2\rho c^2}\left\langle p^2\right\rangle = \frac{1}{4}\frac{\rho a_0^4 b^2 k^4 c^2}{\left(1+k^2a_0^2\right)r^2}\,; \\ W := Wk + Wp = \frac{1}{4}\frac{(kc)^2 b^2 a_0^4 \rho\left(1+2\left(kr\right)^2\right)}{r^4\left(1+k^2a_0^2\right)}\,; \end{gathered} \tag{2.7}$$

$$S := 2\,c\,\sqrt{Wk\,Wp}; \qquad Q := \sqrt{S^2 - I^2}; \tag{2.8}$$

where I is the active intensity, Wk, Wp and W are respectively the kinetic, potential and total energy densities, S is the apparent intensity and Q is the reactivity[10].

From Eqs. 2.6, 2.7 and 2.8, all sound intensity indicators described in section 1.5 of interest are then derived:

$$\begin{gathered} \eta := \frac{I}{cW} = \frac{2\left(kr\right)^2}{1+2(kr)^2}\,; \\ \eta_k := \frac{I}{2cWk} = \frac{(kr)^2}{1+(kr)^2}\,; \qquad \eta_p := \frac{I}{2cWp} = 1\,; \end{gathered} \tag{2.9}$$

$$\begin{gathered} \mu := \frac{Q}{cW} = \frac{2kr}{1+2(kr)^2}\,; \\ \mu_k := \frac{Q}{2cWk} = \frac{kr}{1+(kr)^2}\,; \qquad \mu_p := \frac{Q}{2cWp} = \frac{1}{kr}\,; \end{gathered} \tag{2.10}$$

$$\begin{gathered} \sigma := \frac{S}{cW} = 2\frac{\sqrt{Wk\,Wp}}{W} = \frac{2kr\sqrt{1+(kr)^2}}{1+2(kr)^2}; \\ \sigma_k := \frac{S}{2cWk} = \frac{\sqrt{Wk\,Wp}}{Wk} = \frac{kr}{\sqrt{1+(kr)^2}}\,; \qquad \sigma_p := \frac{S}{2cWp} = \frac{\sqrt{Wk\,Wp}}{Wp} = \frac{\sqrt{1+(kr)^2}}{kr}; \end{gathered} \tag{2.11}$$

$$\xi := \frac{\eta}{\sigma} = \frac{kr}{\sqrt{1+(kr)^2}}\,; \qquad \delta_\xi := \arccos\left(\xi\right) \tag{2.12}$$

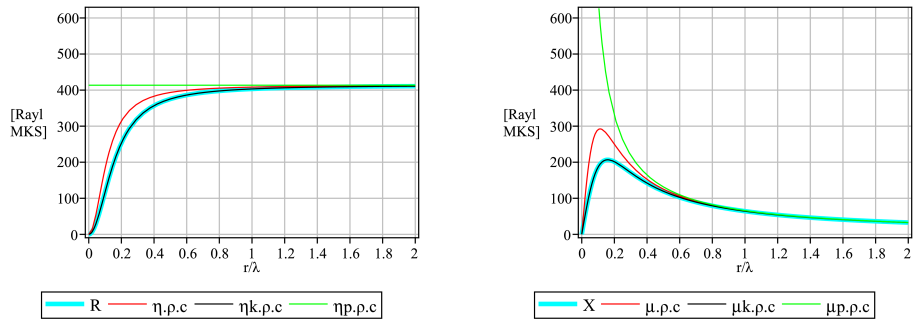

Figure 2.2: Graphical comparison of wave impedance and energy indicators for the divergent spherical wave. Resistance R is plotted on the left and reactance X is on the right. A perfect match is found only between R and X (in cyan) with $\eta_k \rho c$ and $\mu_k \rho c$ (in black) proving the WiSi connection.

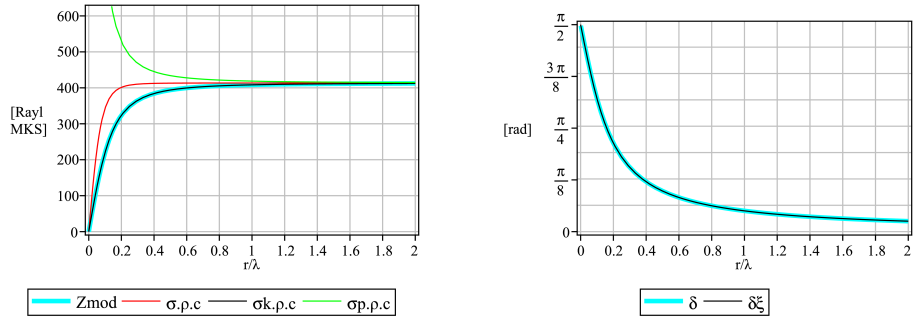

Figure 2.3: Graphical comparison of modulus and phase of wave impedance with energy indicators for the divergent spherical wave. As it was expected, a perfect match is found only between $\left|\hat{Z}\right|$ (in cyan) with $\sigma_k \rho c$ (in black) on the left plot. In the right plot the perfect match between the phase δ calculated from the wave impedance $\hat{Z}$ (in cyan) and the phase δ_ξ calculated from the acoustic power factor ξ is shown.

With all these indicators in our hands, plots of Figures 2.2 and 2.3 are obtained, showing a perfect coincidence only for the quantities η_k, μ_k, and σ_k appearing in Eq.1.59 whose validity is thus graphically proven.

2.1.4 Monochromatic and Three-frequency Cases

In order to analyze the validity of Eq.1.59 in a general multi-frequency case, active and reactive intensities and the total reactivity are calculated for a monochromatic case and a three-frequency case, each from the time-averaging definition and spectral analysis.

The mathematical model of the three-frequency case is given by adding three tones in the time domain.

Results are plotted in Figure 2.4, where active and reactive intensity calculated from time averaging and spectral analysis are shown.

As it is shown in the plot, both active and reactive intensity have a perfect match using the two calculation methods for both cases. Furthermore, the reactivity coincides with the reactive intensity as explained before.

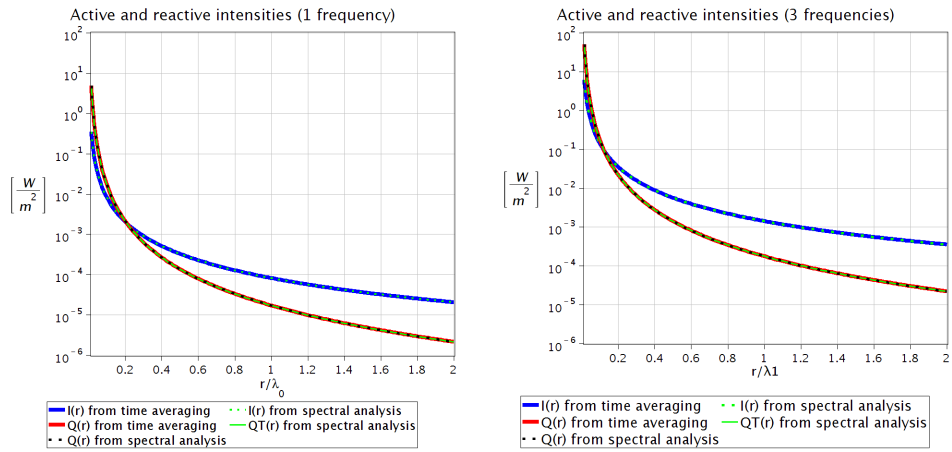

Figure 2.4: Active (blue) and Reactive (red) Intensity in a Divergent Spherical Wave Field for Monochromatic Case (left) and Three-frequency Case (right).

2.2 Quasi-Stationary Wave 1-D

Quasi-stationary plane wave model (QSW) is given by the superposition of two plane waves with the same frequency, traveling in opposite directions: progressive and regressive waves. The first one represents the wave generated by the source which is supposedly to be placed at minus infinite, while the second one represents the same wave reflected on a reflective surface, which is supposed to be placed at plus infinite as it is shown in figure 2.5.

2.2.1 Model

The mathematical model of the QSW is described by the velocity potential function $\phi(x,t)$ as it is shown in the equation 2.13, where A is the amplitude of the progressive wave while the amplitude of the regressive wave is a proportion of A given by $\mathbb{R}$, whose value is between 0 and 1. Progressive and regressive waves have a difference of phase given by ϑ.

The complex pressure is obtained by deriving the velocity potential function in relation to time (2.14), while the complex velocity is obtained by deriving in relation to the space (2.15). Finally, the pressure and velocity signals with physical mean is obtained by taking the real part of each complex quantity.

$$\phi(x,t) = A\,c\left(e^{i(kx-\omega t)} + \mathbb{R}\,e^{i(kx+\omega t+\vartheta)}\right) \tag{2.13}$$

$$\begin{aligned}\hat{p}(x,t) &= -\frac{1}{\rho}\frac{\partial\phi(x,t)}{\partial t} = -i\,\rho\,A\,c\,\omega\,\left(\mathrm{e}^{-ikx} + \mathbb{R}\,e^{i(kx+\vartheta)}\right)e^{i\omega t} \\ p(x,t) &= \Re\left\{\hat{p}(x,t)\right\}\end{aligned} \tag{2.14}$$

$$\begin{aligned}\hat{\boldsymbol{v}}(x,t) &= \nabla\phi(x,t) = -iA\,c\,k\,\left(\mathrm{e}^{-ikx} - \mathbb{R}\,e^{i(kx+\vartheta)}\right)e^{i\omega t} \\ v(x,t) &= \Re\left\{\hat{\boldsymbol{v}}(x,t)\right\}\end{aligned} \tag{2.15}$$

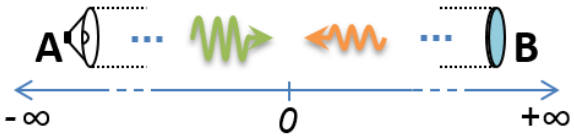

Figure 2.5: Quasi-stationary Wave Model in 1-D.

2.2.2 Impedance Calculation

By replacing $k = \omega/c$ in the equations 2.14 and 2.15, the wave impedance is obtained from the quotient of the complex pressure and the complex particle velocity:

$$\begin{gathered} \hat{Z}(x,\omega) = \rho c \frac{\left(\mathrm{e}^{-ix\omega/c} + \mathbb{R}\, e^{i(x\omega/c+\vartheta)}\right)}{\left(\mathrm{e}^{-ix\omega/c} - \mathbb{R}\, e^{i(x\omega/c+\vartheta)}\right)} \\ R(x,\omega) = \Re\{Z(x,\omega)\}\ ;\ \ I(x,\omega) = \Im\{Z(x,\omega)\} \\ \delta := \arctan\left(\frac{X(x,\omega)}{R(x,\omega)}\right) \end{gathered} \tag{2.16}$$

where R is the acoustic resistance, X is the reactance and δ is the phase difference between pressure and velocity for any circular frequency ω.

Notice that when $\mathbb{R} = 0$, the wave impedance coincides with the characteristic impedance as it was shown in subsection 1.2.1.

2.2.3 Calculation of Energetic Quantities and Indicators

The energetic quantities and their derived indicators are calculated in this subsection. Explicit results are described only when they are of reasonable length and they indicate their inert form when necessary.

The first quantity is the time-independent active intensity obtained from the usual definition Eq.1.35. The expression for the QSW model is shown in equation 2.17. Notice that the space variable x is not present here, so the active intensity is always constant in the space.

$$I(x) = \frac{1}{2}\rho A^2 \omega^2 c\left(1 - \mathbb{R}^2\right); \tag{2.17}$$

In the equation 2.18 shown below, the kinetic, potential and total energy densities are formulated. For kinetic and potential energy equations, x is only present in the cosine term. In the particular situation when $\mathbb{R} = 0$, the energy densities remain constant, otherwise, W_k and W_p have an oscillatory behavior respect x. Besides, the total energy density W remains always constant in the space.

$$\begin{aligned} W_k(x) &= \frac{1}{4}\rho A^2\omega^2\left(1 - 2\mathbb{R}\cos\left(2kx + \vartheta\right) + \mathbb{R}^2\right); \\ W_p(x) &= \frac{1}{4}\rho A^2\omega^2\left(1 + 2\mathbb{R}\cos\left(2kx + \vartheta\right) + \mathbb{R}^2\right); \\ W(x) &= Wk(x) + Wp(x) = \frac{1}{2}\rho A^2\omega^2\left(1 + \mathbb{R}^2\right); \end{aligned} \tag{2.18}$$

As shown in section 1.4, the apparent intensity modulus can be calculated in terms of energy densities W_k and W_p respectively, as shown in equation 2.19. The reactivity is obtained from the apparent and active intensity modulus as follows:

$$S = 2\,c\,\sqrt{Wk\,Wp}; \quad Q = \sqrt{S^2 - I^2} \tag{2.19}$$

As explained in section 1.5, the energetic indicators η, μ, and σ are written in three attempts using the total, kinetic and potential energy densities, in order to find the relationship between sound intensity and wave impedance. The expression for the quasi-stationary wave are shown below:

$$\begin{aligned} \eta &\coloneqq \frac{I}{c\,W} = \frac{(1 - \mathbb{R}^2)}{(1 + \mathbb{R}^2)}\ ; \\ \eta_k &\coloneqq \frac{I}{2c\,Wk} = \frac{(1 - \mathbb{R}^2)}{1 - 2\mathbb{R}\cos\left(2kx + \vartheta\right) + \mathbb{R}^2}\ ; \\ \eta_p &\coloneqq \frac{I}{2c\,Wp} = \frac{(1 - \mathbb{R}^2)}{1 + 2\mathbb{R}\cos\left(2kx + \vartheta\right) + \mathbb{R}^2}\ ; \end{aligned} \tag{2.20}$$

$$\mu \coloneqq \frac{Q}{c\,W}\,; \qquad \mu_k \coloneqq \frac{Q}{2c\,Wk}\,; \qquad \mu_p \coloneqq \frac{Q}{2c\,Wp}; \tag{2.21}$$

$$\sigma \coloneqq \frac{S}{cW}\,; \qquad \sigma_k \coloneqq \frac{S}{2cWk}; \qquad \sigma_p \coloneqq \frac{S}{2cWp}\,; \tag{2.22}$$

$$\begin{aligned} \xi \coloneqq \frac{\eta}{\sigma} &= \frac{(1 - \mathbb{R}^2)}{\sqrt{1 + 2\mathbb{R}^2 - 4\mathbb{R}^2 cos^2(2kx + \vartheta) + \mathbb{R}^4}}\ ; \\ \delta_\xi &\coloneqq \arccos(\xi) \end{aligned} \tag{2.23}$$

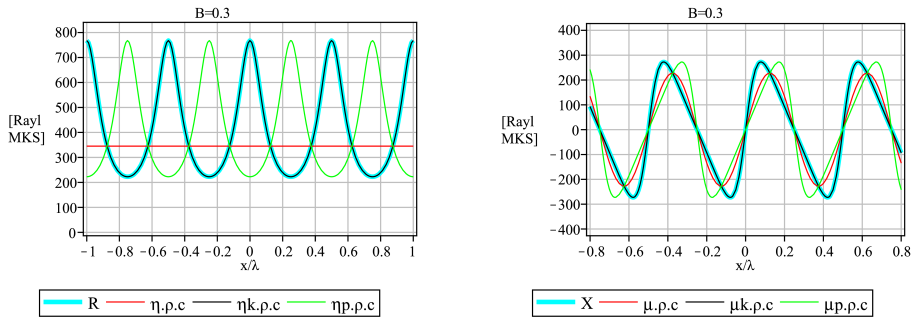

Figure 2.6: Graphical comparison of wave impedance and energy indicators for one-dimensional quasi-stationary waves. Resistance R is plotted on the left and reactance X is on the right. Again, the perfect match is found only between R and X (in cyan) with $\eta_k \rho c$ and $\mu_k \rho c$ (in black) proving also in this case, the wisi connection.

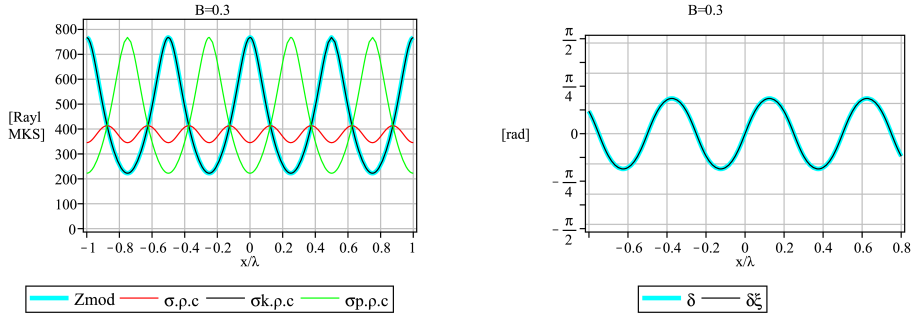

Figure 2.7: Graphical comparison of modulus and phase of wave impedance with energy indicators for one-dimensional quasi-stationary waves. As expected, a perfect correspondence is found only between $\left|\hat{Z}\right|$ (in cyan) with $\sigma_k \rho c$ (in black) on the left plot. In the right plot, the perfect match between the phase δ calculated from the wave impedance $\hat{Z}$ (in cyan) and the phase δ_ξ calculated from the acoustic power factor ξ is shown.

The curves plotted in Figures 2.6 and 2.7 show the results obtained. Also here there is a perfect match between the quantities related with impedance and the energetic indicators associated only with the kinetic energy. Therefore, this is the proof of the validity of Eq.1.59.

2.2.4 Monochromatic and Three-frequency Cases

In the same way as in the previous case, active and reactive intensities and total reactivity are calculated for a monochromatic case and a three-frequency case, using the two calculation methods (time-averaging definition and spectral analysis), in order to analyze the validity of Eq.1.59 in a general multi frequency case.

In Figure 2.8, active and reactive intensities from time averaging and spectral analysis are plotted.

Looking at the left plot in Figure 2.8, active intensity and reactivity have a perfect match between the two calculation methods, while the spectral analysis in the reactive intensity calculation only coincides for positive values. This is because the spectral analysis allows to keep the sign of the reactance as explained in section 1.6.

On the other hand, in the three-frequency case (right plot), the active intensity and reactivity also have a perfect match using the time averaging and spectral analysis methods, but here, the reactive intensity calculated from the spectral analysis is completely different.

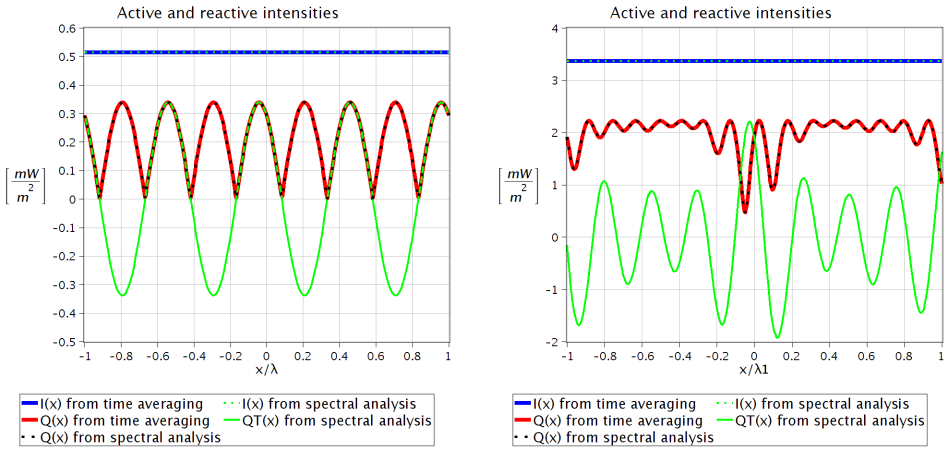

Figure 2.8: Active (blue) and Reactive (red) intensities in a Quasi-stationary Wave Field in 1-D for Monochromatic Case (left) and Three-frequency Case (right)

Hence, we can conclude that the spectral analysis allows to keep the sign of the reactive intensity, but in the multi-frequency cases, the overall frequency is valid only for the active intensity and the reactivity but not for reactive intensity.

2.3 Quasi-stationary Wave 2-D

Let us now see an interesting case in two dimensions when the circulation of energy is present in the sound field i.e. $\boldsymbol{\nabla} \times \boldsymbol{I} \neq \mathbf{0}$. The model is represented in Fig.2.9.

As it was said in the introduction of this chapter, numerical simulations have been executed with Matlab (TM) over synthesized signals and using its standard algebraic and signal processing routines in order to decrease the running time. Therefore, no symbolic expressions are reported in here, and the calculation of the impedance and the energetic quantities are obtained by the usual definitions.

2.3.1 Model

This case study is easily modeled generally by superposing two quasi-stationary waves along the orthogonal axes x and y and by choosing appropriate values for the real reflection coefficients B_x,B_y with time lags ϑ_x and ϑ_y respectively.

The velocity potential function can be written by extending the velocity potential function of the quasi-stationary wave case in 1-D (2.13):

$$\phi\left(x,y,t\right) = A\,c\left(e^{i(\omega t-kx)} + B_x\,e^{i(\omega t+kx+\vartheta_x)} + e^{i(\omega t-ky)} + B_y\,e^{i(\omega t+ky+\vartheta_y)}\right); \tag{2.24}$$

Therefore, as usual, the 2-D pressure and velocity fields are obtained from the velocity potential function as follows:

$$\begin{aligned} \hat{p}\left(x,y,t\right) &= -\rho\frac{\partial\phi(x,y,t)}{\partial t} \\ p\left(x,y,t\right) &= \Re\left\{\hat{p}\left(x,y,t\right)\right\}; \end{aligned} \tag{2.25}$$

$$\begin{aligned} \hat{\boldsymbol{v}}\left(x,y,t\right) &= \boldsymbol{\nabla}\phi(x,y,t) \\ \boldsymbol{v}\left(x,y,t\right) &= \Re\left\{\hat{\boldsymbol{v}}(x,y,t)\right\}. \end{aligned} \tag{2.26}$$

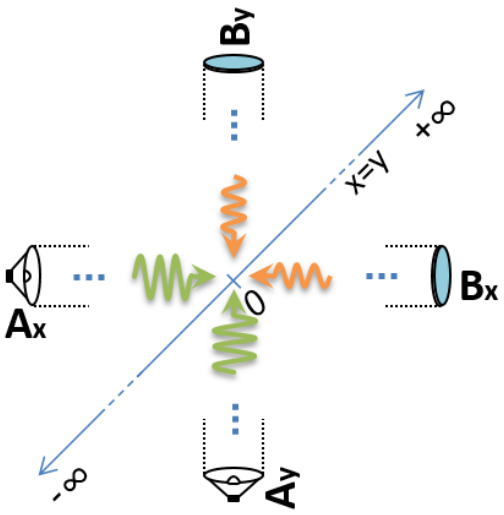

Figure 2.9: Quasi-stationary Wave Model in 2-D.

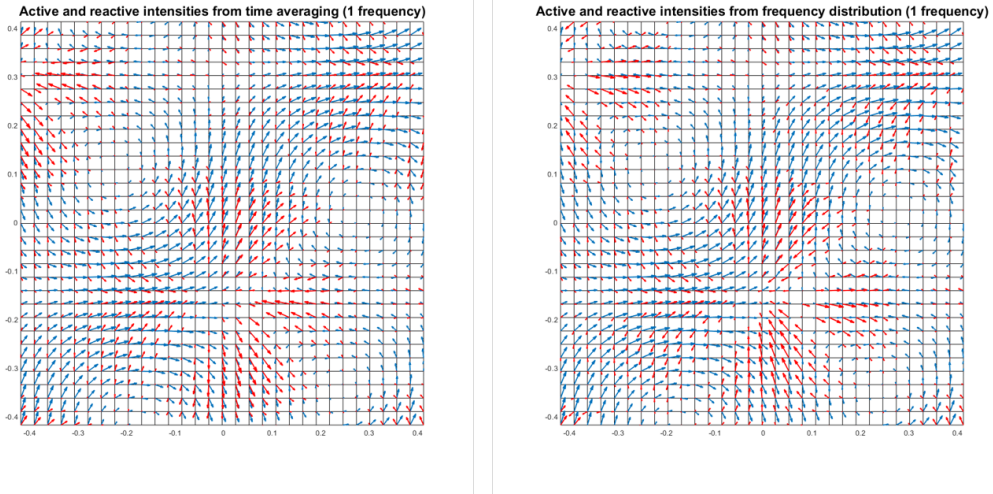

Figure 2.10: Active (blue) and Reactive (red) Intensity in a Quasi-stationary Wave Field in 2-D for Monochromatic Case.

2.3.2 Monochromatic and Three-frequency Cases

The graphical results obtained are reported in figure 2.10 for a monochromatic field and in figure 2.11 for a non-monochromatic one.

On the left side of figure 2.10, active and reactive intensity fields calculated directly from their defining equation 1.55 (i.e. using time-averaging processes) are compared to the same fields (on the right side) calculated from Eqs. 1.65 and 1.67 instead (i.e. using spectral processes). As shown, active and reactive intensity fields coincide in the two sides but their spatial directions, as expected, are generally different. An interesting observation regards the reversal of the reactive intensity direction in certain areas of the right-side field. This is due to the sign information provided by the reactance, which is not present in the time-independent reactive intensity field depicted on the left-side.

In the non-monochromatic case of figure 2.11, where the same comparison as for monochromatic fields is shown, the reactive intensity field $\boldsymbol{Q_T}$ has been calculated using only the

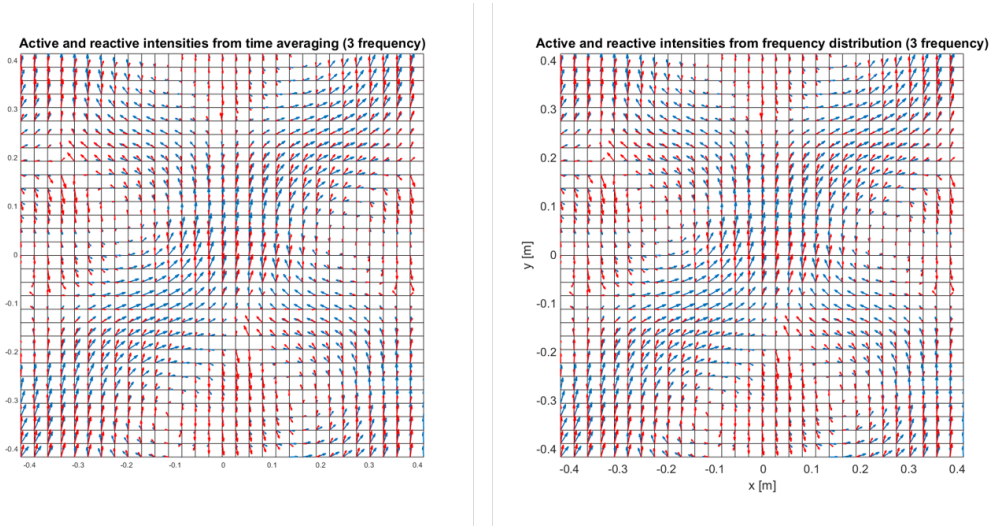

Figure 2.11: Active (blue) and Reactive (red) Intensity in a Quasi-stationary Wave Field in 2-D for Three-frequency Case.

time-averaging process. This is due to the inequality $Q_{i\boldsymbol{T}}(\boldsymbol{x}) \neq \left[\sum_{\omega} Q_{i\boldsymbol{T}}(\boldsymbol{x},\omega)\right]_{i=x,y,z}$ always holds in non-monochromatic cases, and thus reactive intensity can only be calculated as a time-average.

This completes the graphical validation of the acoustic energy-mass equation also for curved sound fields.

Chapter 3

MEASUREMENT INSTRUMENTS AND CALIBRATION METHODS

3.1 Intensimetric Probes

As it was explained in chapter 1, a sound field can be described by two sound field quantities: sound pressure and particle velocity, p and v respectively. The sound intensity is calculated by the product of these two signals, so this is why the probes that measure simultaneously pressure and velocity signals are simultaneously called intensimetric probes. Therefore, in a general case two transducers are required [5].

The transducers for measuring the sound pressure are already highly developed. There are many techniques to obtain the variation of pressure in the medium, but, in general, the concept is always the same: to detect the movement of a membrane that closes a cavity within which the pressure is equal to static pressure, and the pressure variations outside the cavity cause a movement of the membrane [18].

The most used transducers are the dynamic and condenser microphones. The principle operation of the first one is based in the electromagnetic fundamentals. It consists of a coil fixed to the membrane, which the movement of the membrane causes the coil to move in a magnetic field resulting in an electrical signal. On the other hand, the condenser microphones are based on electrical field fundamentals. In practice, a condenser microphone is a capacitor where one of its two plats acts as a flexible membrane, which is deflected due to the pressure variations. These deflections modify the capacitance, which produces a voltage variation when it is polarized by a constant electric voltage.

The development of the transducers to measure particle velocity, however, started many years after the development of pressure transducers. The first consolidated technique was an indirect method which obtains the particle velocity signal from the gradient of the pressure. Therefore, at least two pressure microphones are required. This methodology was the main technique to measure particle velocity and it is used until now. In the last few years, a transducer to measure particle velocity has been developed. It consists of a couple of very thin wires that vary their temperature with the movement of the particles.

This work focuses on these two methods for measuring sound intensity: p-p (pressure-pressure) and p-v (pressure-velocity) intensimetric probes.

3.1.1 P-p technique

This probe is based on measuring the gradient of the pressure to sense the particle velocity signal. As explained in the section 1.1, in linear acoustic fields, the Newton's equation of motion can be simplified as shown in Eq.3.1. Thus, particle velocity can be obtained from the gradient of pressure (Eq.3.2), where the partial derivative is taken with respect to each spatial component (Eq.3.3).

$$\rho \frac{d\mathbf{v}\left(\boldsymbol{x},t\right)}{dt} = -\nabla p\left(\boldsymbol{x},t\right) \tag{3.1}$$

$$\mathbf{v}\left(\boldsymbol{x},t\right) = -\frac{1}{\rho}\int \nabla p\left(\boldsymbol{x},t\right) dt \tag{3.2}$$

$$v_x\left(x,t\right) = -\frac{1}{\rho}\int \frac{\partial p\left(\boldsymbol{x},t\right)}{\partial x} dt \tag{3.3}$$

In practice, the gradient of the pressure is approximated by a finite difference and $v_x\left(x,t\right)$ can be calculated as:

$$v_x\left(\boldsymbol{x},t\right) \simeq -\frac{1}{\rho\Delta x}\int \left(p_2\left(\boldsymbol{x}_2,t\right) - p_1\left(\boldsymbol{x}_1,t\right)\right) dt$$

where $p1$ and $p2$ represent the signals of the two microphones separated by a distance equal to Δx.

Clearly, the measuring point of this array is between the two microphones $\Delta x/2$, which is not coincident with the pressure signal of the microphones. So, the pressure signal of this probe is obtained directly as the arithmetic mean of two pressure signals:

$$p\left(\boldsymbol{x},t\right) = \frac{p_1\left(\boldsymbol{x}_1,t\right) + p_2\left(\boldsymbol{x}_2,t\right)}{2} \tag{3.4}$$

3.1.2 P-v technique

In the last few years, a new generation of particle velocity sensors has been developed based on the measurement of the temperature changes which are proportional to the velocity of the air particles. In fact, the change of temperature in the wires produces a change in its resistivity.

In practice, the probe consists of two ultra-thin platinum wires in parallel, placed very close to each other, which are heated up about 200 °C to 400 °C due to a constant current circulation. Each wire works like a resistance changing its value with the temperature. In this way, the micro air flow modifies the temperature of the wires and the signal is given by the change of its resistivity. The wires are connected in a Wheatstone bridge (see Fig.3.3) in order to convert the resistivity changes into an electrical signal. The bridge is called

Figure 3.1: Example of Axial p-p Intensity Probe: Microphones are in Face to Face Configuration

balanced when the potential difference between B and D is equal to zero. This occurs in the following condition:

$$\frac{R_3}{R_4} = \frac{R_1}{R_2} = \frac{R_{W1}}{R_{W2}} \tag{3.5}$$

In this way, if the resistances R_1 and R_2 are replaced withthe sensor wires R_{W1} and R_{W2}, and R_3 and R_4 are chosen in order to balance the bridge (Eq.3.5), the signal $v(t)$ is equal to zero when the air flow is not present and vice versa, when the air particles are moving across the wires, the temperature changes, the resistivity varies and the bridge is unbalanced producing a potential difference which is the output signal of particle velocity.

Let us now analyze three situations of particle velocity:

- No moving air particles: here, the temperature of the wires remains constant due to no perturbations. Therefore the bridge remains balanced and the signal output is equal to zero.
- Air particles move along the wires: in this situation, the wires change their temperature to the same extent, so, again the bridge remains balanced because the proportion in the condition (Eq.3.5) does not change.
- Air particles move orthogonally across the wires: this is the favorable direction to sense the air flow. Here, the air flow changes the temperature of the wires asymmetrically producing a signal due to the unbalance of the measuring bridge.

The effect of the last two items can be better seen in the polar patterns of Fig.3.4, where the directionality of sensitivity of the probe has been measured [1].

3.2 Calibration of Intensimetric Probes

The processes currently used to calibrate the intensimetric probes require the preliminary knowledge of the acoustic impedance from model fields, which are experimentally made to

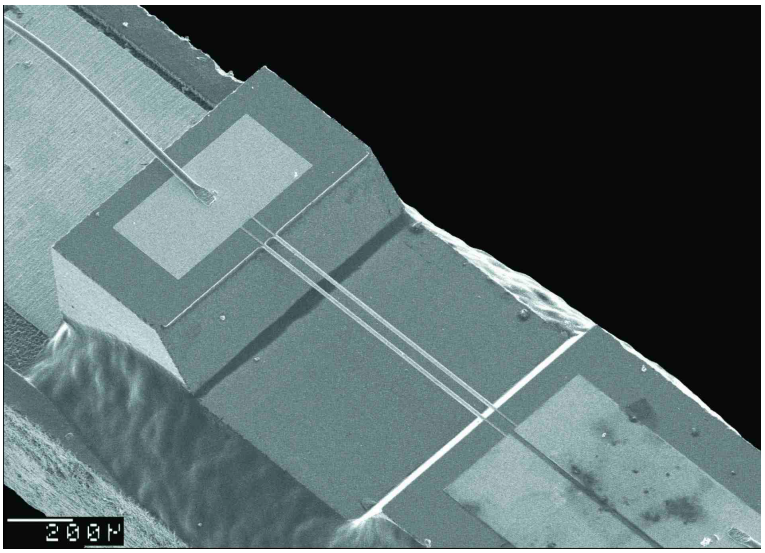

Figure 3.2: Scanning Electron Microscope (SEM) Photo of the Ultra-thin Platinum Wires of a Microflown Probe [1]

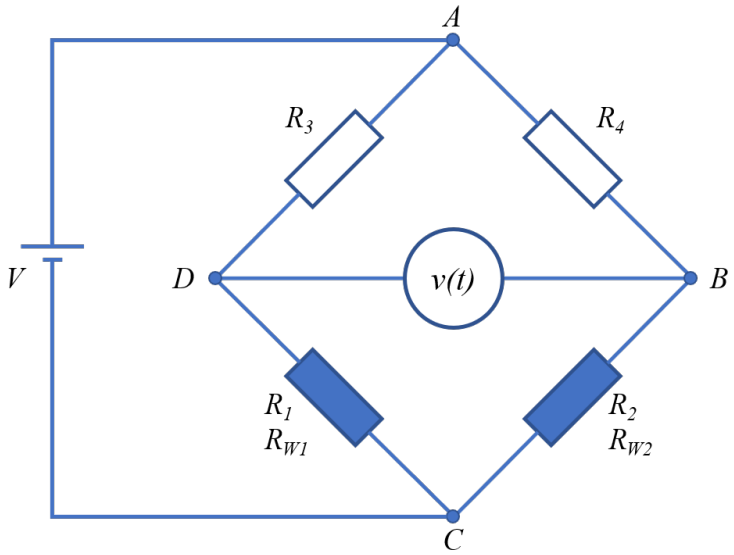

Figure 3.3: Wheatstone Bridge

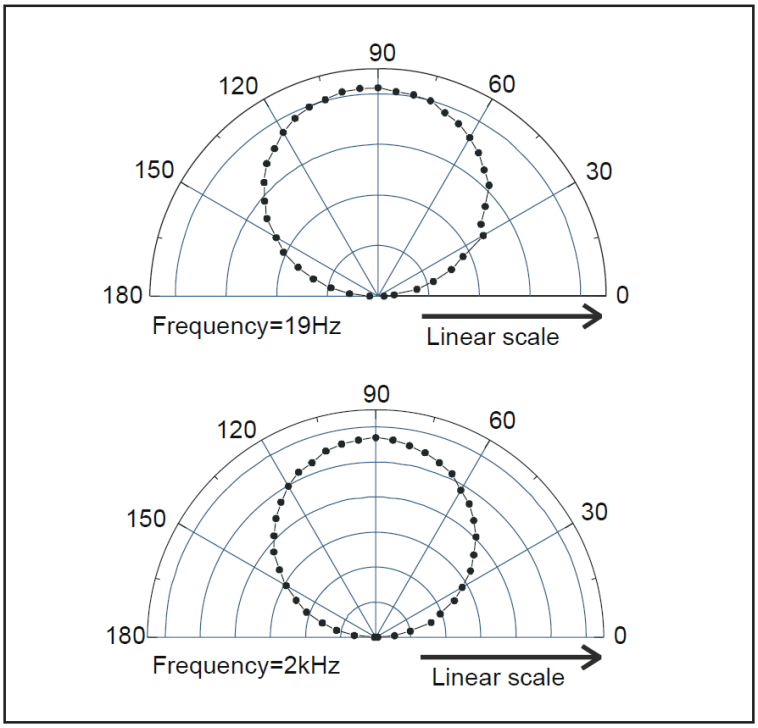

Figure 3.4: Microflown: Polar Patterns at Different Frequencies (Linear scale, Only Half the Response is Shown) [1]

serve as reference fields. Among the most used reference fields, we can mention spherical wave fields generated in an anechoic chamber, stationary wave fields generated into a Kundt tube, etc., [19]. All of these model fields, however, have the disadvantage of including the position of the measuring point in the calculation of the reference acoustic impedance, which can be a possible cause of calibration error.

Two methodologies in which it is not necessary to know the exact position of the measuring point are proposed in this work. The first one is a field generated into an anechoic waveguide where the measuring point is placed in the far field. While in the second case, the reference impedance is obtained as the geometric mean of the impedance in two extreme conditions: closed tube and open tube.

The calibration process consists in finding the scale factors α and β for the pressure and velocity transducers respectively for a fixed frequency, and the calibration functions K and $\hat{\Gamma}$ defined in the frequency domain.

The scale factors transform the values measured in arbitrary units (AU) with the A/D converter, in physical units (Pa and m/s,respectively for p and v), while the calibration function extend the scale factor to the wide spectrum.

The calibration process has been summarized in the following steps [20][21]:

1. Obtain the scale factor of the reference microphone α_{ref}:

$$\alpha_{ref} = \frac{p_{(PF)}[Pa]}{s_{ref(PF)}[AU]}$$

   where $p_{(PF)}$ is the rms value of the pressure given by a pistonphone, and $s_{ref(PF)}$ is the value registered by the sound card with the reference microphone measuring the sound generated by the pistonphone.

2. Fix a reference tone into the wave guide $p_{cal(W)}$: generate a tone at the same frequency

of the pistonphone and save the value measured with the reference microphone.

$$p_{cal(W)} = \alpha_{ref} \left[\frac{Pa}{AU}\right] s_{ref(W)}[AU]$$

$s_{ref(W)}$ is the value of the reference tone measured with the reference microphone in AU of the sound card.

3. Measure the pressure spectrum with the reference microphone $\hat{P}_{ref}$
4. Obtain the scale factors of the pressure and the velocity transducers:

$$\alpha_{probe} = \frac{p_{cal(W)}[Pa]}{s_{p(W)}[AU]}$$

$$\beta_{probe} = \frac{p_{cal(W)}[Pa]}{s_{v(W)}[AU]} \cdot \frac{1}{\rho c} \left[\frac{m \cdot s^{-1}}{Pa}\right]$$

where $s_{p(W)}$ and $s_{v(W)}$ are the calibration tone measured with the pressure and the velocity transducers respectively.

5. Measure the pressure and the velocity spectra with the pressure and the velocity transducers of the probe $\hat{P}_{probe}$ and $\hat{V}_{probe}$
6. Calculate the calibration functions:

$$K(\omega) = \left|\frac{\hat{P}_{ref}}{\hat{P}_{probe}}\right| \in \mathbb{R} \tag{3.6}$$

$$\hat{\Gamma}(\omega) = \frac{\hat{P}_{probe}}{\hat{V}_{probe}} \frac{1}{\hat{Z}_0} \in \mathbb{C} \tag{3.7}$$

where $\hat{Z}_0$ is the reference impedance.

The general process sketched above can be executed in different field conditions, each modeled by the corresponding reference impedance $\hat{Z}^0$ (see for instance [22][19]). Yet in particular, wishing to improve the calibration precision, the acoustic wave guide methodology introduced in [20] can be used with different terminations (a), (b) and (c) whose setup is shown in figure 3.5, therefore to create purely active and reactive field conditions quickly and easily..

As a matter of fact, using the setup 3.5, the measures are taken into a waveguide with three boundary conditions: anechoic (a), closed (b) and open (c). The tube, which is $38.5\,\mathrm{m}$ long when in anechoic configuration, is instead cut to $11\,\mathrm{m}$ in the open and closed configuration. In each configuration, the distance of the calibration point from the source is fixed to $10.8\,\mathrm{m}$. The sound field inside the wave guide is generated through an acoustic impedance adapter (trombone) linked to the tube, with a loudspeaker excited, for instance, with a white-noise voltage signal.

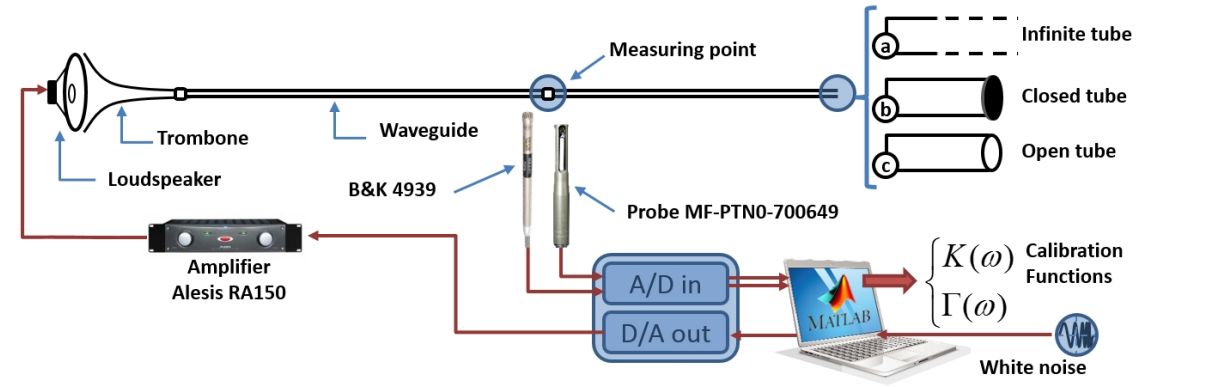

Figure 3.5: Calibration Setup: (a) Active Calibration, (b,c) Reactive Calibration.

3.2.1 Anechoic Calibration

The calibration function $\hat{\Gamma}_A(\omega)$ using the anechoic setup is obtained by measuring the pressure and velocity inside the wave guide in a purely active configuration. In this case, a progressive plane wave is present within the tube and, accordingly, the reference wave impedance $\hat{Z}^0$ is supposed to be equal to the characteristic impedance ρc (case (a) of figure 3.5). From equations 3.6 and 3.7, the anechoic calibration function $\hat{\Gamma}_A(\omega)$ is then obtained as:

$$\hat{\Gamma}_A(\omega) = \frac{\hat{P}}{\hat{V}} \cdot \frac{1}{\rho c} \tag{3.8}$$

and, together with K, can be applied to get the corrections to pressure and velocity in the frequency domain, especially in active fields.

3.2.2 Reactive Calibration

The reactive calibration method is based on the transmission line theory [8] where the reference impedance $\hat{Z}^0$ is modeled as the geometric mean between the theoretical closed-tube impedance $\hat{Z}^0_{oc}$ and the open-tube impedance $\hat{Z}^0_{sc}$, using respectively the setups shown as case (b) and (c) in figure 3.5[23]. Here, we take full advantage of the electrical analogy (Fig.3.6) where a closed tube corresponds to an open circuit, while an open one is analogous to a short circuit. In fact, as it can be demonstrated that, the geometric mean $\sqrt{\hat{Z}^0_{oc}\hat{Z}^0_{sc}}$ of these two reactive impedances is equal to the characteristic impedance ρc,(see [8, Eq. 1.07, p. 36]), i.e. $\sqrt{\hat{Z}^0_{oc}\hat{Z}^0_{sc}} = \rho c$. Thus, using this interesting energetic property of plane waves, the reactive calibration function $\hat{\Gamma}_R(\omega)$ can be calculated from equations 3.6 and 3.7 in a very similar way as in the first step, as follows :

$$\hat{\Gamma}_R(\omega) = \sqrt{\frac{\hat{Z}^m_{oc}}{\left[\hat{V}_{oc}\right]} \cdot \frac{\hat{P}_{sc}}{\left[\hat{V}_{sc}\right]}} \cdot \frac{1}{\rho c} \tag{3.9}$$

Clearly $\hat{\Gamma}_R$ is expected to operate the optimal correction to pressure and velocity in the frequency domain, when measures are executed in highly reactive field conditions.

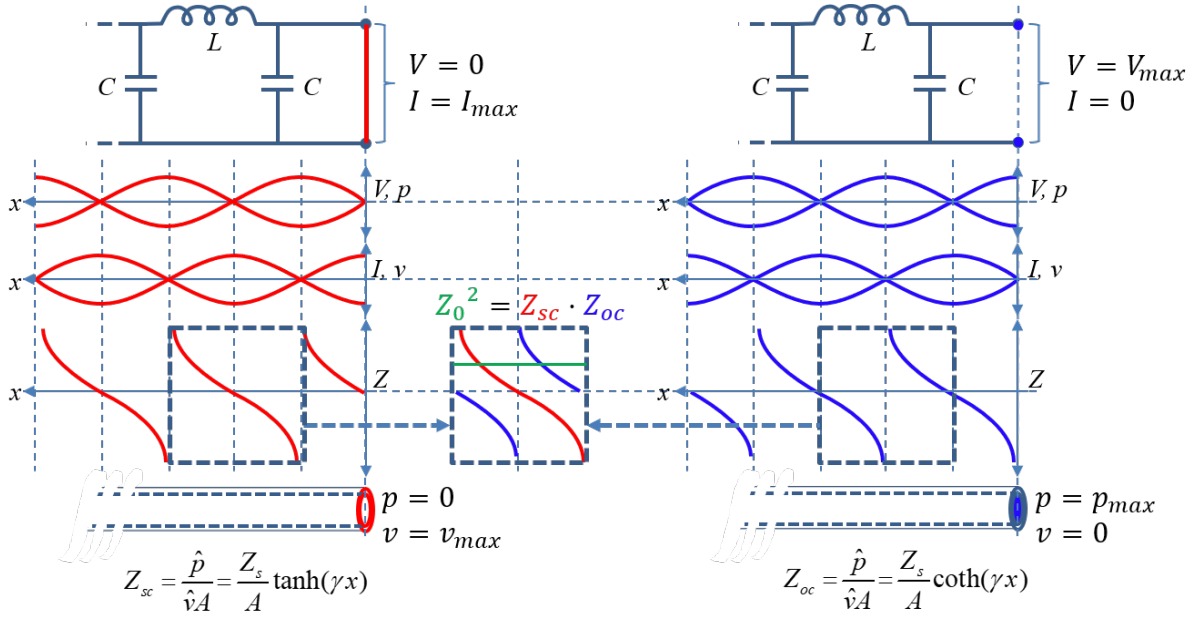

Figure 3.6: Electrical analogy. Open tube (red) and Closed tube (blue)

In general field conditions, anyway, a simple arithmetic average of $\hat{\Gamma}_A(\omega)$ and $\hat{\Gamma}_R(\omega)$ can be expected to work optimally. This expectation is confirmed in figure 3.7 where the comparison among correction functions K, $\hat{\Gamma}_A$, $\hat{\Gamma}_R$ and the average function $\hat{\Gamma}(\omega) = \left(\hat{\Gamma}_A(\omega) + \hat{\Gamma}_R(\omega)\right)/2$ obtained for an axial intensity probe under calibration in the facility of figure 3.5 is shown.

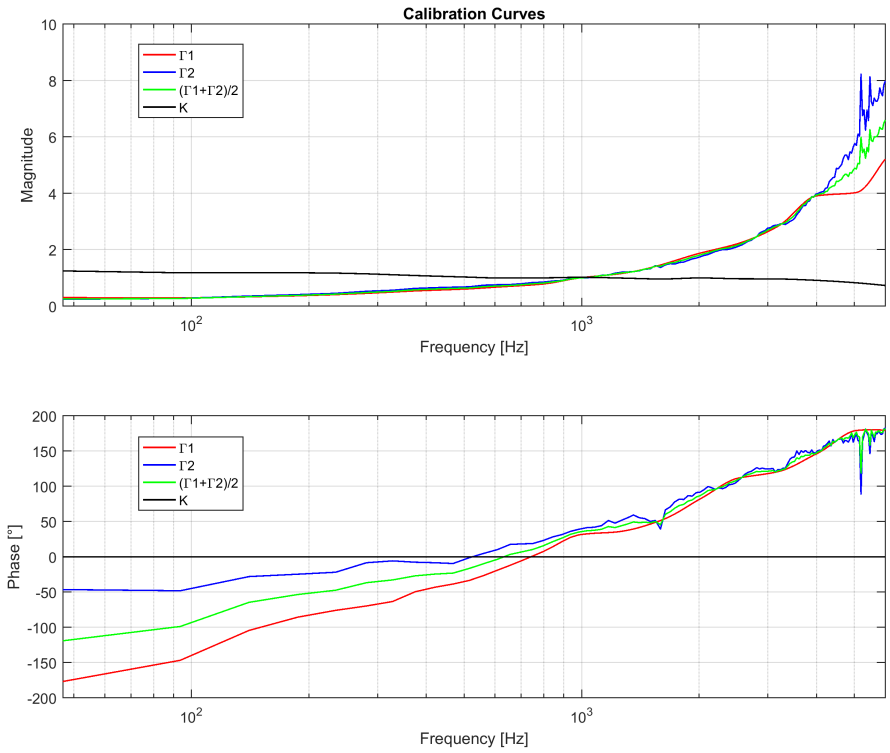

Figure 3.7: Comparison of correction functions K, $\hat{\Gamma}_A$, $\hat{\Gamma}_R$ and $\hat{\Gamma}(\omega) = \left(\hat{\Gamma}_A(\omega) + \hat{\Gamma}_R(\omega)\right)/2$ obtained for an axial pressure-velocity probes, using the active (red curves) and reactive (blue curves) calibration methods.

Chapter 4

MEASURING DEVICE AND MEASUREMENTS IN REAL ENVIRONMENTS

This chapter is devoted to the formulation of acoustic signal processing algorithms for measuring complex sound intensity [24], following the methodology defined in chapter 1. As it has been demonstrated in the first chapter, complex intensity can be calculated from a spectral equation (Eq.1.59) linking the active and reactive intensity, respectively, to the real and imaginary part of wave impedance, through a frequency dependent common factor given by the particle velocity auto-spectrum (energy-mass equation).

From the metrological and instrumental point of view, this means that complex sound intensity can be measured by means of usual dual-channel signal processing analyzers but finalized with appropriate algebraic operations in the frequency domain. The outline of a precision device able to measure both the active and reactive sound intensity will be reported in section 4.1. The calibration process described in section 3.2 is also included in the layout so as to make it immediately usable. A prototype implemented in a stand-alone hardware is shown in the appendix.

Finally, some measures made in a waveguide and in the squared tube will be shown in sections 4.2 and 4.3 respectively.

4.1 Algorithm for Measuring Complex Sound Intensity and its Flowchart

Now, the measuring device algorithm for calculating complex sound intensity from wave impedance and velocity autospectrum will be herein reported, based on fundamentals exposed in chapter 1.

As shown in section 1.5, the acoustic energy-mass equation (Eq.1.59) at any point $\boldsymbol{x}$ of a general field can be expressed in terms of components

$$\hat{S}_i(\boldsymbol{x},\omega) = \hat{Z}_i\left(\boldsymbol{x},\omega\right)\left|\hat{V}_i\left(\boldsymbol{x},\omega\right)\right|^2 \tag{4.1}$$

where the three wave impedances $\hat{Z}_i(\omega)$ and the particle velocity autospectra $\left|\hat{V}_i(\omega)\right|^2 = \hat{V}_i\left(\hat{V}_i\right)^*$ are measured in the orthonormal basis $\boldsymbol{e}_{i=x,y,z}$ spanning the active intensity vector

field [1].

The same equation can be written in a simpler manner, in terms of the *wave admittance vector* ([15, footnote on p. 153]). This can be defined as a complex vector quantity

$$\hat{\boldsymbol{Y}}(\omega) \coloneqq \frac{\mathscr{F}[v_i(\boldsymbol{x},t)]}{\mathscr{F}[p(\boldsymbol{x},t)]} \equiv \frac{\hat{V}_i(\boldsymbol{x},\omega)}{\hat{P}(\boldsymbol{x},\omega)} = G_i(\boldsymbol{x},\omega) + i\,B_i(\boldsymbol{x},\omega)$$

obtained from the complex ratio of the Fourier-transformed components $\hat{V}_i(\boldsymbol{x},\omega)$ of $v_i(t) = \boldsymbol{v}\cdot\boldsymbol{e}_i$ at $\boldsymbol{x}$, to the common pressure $\hat{P}(\boldsymbol{x},\omega)$. The energy-mass equation then becomes:

$$\hat{S}_i(\omega) \coloneqq I_i(\omega) + i\,[Q_T]_i(\omega) = \bar{Y}_i(\omega)\left|\bar{P}(\omega)\right|^2 \tag{4.2}$$

where the complex intensity spectrum $\hat{\boldsymbol{S}}(\omega)$, defined in terms of the spectral components of active and reactive intensities $I_i(\omega)$ and $[Q_T]_i(\omega)$, is now obtained from the pressure autospectrum $\left|\bar{P}(\omega)\right|^2$ and the real and imaginary parts $G_i(\omega)$ and $B_i(\omega)$ (respectively called conductance and susceptance) of the wave admittance vector components, measured at the same point $\boldsymbol{x}$.

However, a lot of care must be taken when calculating the reactive intensity spectral components $[Q_T]_i(\omega)$. In fact, these components result from the application of the reactivity tensor $\mathbb{Q}(\boldsymbol{x},\omega)$ to the unit vector $\boldsymbol{T}(\boldsymbol{x},\omega_n) = \boldsymbol{I}(\boldsymbol{x},\omega_n)\cdot|\boldsymbol{I}(\boldsymbol{x},\omega_n)|^{-1}$ defining the direction of the spectral active intensity $\boldsymbol{I}(\boldsymbol{x},\omega_n)$ and, to make matters worse, a diagonalization process is required for computing the reactivity tensor as $\mathsf{Q}(\boldsymbol{x},\omega) = \sqrt{\mathsf{Q}^2(\boldsymbol{x},\omega)}$ for each frequency. Fortunately enough, the diagonalization process of $\mathsf{Q}(\boldsymbol{x},\omega)$ is embedded in the matrix square root routines [25] implemented in the Matlab code, used here for developing the complete measuring device algorithm.

To be operational since the beginning, the expression of $\mathbb{Q}^2(\boldsymbol{x},\omega)$ can be written down, in agreement with 4.2, as

$$\left[\mathbb{Q}^2(\omega)\right]_{ij} \coloneqq B_i(\omega)\left|\hat{P}(\omega)\right|^2 \cdot B_j(\omega)\left|\bar{P}(\omega)\right|^2 \tag{4.3}$$

where $B(\omega)$ is the susceptance and $\left|\hat{P}(\omega)\right|^2$ is the pressure autospectrum. Then, the matrix square root $\sqrt{\mathbb{Q}^2(\omega)}$ is calculated for each frequency component, to obtain the spectral reactivity tensor $\mathbb{Q}(\boldsymbol{x},\omega) = \sqrt{\mathbb{Q}^2(\boldsymbol{x},\omega)}$. Once $\mathbb{Q}(\boldsymbol{x},\omega)$ has been calculated, the spectral reactive intensity vector $\boldsymbol{Q}_T(\omega)$ is readily obtained as

$$\boldsymbol{Q}_T(\omega) \coloneqq \mathbb{Q}(\omega)\,\boldsymbol{T}(\omega)\ . \tag{4.4}$$

After this operative preamble, the complete verbal algorithm for a possible measuring device of the 3D complex intensity can be stated as follows:

1. Capture the rough pressure and velocity signals $p^m(t)$ and $v_i^m(t)$ respectively, using a 3D intensimetric probe at point $\boldsymbol{x}$ in an arbitrary orthonormal basis $\boldsymbol{e}_{i=x,y,z}$.

2. Transform these four signals into the frequency domain to obtain $\hat{P}^m(\omega)$ and $\hat{V}_i^m(\omega)$.

3. Obtain the correct spectra $\hat{P}(\omega)$ and $\hat{V}_i(\omega)$ by applying the calibration functions $K(\omega)$ and $\hat{\Gamma}_i(\omega)$ in the frequency domain.

[1] The subscript i-th must not be confused with $i = \sqrt{-1}$, which represents the imaginary part component

4. Calculate the complex admittance vector $\hat{Y}_i(\omega)$.
5. Calculate the pressure and velocity autospectra $\left|\hat{P}(\omega)\right|^2$ and $\left|\hat{V}_k(\omega)\right|^2$.
6. Calculate the spectral components of active intensity $I_i(\boldsymbol{x},\omega)$ from equation 4.2.
7. Calculate the frequency overall magnitude of active Intensity $I_i(\boldsymbol{x}) = \sum_{\omega} I_i(\boldsymbol{x},\omega)$.
8. Calculate the spectral reactivity tensor $\mathbb{Q}_{ij}(\boldsymbol{x},\omega)$.
9. Calculate the spectral components of reactive intensity $[Q_T(\boldsymbol{x},\omega)]_i$.
10. Calculate the total reactivity $Q(\boldsymbol{x})$.

$$Q(\boldsymbol{x}) = \sqrt{\langle p^2\rangle \langle \boldsymbol{v}^2\rangle - I^2} = \sqrt{\sum_{i=x,y,z}\left[\sum_{\omega}\left|\hat{P}(\boldsymbol{x},\omega)\right|^2 \cdot \sum_{\omega}\left|\hat{V}_i(\boldsymbol{x},\omega)\right|^2 - \left(\sum_{\omega} I_i(\boldsymbol{x},\omega)\right)^2\right]}.$$

The flowchart of the algorithm above is shown in figure 4.1.

4.1.1 Flowchart

The diagram is separated in four sectors: I, II, III, IV. The first one is the device input and consists in the acquisition and conditioning of the signals captured by the 3D sound intensity probe. The output from this sector is made up by four spectral arrays calibrated in magnitude and phase. The spectrum of complex intensity is calculated in the second sector, while the third sector implements the device displayed output. The special sector IV is devoted to execute calibration tasks before starting the measurement session. Each of these sectors will be detailed below.

4.1.1.1 Flowchart: Sector I

As shown in figure 4.1, the signals are captured by a 3D sound intensity probe using an analog-to-digital converter and then processed through the FFT algorithm with spectral resolution Δn. The four spectral arrays ($n = 1, .., N$) are then calibrated in the calibration block implementing the following equations:

$$\begin{aligned} \hat{P}(\omega_n) &= \hat{P}^m(\omega_n)\cdot K(\omega_n) \\ \hat{V}_i(\omega_n) &= \hat{V}_i^m(\omega_n)\cdot K(\omega_n)\cdot \hat{\Gamma}_i(\omega_n)\ . \end{aligned} \tag{4.5}$$

The calibration functions K and $\hat{\boldsymbol{\Gamma}}$ in equations 4.5 are retrieved from the Memory CAL block where the linear combiner is used to combine $\hat{\boldsymbol{\Gamma}}_A$ and $\hat{\boldsymbol{\Gamma}}_R$ depending on the field conditions according the equation $\hat{\boldsymbol{\Gamma}} = \hat{\boldsymbol{\Gamma}}_A \cdot r + \hat{\boldsymbol{\Gamma}}_R \cdot (1-r)\ ;\ 0 \leqslant r \leqslant 1$, where $r = 0$ is used in the anechoic field situations and $r = 1$ stands for purely reactive fields.

The calibration operations to obtain K and $\hat{\boldsymbol{\Gamma}}$ will be detailed in subsection 4.1.1.4.

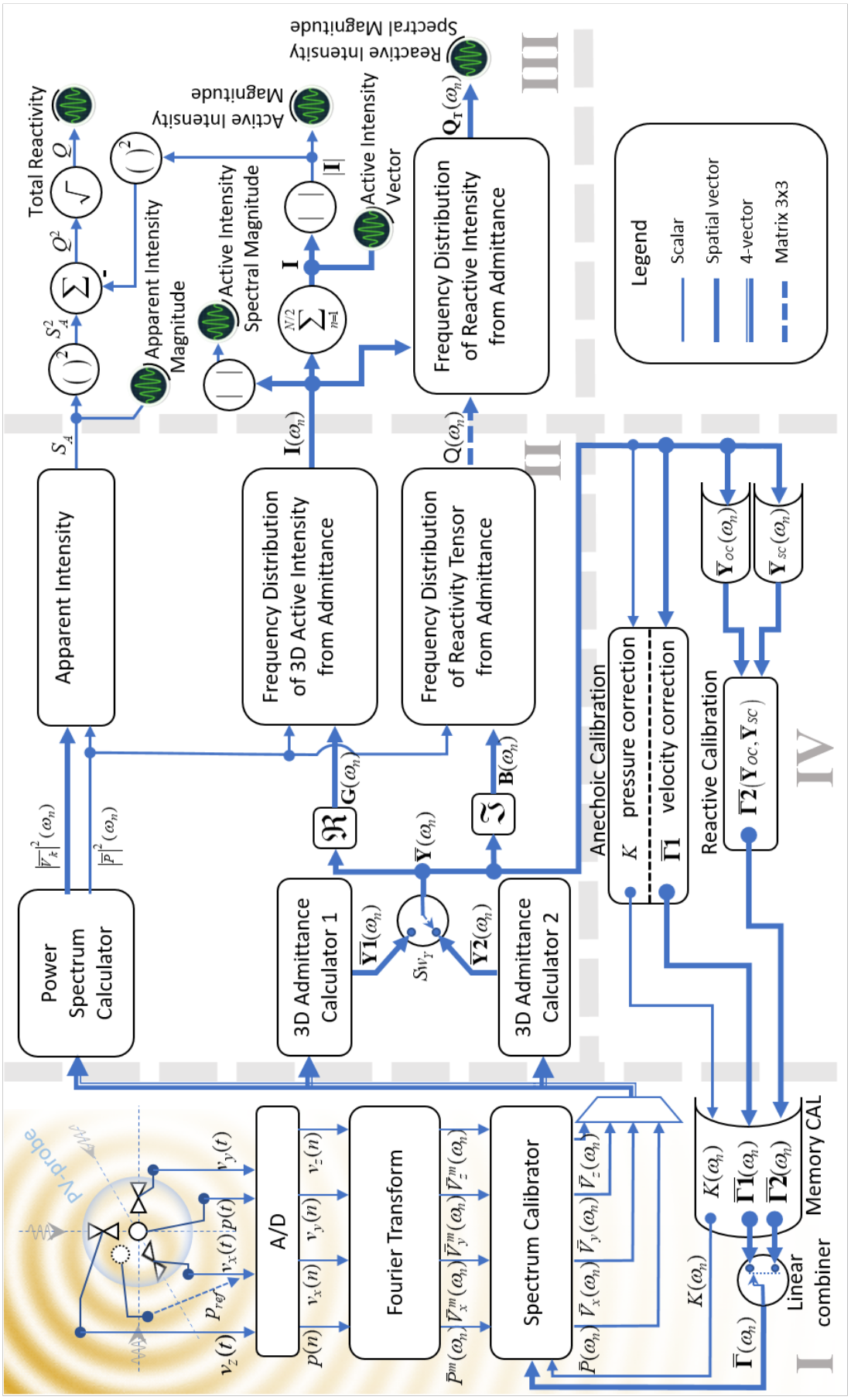

Figure 4.1: Flowchart of a precision device for measuring the 3D complex intensity from wave admittance.

4.1.1.2 Flowchart: Sector II

On the left side of sector II, three main blocks are shown.

In the first block from the top, the power spectra of the pressure and the velocity components are calculated as shown below:

$$\left|\hat{P}(\omega_n)\right|^2 = \hat{P}(\omega_n)\hat{P}^*(\omega_n); \quad \left|\hat{V}_i(\omega_n)\right|^2 = \hat{V}_i(\omega_n)\hat{V}_i^*(\omega_n); \tag{4.6}$$

In the second and third block from the top, the vector wave admittance $\hat{\boldsymbol{Y}}\,(\omega_n)$ is computed using the auto and cross spectra of pressure and velocity following the two different procedures [26] shown in formulas 4.7 and 4.8. The switch Sw_Y is used to choose the mode in which the admittance calculation is made, according to signal/noise ratio levels between pressure and velocity signals. The expression 4.7 is used when the SNR level of velocity signal is higher than the one of the pressure signal, however, when vice-versa, the expression 4.8 is used [27].

$$\hat{\boldsymbol{Y}}1(\omega_n) = \frac{\hat{V}_i\hat{V}_i^*}{\hat{P}\hat{V}_i^*}; \tag{4.7}$$

$$\hat{\boldsymbol{Y}}2(\omega_n) = \frac{\hat{V}_i\hat{P}^*}{\hat{P}\hat{P}^*}\ . \tag{4.8}$$

The output from switch Sw_Y is in any case the optimized admittance $\hat{\boldsymbol{Y}}\,(\omega_n)$ ready for the next calculations based on energy-mass expression 1.63.

The spectrum of the active intensity and spectral reactivity tensor are then calculated in the the two blocks on the right side of sector II. The first one is calculated using the following expression, where $G(\omega_n)$ is the real part of the admittance (conductance):

$$I_i(\omega_n) = G_i\,(\omega_n)\left|\hat{P}\,(\omega_n)\right|^2\ . \tag{4.9}$$

The spectral reactivity tensor is calculated from the susceptance $B\,(\omega_n)$ and the autospectrum of pressure $\left|\hat{P}\,(\omega_n)\right|^2$ where each element of the squared tensor is obtained by using the expression shown in 4.3, and then the matrix square root process has to be applied to obtain $\mathbb{Q}\,(\omega_n)$.

On the top-right of sector II, the apparent intensity S_A is defined in terms of its components $[S_A]_i \coloneqq \sqrt{\langle p^2(t)\rangle\,\langle v_i^2(t)\rangle}$. This definition, can be calculated in the frequency domain using the energy relationship $\langle x^2(t)\rangle = \int |X|^2\,(\omega)\cdot d\omega$ (see ref. [28, eq. 2.74, p. 46]), so the apparent intensity components can be calculated from pressure and velocity spectra as:

$$S_A \coloneqq \sqrt{\langle p^2\rangle\,\langle \boldsymbol{v}^2\rangle} = \sqrt{S_x^2 + S_y^2 + S_z^2} \tag{4.10}$$

$$[S_A]_i \coloneqq \sqrt{\langle p^2(t)\rangle\,\langle v_i^2(t)\rangle} \equiv \sqrt{\sum_{n=0}^{N/2}\left|\hat{P}(\omega_n)\right|^2 \cdot \sum_{n=0}^{N/2}\left|\hat{V}_i(\omega_n)\right|^2}\ . \tag{4.11}$$

4.1.1.3 Flowchart: Sector III

The device display output is implemented in the third sector.

The magnitude of the time-independent apparent intensity is computed from its components given in equation 4.11 so to obtain $S_A \coloneqq \sqrt{\langle p^2 \rangle \, \langle \boldsymbol{v}^2 \rangle}$ from Eq. 4.10.

The frequency distribution of the active intensity $\boldsymbol{I}(\omega_n)$ has been already calculated in the sector II through equation 4.9, while the frequency distribution of the reactive intensity $\boldsymbol{Q_T}(\omega_n)$ is obtained simply by applying, frequency by frequency, the spectral reactivity tensor $\mathbb{Q}\,(\boldsymbol{x}, \omega)$ to the unit vector $\boldsymbol{T}(\boldsymbol{x}, \omega_n) = \boldsymbol{I}(\boldsymbol{x}, \omega_n) \cdot |\boldsymbol{I}(\boldsymbol{x}, \omega_n)|^{-1}$ as shown in equation 4.4.

The time-independent active intensity vector and its magnitude are computed directly from the spectral components:

$$I_i = \sum_{n=0}^{N/2} I_i(\omega_n); \qquad |\boldsymbol{I}| = \sqrt{I_x^2 + I_y^2 + I_z^2}\,, \tag{4.12}$$

and the time independent reactive intensity magnitude is calculated from the following expression:

$$Q = \sqrt{S_A^2 - \boldsymbol{I}^2}\ . \tag{4.13}$$

4.1.1.4 Flowchart: Sector IV

Sector IV of figure 4.1 shows how to implement a possible calibration mode for the device.

A sequence of tasks and measures have to be carried out by the device's operator in order to obtain the calibration functions $\hat{\boldsymbol{\Gamma}}_A$ and $\hat{\boldsymbol{\Gamma}}_R$.

Sector IV is mainly composed by two memory blocks and two calibration blocks called *active* and *reactive* calibration. The output from sector IV is connected to the memory CAL block in sector I.

When the device is not yet calibrated, functions K, $\hat{\boldsymbol{\Gamma}}_A$ and $\hat{\boldsymbol{\Gamma}}_R$ are initialized to 1, and the following sequence has to be processed for each component:

1. Put the wave-guide in anechoic configuration while the device is standing for the confirmation that setup is ready.

2. The process starts by calculating the correction function K of Eq.3.6 from signals p_{ref} and p^m captured respectively by a reference microphone and the microphone of the probe under calibration in the anechoic wave-guide which is excited for instance with white noise. Computations are executed through the Admittance Calculator blocks in sector II simply by feeding the $\hat{V}_x$ channel with P_{ref}.

3. Calculate the functions $\hat{\boldsymbol{\Gamma}}_A$ of equation 1 from signals p^m, v_x^m, v_y^m, and v_z^m captured with configuration of step 1, using the 3D Admittance Calculator blocks.

4. Save K and $\hat{\boldsymbol{\Gamma}}_A$ in the Memory CAL block of sector I, for later use as optimal identity calibration of the probe in *active* field conditions.

5. Put the wave-guide in closed tube configuration while the device is standing for the confirmation that setup is ready;
6. When ready, measure the closed tube (Open Circuit) admittance components $\left[\hat{Y}_{oc}^{m}\right]_{i}$ and store them for later use in step 9, to calculate the second (reactive) calibration $\hat{\mathbf{\Gamma}}_{R}$.
7. Put the waveguide in open tube configuration while the device is standing for the confirmation that setup is ready.
8. When ready, measure the open tube (Short Circuit) admittance components $\left[\hat{Y}_{sc}^{m}\right]_{k}$ and stack them for later use in step 9 together with $\left[\hat{Y}_{oc}^{m}\right]_{k}$ as supplement data to calculate $\hat{\mathbf{\Gamma}}_{R}$.
9. Calculate the functions $\hat{\mathbf{\Gamma}}_{R}$ of equation 3.9 from $1/\left[\hat{Y}_{oc}^{m}\right]_{k}$ and $1/\left[\hat{Y}_{sc}^{m}\right]_{k}$ previously stored in steps 6 and 8 and save them for later use as optimal identity calibration of the probe in *reactive* field conditions.
10. Calculate the average correction function $\hat{\mathbf{\Gamma}}$ from a linear combination of $\hat{\mathbf{\Gamma}}_{A}$ and $\hat{\mathbf{\Gamma}}_{R}$ to optimize the calibration error in general fields.

4.2 Measurements in a Waveguide

In order to test the algorithm shown above and to verify the fundamentals described in chapter 1 in real fields, some measurements taken into the waveguide in three different conditions will be exposed in this section. Furthermore, the two calibration methods obtained in anechoic and reactive fields will be used in order to compare both in different situations.

The measuring setup is shown in Fig.4.2 and consists of a waveguide of forty meters long, which is excited with a loudspeaker. The junction between the loudspeaker and the waveguide is made through a trombone which acts as an impedance adapter. The waveguide has a segment of five meters long with twenty-four measuring points separated by twenty centimeters each, where the first hole is at six meters from the source. After the measuring segment, the waveguide can be opened or closed at eleven meters of the source, with the purpose of changing the acoustic field into the tube.

The loudspeaker is excited by a power amplifier which receives the audio signal from the computer through an A/D converter (National Instruments). In the three cases, the waveguide is excited with white noise and the signal processing is made in octave bands .

The measurements are taken with a Microflown probe PTN0-700649, which is connected to the sound card through the signal conditioner. For each case, active and reactive calibrations are used.

The measurement software was programmed in Matlab(TM) following the algorithm described in section 4.1.

4.2.1 Anechoic Waveguide

In the anechoic setup, the waveguide is forty meters long to avoid the regressive waves influence. In this situation, the sound field approximates to a plane progressive wave, where the energy speed and the active intensity are maximum and the reactivity is ideally equal to zero.

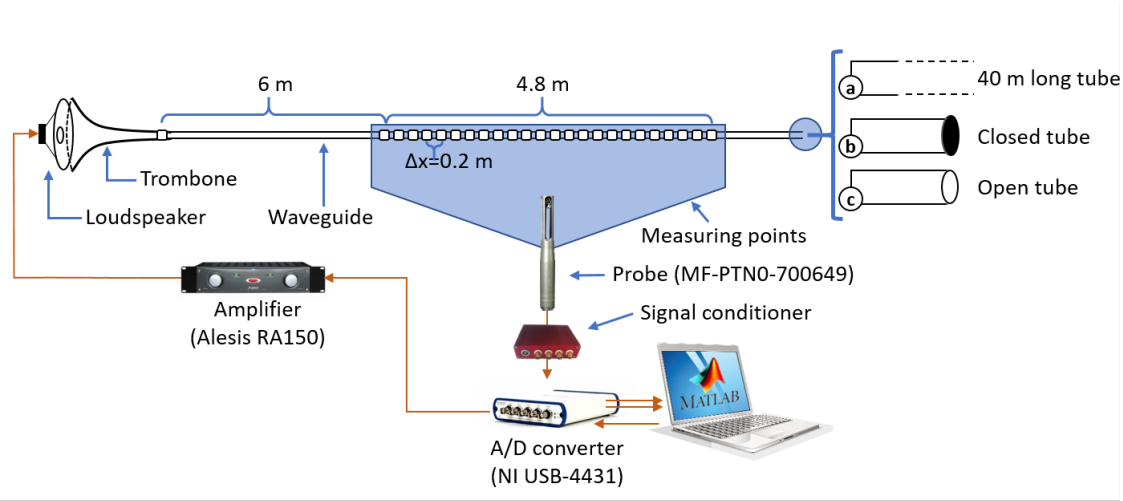

Figure 4.2: Waveguide Measurement Setup.

As shown in Fig.4.3 a similar situation occurs in the plots: η is constant and near to 1, and active intensity is $10\,dB$ biggest than total reactivity, and both have a negative slope due to the attenuation.

In fact, in this case, the measurement setup is very similar to the calibration setup, therefore, clearly the results should be good, because this was an imposed condition in the calibration process.

If we look carefully at the energy speed plot, the frequencies where the energy flows more quickly are the middle frequencies (in green).

This behavior is not expected because the high frequencies must be quicker than the low frequencies.

Let us now see what happens when the reactive calibration is used in the anechoic waveguide.

Looking at Fig.4.4, the energy speeds for each frequency band are correctly sorted (low frequencies are slower than high frequencies), which means that the field is more reactive for the low frequency.

Also here, the active and reactive intensities have a negative slope for each octave band due to the attenuation, but now the reactivity has been increased for the low frequencies.

If we observe the simulation results for the spherical divergent wave in Fig.2.4, we find that in the near field, active and reactive intensities have similar values, but the reactive intensity decreases more rapidly than the active intensity.

Comparing the simulation and the real results, we find that behavior also happens in the experimental situation, where the difference between active and reactive intensities increases with the frequency.

Therefore, we can say that the anechoic waveguide is more similar to a radius of a sphere and the most suitable model for the anechoic waveguide is the divergent spherical wave.

We can thus state that the most precise calibration method is the reactive method.

4.2.2 Open and Closed Waveguide

Now the measures are made in two extreme conditions of the wave guide: open tube and closed tube. Also, active and reactive calibration are used, and the plots show the speed of energy normalized to c, active intensity and total reactivity.

The Fig.4.5 and 4.6 show the results for the closed waveguide using the anechoic and reactive calibration respectively, while the Fig.4.7 and 4.8 show the results for the open

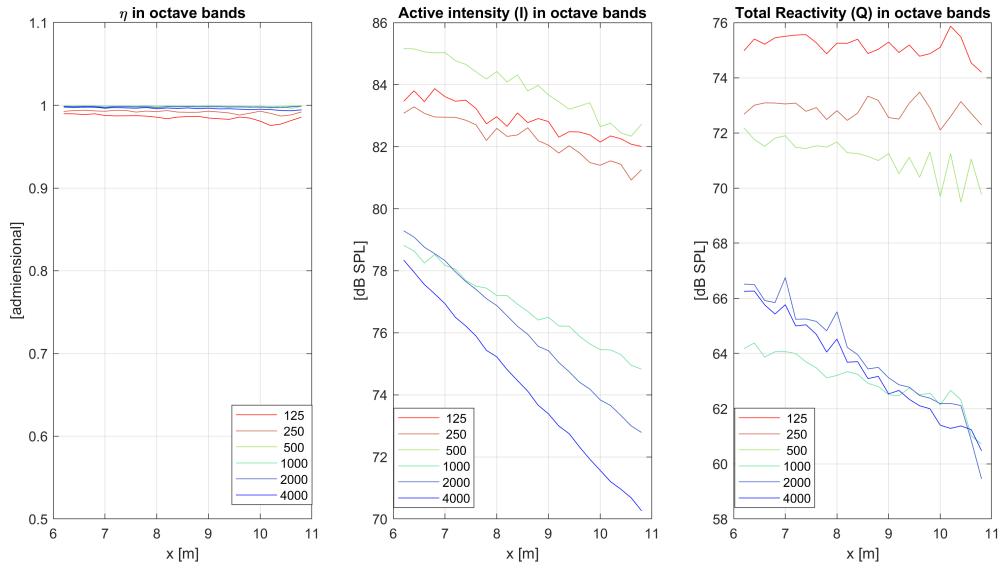

Figure 4.3: Anechoic Waveguide (anechoic calibration): a) c-normalized speed of the energy particle, b) active intensity, c) total reactivity. Low frequencies in red, medium frequencies in green, high frequencies in blue.

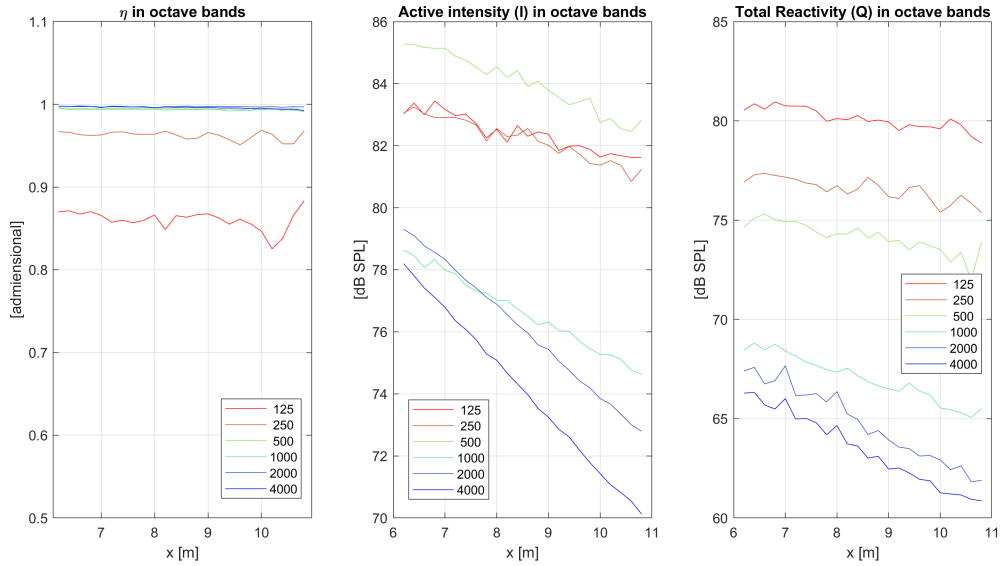

Figure 4.4: Anechoic Waveguide (reactive calibration): a) c-normalized speed of the energy particle, b) active intensity, c) total reactivity. Low frequencies in red, medium frequencies in green, high frequencies in blue.

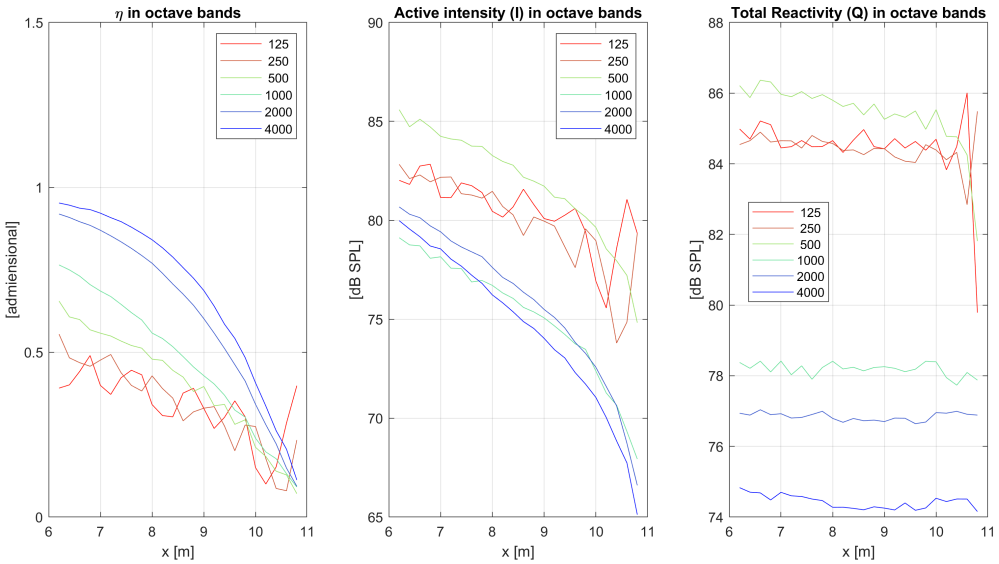

Figure 4.5: Closed Waveguide (anechoic calibration): a) c-normalized speed of the energy particle, b) active intensity, c) total reactivity. Low frequencies in red, medium frequencies in green, high frequencies in blue.

waveguide for the two calibrations.

There are no significant differences in the four figures. Here, the speed of energy decreases when the energy is arriving to the end of the tube. Also, the active intensity has a negative slope due to the attenuation, while the total reactivity is approximately constant.

When comparing the measurement results with the simulation results for the quasi-stationary wave (Fig.2.8), it is possible to see a similar behavior; the only difference is that in the model the attenuation is not considered.

4.3 Measurements in a Square Tube

In this section, measurements made into a square tube of section equal to $28\,cm$ are taken in order to test the algorithm in a 3-D environment.

The measurement setup is shown in Fig.4.9 which is composed by a four-meter-long squared rigid tube and the side equals to twenty eight centimeters. The frequency cut-off is equal to $600\,Hz$. The sound field is generated by a loudspeaker placed in one of the extremes of the tube and a reflective surface is positioned in the opposite extreme. The sound field is measured with a 3-D p-v probe placed at $1.5\,m$ from the source.

The first test consists of examining the directionality of a 3-D sound intensity probe by measuring the direction of the active intensity.

Thus, two clusters are used as an excitation signal: below and above cut-off frequency.

The results are shown in Fig.4.10, the active intensity is plotted on the left for the low cluster and on the right for the high cluster. As it is clearly shown, in the low cluster, the arrows for each frequency are oriented in the same direction along the tube, while for the high cluster, the arrows have different directions. This is due to the transversal components that appear upon the cut-off frequency. Therefore, it is possible to measure the spread effect of the active intensity for each frequency component.

The second test is to measure the active and reactive intensity spectra in two different reflective surfaces: foam rubber and plaster.

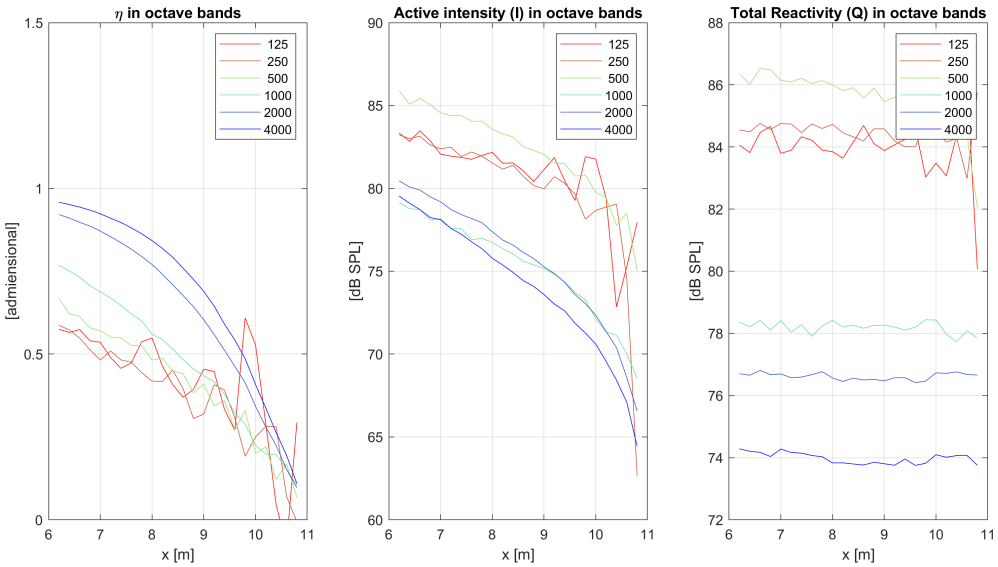

Figure 4.6: Closed Waveguide (reactive calibration): a) c-normalized speed of the energy particle, b) active intensity, c) total reactivity. Low frequencies in red, medium frequencies in green, high frequencies in blue.

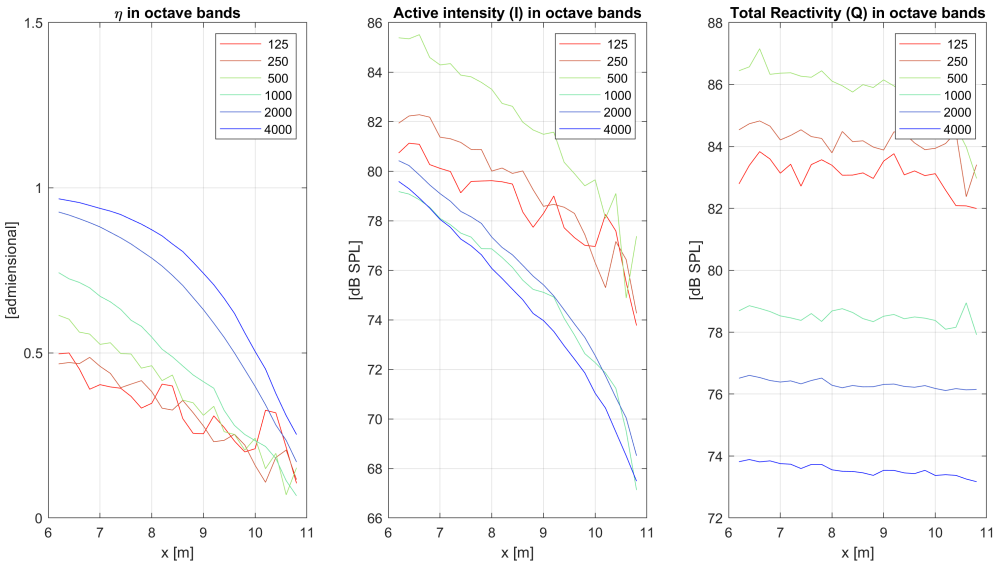

Figure 4.7: Open Waveguide (anechoic calibration): a) c-normalized speed of the energy particle, b) active intensity, c) total reactivity. Low frequencies in red, medium frequencies in green, high frequencies in blue.

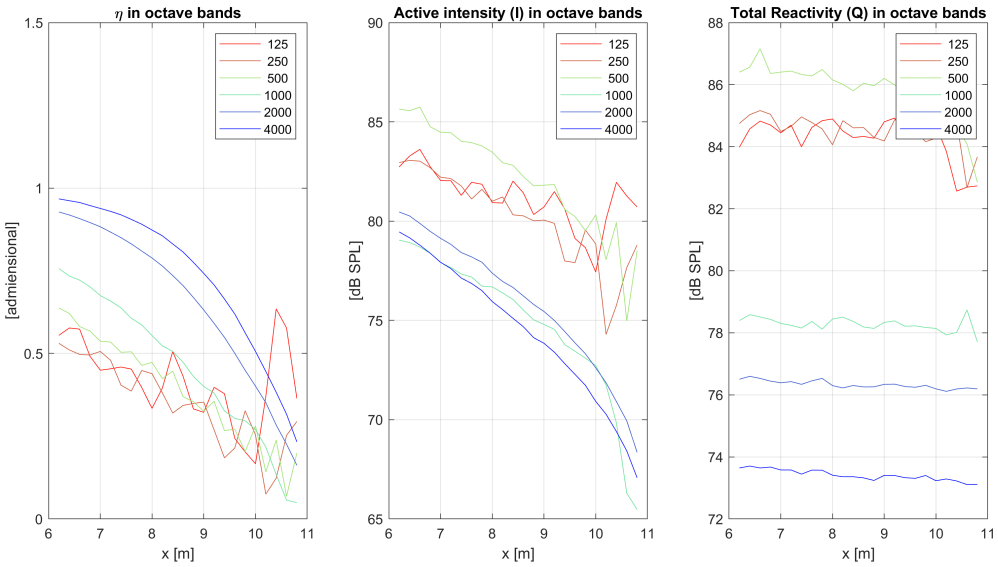

Figure 4.8: Open Waveguide (reactive calibration): a) c-normalized speed of the energy particle, b) active intensity, c) total reactivity. Low frequencies in red, medium frequencies in green, high frequencies in blue.

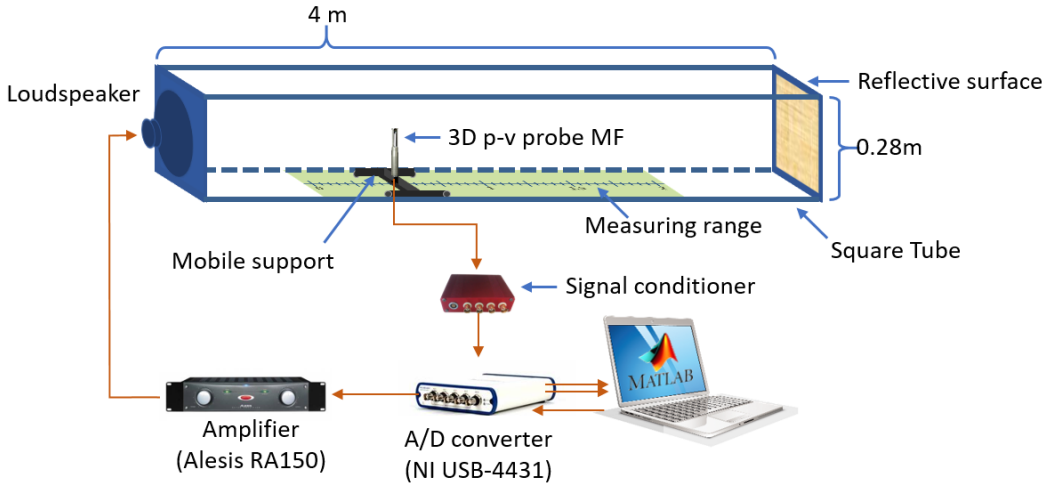

Figure 4.9: Square Tube Measurement Setup

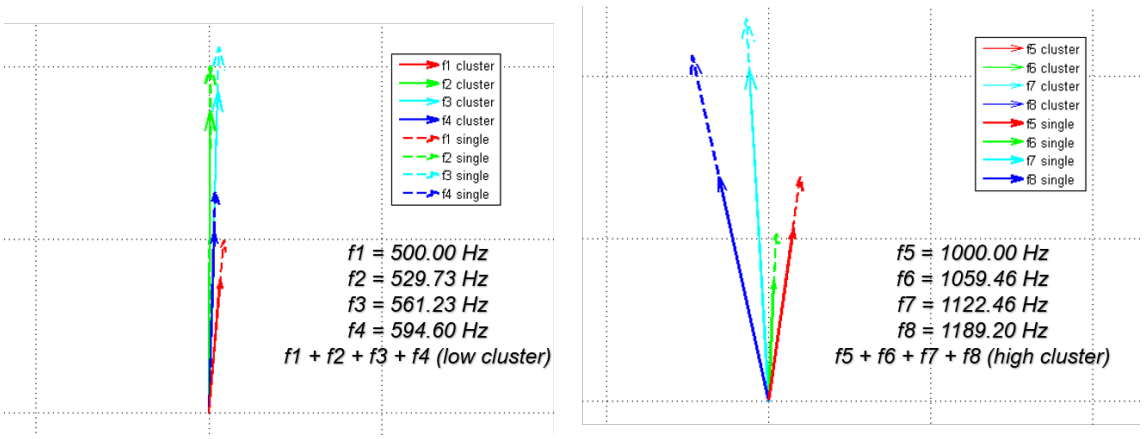

Figure 4.10: Spread Effect. Low Cluster on the Left. High Cluster on the Right

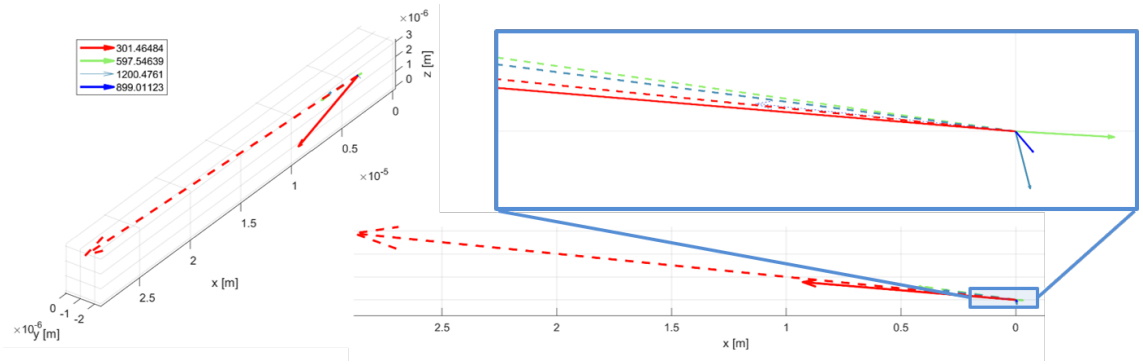

Figure 4.11: Foam Rubber Case. Spectral complex sound intensity: active intensity (dashed) and reactive intensity (solid). Low frequencies in red, medium frequencies in green, high frequencies in blue.

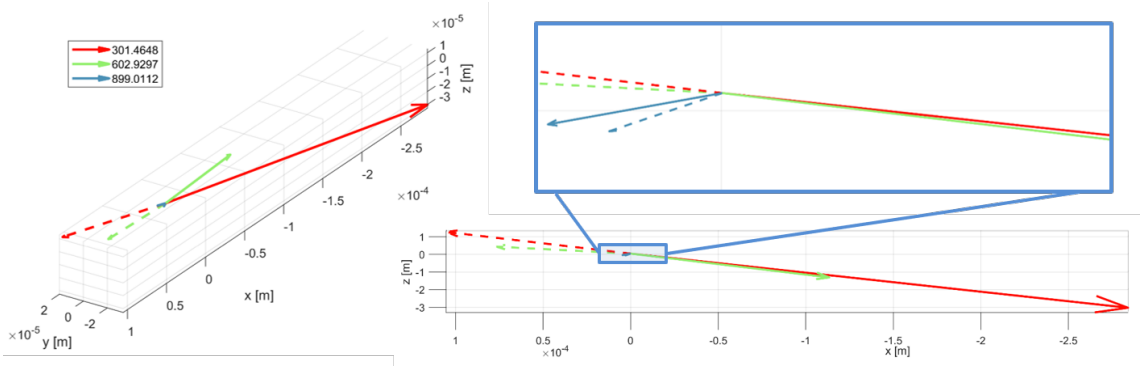

Figure 4.12: Plaster Case. Spectral complex sound intensity: active intensity (dashed) and reactive intensity (solid). Low frequencies in red, medium frequencies in green, high frequencies in blue.

The sound field is generated by one cluster composed of four frequencies below and above the cut-off frequency.

In the foam rubber case (Fig.4.11), the active intensity (dashed arrows) is predominant for all frequencies in the direction of the reflective surface. This is due to the foam rubber being a good energy absorber, so the energy flows from the loudspeaker to the foam rubber easily.

In the plaster case (Fig.4.12), the reactive intensity is bigger than the active intensity. This is due to the plaster reflecting more energy than the foam rubber, therefore, the active intensity is weaker than reactive intensity.

Thus, we can conclude that the algorithm proposed here allows measuring the complex sound intensity in different acoustic fields for each frequency component.

Chapter 5

TYMPANOMETRIC APPLICATION

The purpose of this chapter is to describe the methods used for the execution of a prototype probe for measuring the acoustic admittance into the human ear canal in the frequency range $100 - 5000\,Hz$.

This chapter describes the acoustic fundamentals to develop an electroacoustic system for clinical audiological uses based on an acoustic impedance probe.

The measurement process, performed with the previously calibrated probe, involves the synthesis of a sound stimulus sent to the patient's external ear canal and the simultaneous recording of the two acoustic signals coming from the probe. This process is run by a computer (through an A/D converter) which processes all algorithms necessary for the acoustic identification of the system under analysis. The results are visualized in standard plots of acoustic impedance/admittance in the complex forms. In Fig.5.1 a general diagram of the complete system is shown.

5.1 Physical Fundamentals

In this section, the physicals bases for the clinical audiometric device are explained in order to understand the working principle described in the next section [29].

5.1.1 Wave Impedance: Acoustic Resistance, Inertance and Compliance

As it was defined in the subsection 1.2.1 the acoustic impedance is the time independent quotient of the complex sound pressure and complex particle velocity. This relationship also represents the transfer function of the acoustic system, which describes the behavior of the acoustic field when the system is perturbed.

The acoustic system into the ear canal can be simplified by measuring just a single spatial component of the particle velocity, since the vibrations occur only along the ear canal. This simplification allows to introduce the concept of acoustic impedance to study the vibration mechanism of air inside a "compact" cylinder, which is a tube with a length $L \ll \lambda_{min}$ where λ_{min} indicates the shorter wavelength of the sound that causes the air particle vibration.

There are three physical causes that contribute to oppose the motion of the air particle: friction, inertia and elasticity of the air. These three properties of air are respectively referred in acoustics as: resistance, inertance and compliance. The first one constitutes the real part of the impedance, while the algebraic sum of the other two constitutes its imaginary part also called reactance.

The acoustic impedance is therefore the complex quantity that, for each single frequency, regulates the vibratory motion of the any compact air particle when it is crossed by a sound

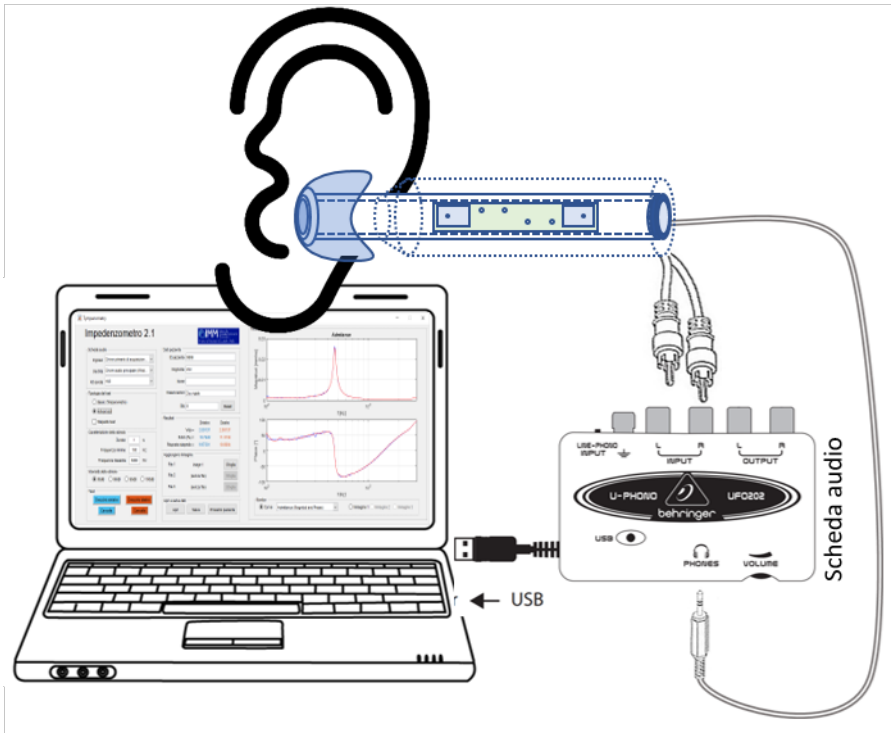

Figure 5.1: General Diagram of the Complete System.

wave.

5.1.2 Helmholtz Resonator

We now study an acoustic phenomenon of easy practical experimentation: the Helmholtz resonator [15].

As shown in the Fig.5.2, its operating principle is analogous to the mass-spring system, which translates into acoustics with the inertance and compliance parameters. The action of blowing in the "bottle neck" generates the sound pressure necessary to excite the resonance.

This virtuous mechanism is established only when the force that accelerates the mass of air contained in the neck of the bottle is exactly balanced, in every instant of the cycle of oscillation, by the elastic restoring force of the volume of air contained within it.

In practice, among all the possible circular frequencies ω by which the inertance and compliance system can oscillate, there is only one frequency that allows this perfect cooperation of forces: the natural frequency of the system. This circular frequency which will be shown in the following equation with ω_0 characterizes the vibration mode of the system and it is easily quantifiable in terms of the parameters of inertance M and acoustic compliance C with the following equation:

$$\omega_0 = \frac{1}{\sqrt{MC}}\,. \tag{5.1}$$

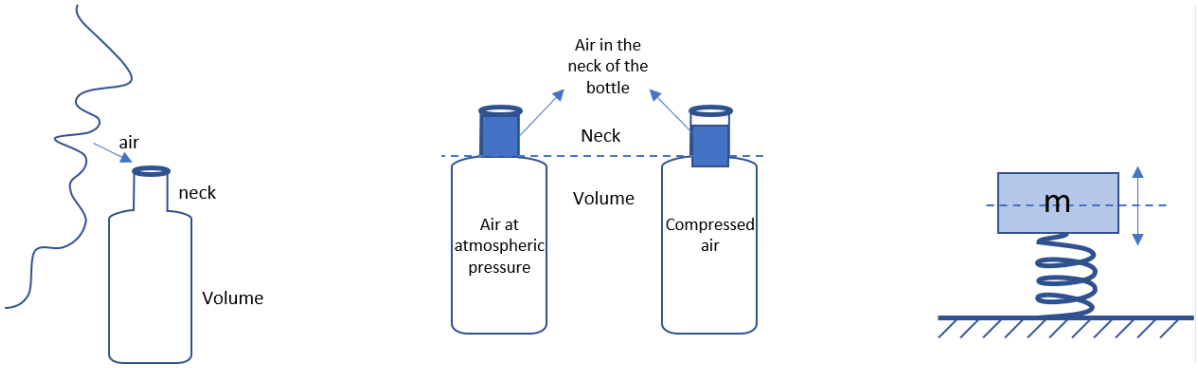

Figure 5.2: Working Principle of the Helmholtz Resonator.[2]

5.1.3 Quality Factor and Acoustic Resistance

The mass-spring resonance model described in the previous paragraph provides that, once activated the oscillating motion at the natural frequency ω_0 , it never stops, i.e. that the mechanism is able to self-feed even in the absence of an external force. This is clearly an ideal behavior that, when in the absence of external force, the amplitude of the oscillation would remain constant over time.

This behavior can be quantified by introducing the concept of damping into the analysis of the oscillatory motion. The damping is physically represented by a force which (unlike those related to inertance and compliance) is always opposed to the oscillatory motion in every moment of the cycle, with the effect of continuously subtracting energy from the oscillating system. In fact, if the stationary average acoustic energy density of the oscillating system is indicated with $\langle w \rangle$, the damping parameter (energy decay constant) is defined by

$$\Omega \approx -\frac{1}{\langle w \rangle} \frac{d \langle w \rangle}{dt} \tag{5.2}$$

which indicates that the energy density $\langle w \rangle$ decays by a factor of $1/\exp(1) \approx 37\,\%$ each time that the duration of the oscillation increases by a factor of $1/\Omega$. Thus, in an ideal case when $\Omega = 0$ the energy never decays.

The dimensional analysis of the energy decay constant Ω allows to determine its physical meaning as the bandwidth of the energy decay. The Fig.5.3 shows the relation of the energy decay constant with the bandwidth of the acoustic power absorbed by the external forces interacting with a inertance-compliance system oscillating with natural frequency $\omega_0 (2\pi)^{-1}$ forced to vibrate at the circular frequency ω by interactions with its boundary conditions.

The bandwidth is calculated as the difference between the frequencies where the absorbed power is equal to 50 %, which is called the "half-power bandwidth" and it is given by $\Omega = \omega_2 - \omega_1$.

Finally, the quality factor or Q-factor is defined as

$$Q = \frac{\omega_0}{\Omega}$$

which indicates how efficient an oscillator or resonator is. Low values of Q mean that the resonator is not efficient and loses a lot of energy, while $Q \to \infty$ corresponds to an ideal resonator.

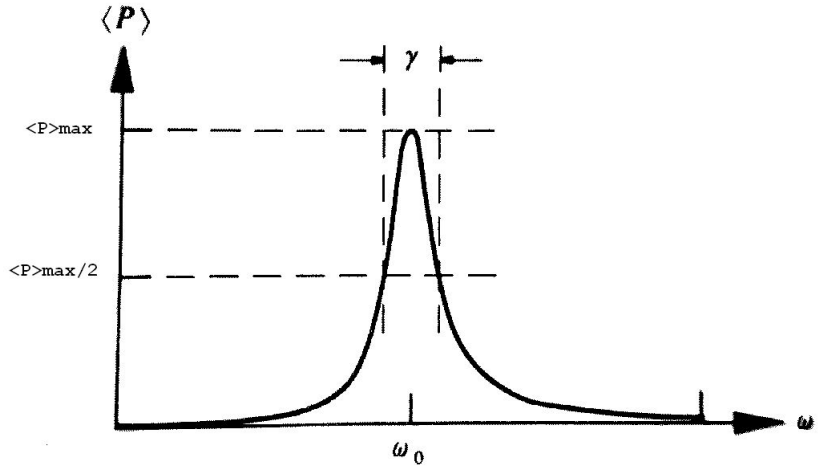

Figure 5.3: Frequency Response Curve of an Inertance-compliance System Oscillating at the Angular Frequency ω_0.[3]

5.1.4 Energy Absorbance

The energy absorbance is a quantity that indicates the proportion of energy that is absorbed into the system, i.e. the energy that is going out from the inertance-compliance oscillating system. In general, there are two possibilities: the energy is absorbed by the friction into the system itself or it is transferred to another system. This is a very important indicator in the audiometric evaluation because it allows us to know how much energy is transferred to the tympanometric membrane.

The energy absorbance is obtained from the reflection coefficient ϱ:

$$EA = 1 - \varrho^2$$

which is calculated in terms of the c-normalized speed of energy η (Eq.1.56) as follows:

$$\varrho = \sqrt{\frac{1-\eta}{1+\eta}}$$

The spectrum of the energy absorbance $EA(\omega)$ can be also obtained using the algorithms described in section 4.1 to calculate the spectral active intensity.

5.2 Working Principle of the Audiometric Device and Comparison with Standard Tympanometry

The audiometric device consists of an intensimetric probe which is used to measure the acoustic impedance into the ear canal.

The acoustic variables are measure into a small tube, which is inserted in the ear canal as it is shown in the Fig.5.4 The model that fits better is the Helmholtz resonator which was described in subsection 5.1.2. The junction of the ear canal with the probe forms a system like a bottle, where the ear canal represents the volume and the probe represents the neck.

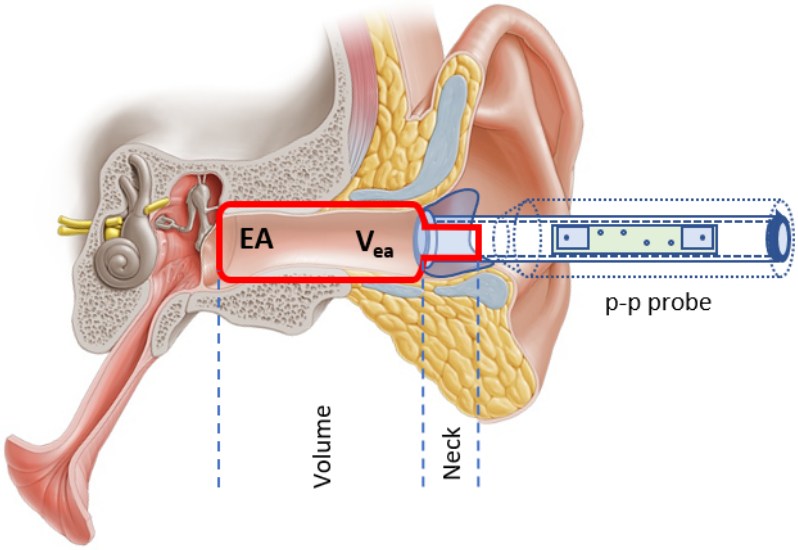

Figure 5.4: Analogy of the of the Ear Canal-probe Model.

In this way, an inertance-compliance oscillating system is composed, where the natural frequency is linked to the volume of the ear canal, which can be calculated from the resonant frequency as:

$$V = f(\omega_0) \tag{5.3}$$

where f is a function with the form of the Eq.5.1.

As it was described in the previous section, the impedance measurement allows knowing the energetic behavior into the ear canal. This is very important in the audiometric study because it serves as an indicator about the mobility of the tympanometric membrane.

The two indicators Q-factor and EA can be used for this analysis, however, the spectral energy absorbance allows to obtain more information than the Q-factor, but implies additional calculation.

The standard tympanometry is a methodology based on measuring the vibration of the reflected tone at 226 Hz, while the static pressure into the ear canal varies from -300 daPa to $+200$ daPa. A typical tympanogramic curve is shown in Fig.5.5. The main variables given by the standard method [30] are shown in the first column of the Table 5.1

Clearly, while it is not possible to find a direct connection between the two methods, due to the audiometric device working only at a static pressure, a correlation based on the functionality of the ear is still possible and it is described in the following table:

Standard Tympanometry	Audiometric Device
V_{ea}: Volume of the Ear Canal	It is calculated from ω_0 (Eq.5.3)
Y_{tm}: Admittance Peak	It is obtained from the admittance curve.
Symmetry of Y: Mobility of the Tympanic Membrane	Can be known from the Q and EA

Table 5.1: Comparison between Standard Tympanometry and Audiometric Device

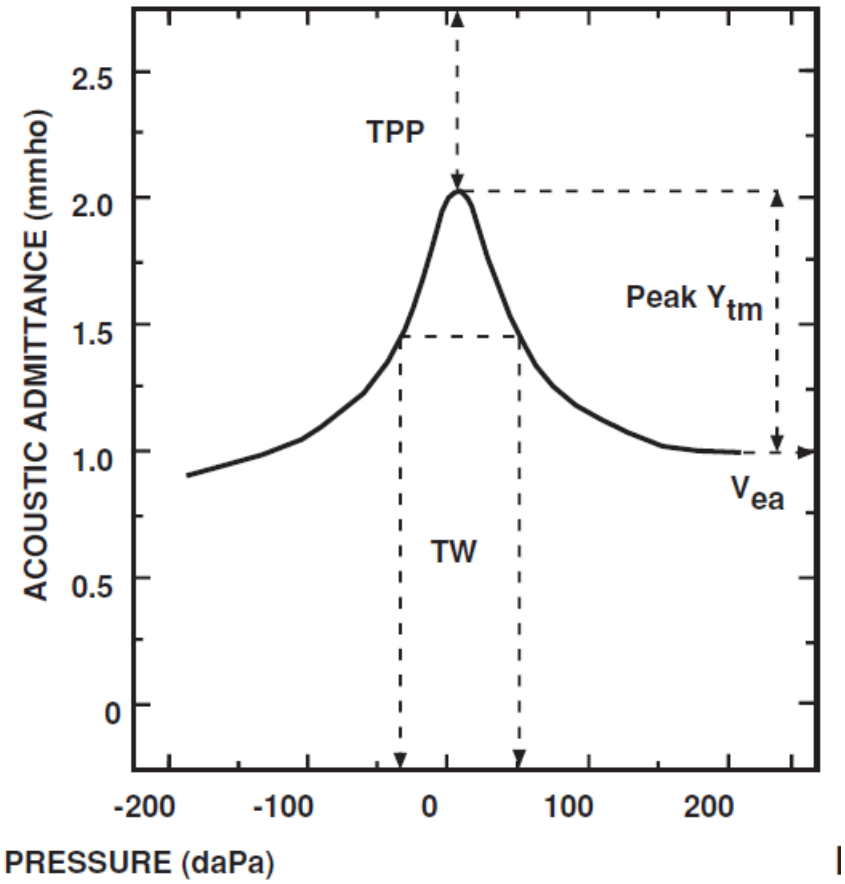

Figure 5.5: Standard Tympanometry Curve.[3]

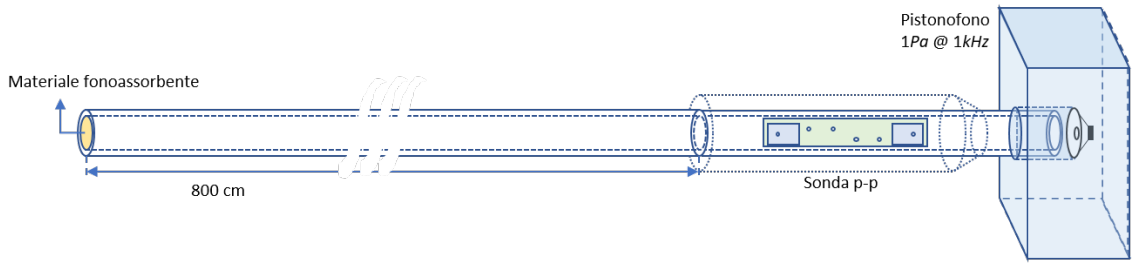

Figure 5.6: Calibration Setup for a Fixed Frequency.

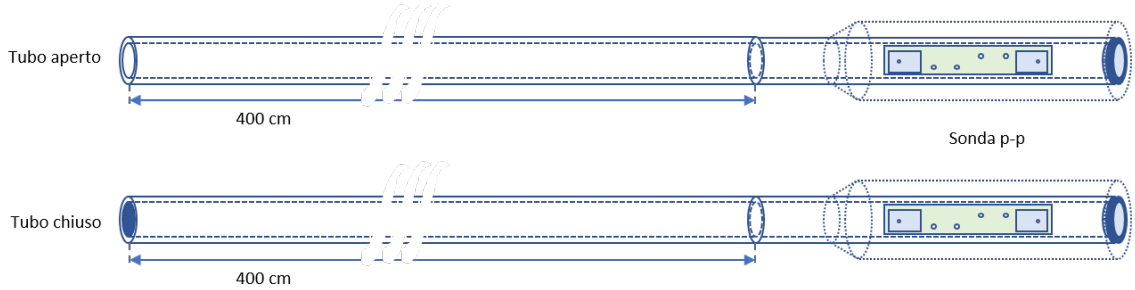

Figure 5.7: Calibration Setup in a Reactive Field.

5.3 Calibration of the Probe

The calibration process of the clinical audiometric device consists in three parts: calibration of the sensors of the probe, calibration of the output level of the A/D converter and calibration the equivalent volume. The first step is already described in section 3.2 where the scale factors α and β are obtained by using the calibration setup shown in Fig.5.6 Here, the reference tone is directly generated by a pistonphone.

The function $\hat{\Gamma}$ is obtained by using the setup shown in Fig.5.7 where the waveguide is excited with the same speaker of the probe. A typical calibration curve of Γ is shown in Fig.5.8.

The output level of the A/D converter is calibrated, measuring the sound pressure level generated by the probe speaker which has to be equal to 94 dB_SPL.

Finally, the calibration of the equivalent volume curve consists in measuring the resonant frequency in at least 3 different reference volumes with the probe (for example 4 cc, 2 cc, and 0.2 cc). The values measured are marked in a plot frequency-volume. The volume calibration curve is found by fitting the plotted points. The Fig.5.9 shows the calibration setup, while Fig.5.10 shows a typical calibration curve for the equivalent volume.

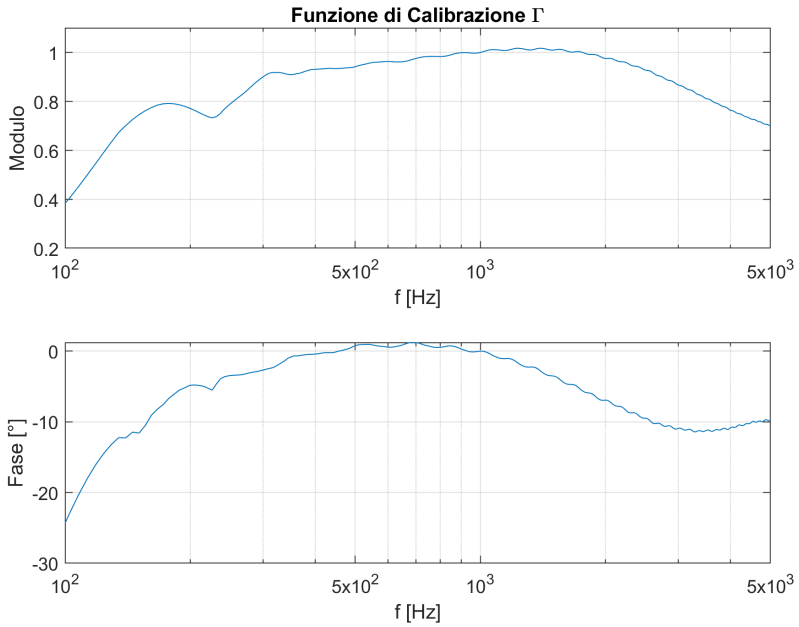

Figure 5.8: Typical Calibration Curve $\hat{\Gamma}$ for a intensimetric probe.

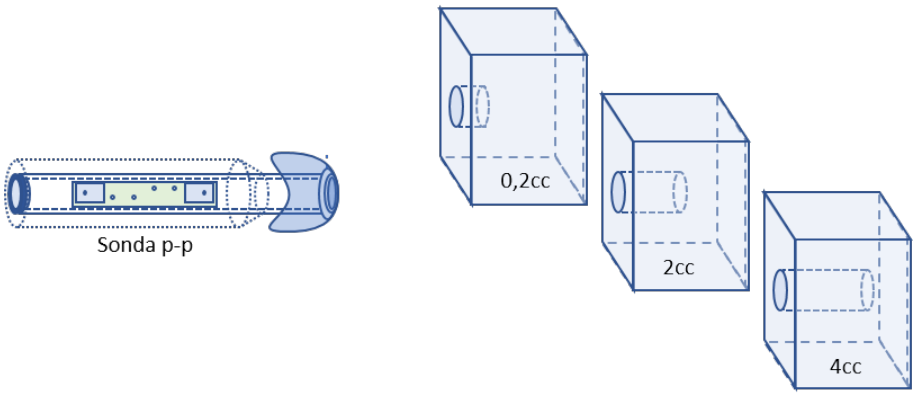

Figure 5.9: Calibration Setup to Obtain the Equivalent Frequency-volume Calibration Function.

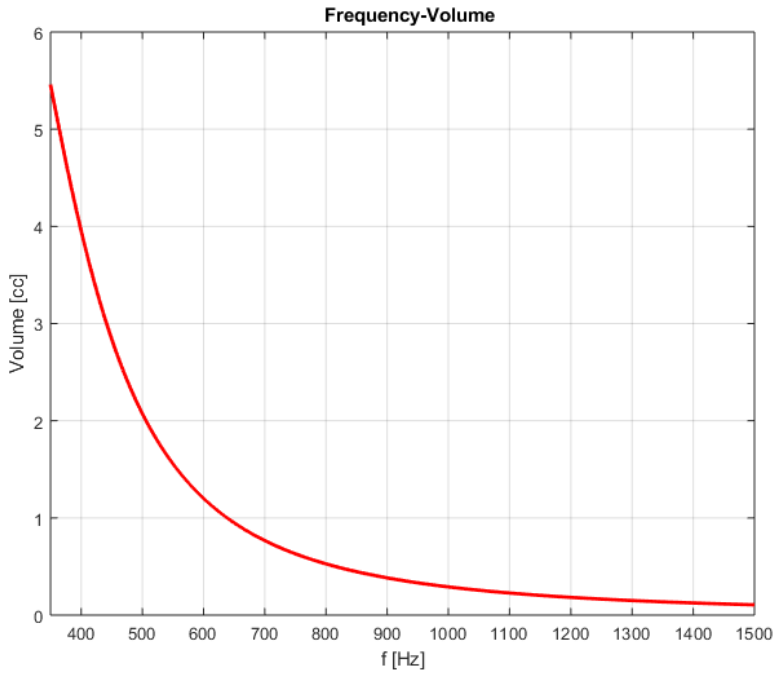

Figure 5.10: Typical Curve of the Equivalent Frequency-volume Function.

Chapter 6

CONCLUSIONS

In this work, the complete process to develop a device to measure the complex sound intensity from the wave impedance has been exposed. Starting from the known fundamentals in acoustics, new concepts and definitions have been introduced. Rigorous definitions of Active and Reactive sound intensities have been given on the basis of the decomposition of particle velocity through the orthogonalization process of pressure and velocity signals in the Hilbert space. Thus, the complex sound intensity has been accordingly defined as an element of the complex vector space, where the active intensity vector is the real part and the imaginary part is given by the application of the reactivity tensor to the versor in the direction of the active intensity.

One of the main aims of this work was to find a relationship between the complex sound intensity defined as a time-independent quantity and its "spectrum" in the frequency domain, which has been possible to reach by finding the fundamental relationship between Wave Impedance and Sound Intensity. Three different acoustic fields (DSW, QSW-1D, and QSW-2D) were simulated in order to validate the relationship between the graphical matching of the acoustic resistance with the kinetic energy conductance and that of the reactance with the kinetic energy susceptance.

This measurement method based on the wave impedance provides more information, given by the signum of the reactance/susceptance, which usually is lost in the square and square root operations. In the section 1.6 a particular method to keep all information from the susceptance has been described. Also, this contribution was verified by simulation.

The simulated fields were the divergent spherical wave (3-D) and quasi-stationary wave in 1-D and 2-D, where symbolic simulation provided by Maple(TM) was used in the two firsts, while in the last case, numerical simulation provided by Matlab(TM) was necessary to reduce the computation time. In each case, the impedance and other important quantities were calculated from the velocity potential function in order to obtain graphical results. The analysis was made for one single tone (monochromatic case) and three-tones cases, and it was verified that the frequency overall active intensity can be obtained directly from the sum of each of its frequency components, while for the reactive intensity it is not possible, only the total reactivity can be obtained as the square root of the difference between squared overall apparent intensity and squared overall active intensity 1.69.

Probes for measuring the sound intensity based on two different principles (pressure-pressure and pressure-velocity) have been evaluated.

The general calibration process described consists of finding the scale factors α and β, and the calibration functions K and $\hat{\Gamma}$ from a known reference impedance. Two calibration methodologies have been presented for two different fields: anechoic and reactive.

An algorithm for measuring the complex sound intensity from the wave impedance has been proposed, and the process has been shown in a flow chart.

Measurements in real environments, in one and three dimensions, have allowed to verify the algorithm and acoustic fundamentals by comparing it with the simulation results.

The acoustic fields chosen for the execution of the measurements were a waveguide with three different terminations: anechoic, closed and open; and a squared tube with a section equal to $28\,cm$. The two calibration functions (anechoic and reactive) were used in each measurement in the waveguide, concluding that the reactive calibration fits better with the simulation results because, in fact, the anechoic setup is more similar to a divergent spherical wave model than the plane progressive wave model.

Finally, the algorithms of the measuring device of the complex sound intensity were used in a real case for an audiometric clinical investigation, where the traditional technique was satisfactorily replaced for a non invasive test, and additional information was given by the energy absorbance quantity.

Bibliography

[1] Hans-Elias de Bree. An overview of microflown technologies. *ACTA ACUSTICA UNITED WITH ACUSTICA*, 127(1):264–270, 2003.

[2] https://newt.phys.unsw.edu.au/jw/helmholtz.html.

[3] Raymond D. Kent, editor. *Tympanometry in Clinical Practice*. The MIT Press, 2004.

[4] Frank Fahy. *Sound intensity*. CRC Press, 1989.

[5] Finn Jacobsen. *Springer Handbook of Acoustics*, chapter 25. Sound Intensity, pages 1053–1075. Springer-Verlag New York, 2014.

[6] Wenbo Duan, Ray Kirby, Jevgenija Prisutova, and Kirill V. Horoshenkov. Measurement of complex acoustic intensity in an acoustic waveguide. *The Journal of the Acoustical Society of America*, 134(5):3674–3685, 2013.

[7] M.G. Prasad and S.Y. Ham. A note on the relation between complex acoustic intensity and specific acoustic impedance. *Journal of Sound and Vibration*, 118(3):549–554, 1987.

[8] E. Meyer and E.-G. Neumann. *Physical and Applied Acoustics: An Introduction*. Academic Press, 1972.

[9] Philip McCord Morse. *Vibration and sound*. McGraw-Hill New York, 2nd edition, 1948.

[10] Domenico Stanzial, Giorgio Sacchi, and Giuliano Schiffrer. On the physical meaning of the power factor in acoustics. *J. Acoust. Soc. Am.*, 131(1):269–280, 2012.

[11] Nicholas J. Higham. Computing real square roots of a real matrix. *Linear Algebra and its Applications*, 88-89:405 – 430, 1987.

[12] Domenico Stanzial and Carlos Esteban Graffigna. On the connection between wave impedance, sound intensity and kinetic energy in monochromatic fields. *Proceedings of Meetings on Acoustics*, 28(1):045004, 2016.

[13] Domenico Stanzial and Giuliano Schiffrer. On the connection between energy velocity, reverberation time and angular momentum. *Journal of Sound and Vibration*, 329(7):931–943, 2010.

[14] Domenico Stanzial and Carlos E. Graffigna. On the general connection between wave impedance and complex sound intensity. *Proceedings of Meetings on Acoustics*, 30(1):055013, 2017.

[15] William Cronk Elmore and Mark A Heald. *Physics of waves*. Dover publications, Inc. New York, 1985.

[16] L.L. Beranek. *Acoustical Measurement*, chapter 7. Measurement of Acoustic Impedance, Choice of Sign of Reactance, pages 298–299. AIP Revised Edition, 1988.

[17] Dudley H Towne. *Wave phenomena*. Addison-Wesley, Massachusetts (USA), 1967.

[18] Hans-Elias de Bree. *The Microflown E-book*. Online, 2009.

[19] Tom Basten and Hans-Elias de Bree. Full bandwidth calibration procedure for acoustic probes containing a pressure and particle velocity sensor. *J. Acoust. Soc. Am.*, 89:163–172, 2010.

[20] Domenico Stanzial, Giorgio Sacchi, and Giuliano Schiffrer. Calibration of pressure-velocity probes using a progressive plane wave reference field and comparison with nominal calibration filters. *J. Acoust. Soc. Am.*, 129(6):3745–3755, 2011.

[21] Domenico Stanzial and Carlos E. Graffigna. Protocollo di calibrazione in ampiezza e fase per sonde pressione-velocità in un campo di riferimento a onde piane progressive. *Online Proceedings 44° Convegno Nazionale AIA 2017*, 2017.

[22] Finn Jacobsen and Virginie Jaud. A note on the calibration of pressure-velocity sound intensity probes. *J. Acoust. Soc. Am.*, 120(2):830–837, 2006.

[23] Domenico Stanzial and Carlos E. Graffigna. Funzione di calibrazione in ampiezza e fase per sonde pressione-velocità ottenuta in campi di riferimento reattivi. *Online Proceedings 45° Convegno Nazionale AIA 2018*, 2018.

[24] Domenico Stanzial and Carlos E. Graffigna. Precision device for measuring the three dimensional spectra of complex intensity. *Proceedings of Meetings on Acoustics*, 30(1):055014, 2017.

[25] Nicholas J. Higham. Computing real square roots of a real matrix. *Linear Algebra and Appl.*, 88:405–430, 1987.

[26] David A Bies and Colin H Hansen. *Engineering noise control: theory and practice*. CRC press, 2009.

[27] H. Herlufsen. Dual channel fft analysis (part i). *Technical Review*, 1, 1984.

[28] U. Ingard. *Acoustics*. Infinity Science Series. Jones & Bartlett Learning, 2008.

[29] C. Graffigna D. Stanzial. Prototipazione di una sonda audiometrica pressione-pressione. Technical report, Neuranix, 2018.

[30] American national standard, specications for instruments to measure aural acoustic impedance and admittance (aural acoustic immitance), ansi s3.39-1987. 2007.

[31] https://www.raspberrypi.org/.

[32] http://www.numpy.org/.

[33] Matthias Geier. Python-sounddevice. 2019.

[34] https://matplotlib.org/.

Appendix A

Implementing the Algorithm in a Device

This section describes how it would be possible to implement the algorithms described in section 4.1 in a stand-alone hardware.

A.1 Hardware

Raspberry Pi (R) is chosen as main hardware. This hardware consists in a credit-card sized computer [31] which is attached to a 7-inch touchscreen display that allows the interaction with the user (see Fig. A.1). Some specifications from the official website [31] are the following:

- Broadcom BCM2837B0, Cortex-A53 (ARMv8) 64-bit SoC @ 1.4GHz
- 1GB LPDDR2 SDRAM
- 2.4GHz and 5GHz IEEE 802.11.b/g/n/ac wireless LAN, Bluetooth 4.2, BLE
- Gigabit Ethernet over USB 2.0 (maximum throughput 300 Mbps)
- 4 USB 2.0 ports
- 7 inch Raspberry Pi touchscreen display
- Micro SD port for loading your operating system and storing data
- 5V/2.5A DC power input

The input and output signals are converted through an external sound card which is connected to the micro-PC.

In our first prototype, the sound card used is a Focusrite Scarlett 18i8, which has four balanced microphone inputs and two stereo unbalanced outputs. This sound card is compatible with Windows, MacOS, and Linux.

A.2 Software

On the Raspberry Pi it is possible to run a lot versions of operating systems (mainly Linux versions). Here we use the official Linux version made for Raspberry named “Raspbian”, which is a based on Debian and it is available online in the official Raspberry website ([31]).

The code was written in Python, which is a an open source and general purpose programming language. Some advantages are that it is readable and clean code based and it is designed with features to facilitate data analysis and visualization. Furthermore, Python

Figure A.1: Measuring Device Hardware.

Figure A.2: Sound Card and Probe.

is compatible with many platforms and systems given that it has many open source frameworks and libraries.

This section will show the main libraries used to program our application in Python. Some code lines will be included in order to show the main routines about play and acquisition signal, signal processing, and plotting curves.

A.2.1 Numpy and SciPy Python Library

These libraries contains the fundamental package for scientific computing in Python [32] . Some functionalities used in the application are:

- A powerful N-dimensional array object
- Useful linear algebra, Fourier transform, and random number capabilities
- Tools for integrating C/C++

The installation of the libraries is very easy using the package manager "pip". The installation commands using pip for Python 3 in Linux are the following:

```
sudo pip3 install numpy
sudo pip3 install scipy
```

Some functions of these libraries used in the program are shown below:

- Defining array: here x, y, z are numbers (integers, float, complex, etc.) that conform the elements of the array A.

  ```
  A = numpy.array([x,y,z])
  ```

- Module: here Z is a complex number and Z_mod is the module of Z.

  ```
  Z_mod = numpy.abs(Z)
  ```

- Phase: here Z is a complex number and Z_phase is the phase of Z in rad.

  ```
  Z_phase = numpy.angle(Z)
  ```

- Real part: here Z is a complex number and R is the real part of Z.

  ```
  R = numpy.real(Z)
  ```

- Imaginary part: here Z is a complex number and X is the imaginary part of Z.

  ```
  X = numpy.imag(Z)
  ```

- Conjugate: here Z is a complex number and Z_conj is the conjugate of Z.

  ```
  Z_conj = numpy.conjugate(Z)
  ```

- Transpose: here A is a matrix and B is the transpose matrix of A.

  ```
  B = numpy.transpose(A)
  ```

- Cross Spectrum: here p and v are signals in the time domain sampled at frequency Fs. GPV is the cross spectrum of p and v, and F is the frequency vector of GPV.

```
F,GPV = scipyi.signal.csd(p, v, fs = 44100, window="hann",...
...,nfft = 8192, return_onesided = True, scaling = "spectrum")
```

- Power Spectrum (Welch algorithm): here p is a signal in the time domain sampled at frequency Fs, while P is the power spectrum of p, and F is the frequency vector of P.

```
F,GPV = scipyi.signal.welch(p, fs = 44100, window="hann",...
...,nfft = 8192, return_onesided = True, scaling = "spectrum")
```

A.2.2 Sounddevice Python Library

Sounddevice is a Python library [33] used to play and record signals through a sound card installed in the host operating system.

Also here, the installation process is made through the package manager pip. The command in Linux is the following:

```
sudo pip3 install sounddevice
```

Below a basic routing to play and rec a signal is shown:

- List the available sound devices:

```
sounddevice.query_devices()
```

- Define the default parameters:

```
sounddevice.default.samplerate = 44100
sounddevice.default.device=[dev_in_id,dev_out_id]
sounddevice.default.channels = [4,1]
```

- Play and rec sentence:

```
rec_data = sounddevice.playrec(play_data)
```

A.2.3 Matplotlib Python Library

Matplotlib [34] is a powerful Python library which allows to plot any kind of graph. Furthermore with matplotlib, it is possible to have full control of line styles, font properties, axes properties, etc.

The installation command in Linux is:

```
sudo pip3 install matplotlib
```

The typical plot routine is shown below:

- Define plot area: figure and canvas objects are created, “fig” and “canvas” respectively. The canvas object links the figure object with the frame where the plots will be shown.

```
fig = plt.Figure()
canvas = FigureCanvasTkAgg(fig, plot_frame)
canvas.get_tk_widget().pack()
```

- Plot figure: figure object is cleared, a new plot object is created, and data is plotted.

```
fig.clf()
fig_plt = self.fig.add_subplot(111)
self.fig_plt.semilogx(F, np.abs(Z),color = 'blue')
```

- Define plot properties: here some plot properties are set, for example, the abscissa and the ordinate labels, title, legend, limits of the plot and show the grid.

```
fig_plt.set_xlabel('frequency [Hz]')
fig_plt.set_ylabel('Z')
fig_plt.set_title('Power spectra')
fig_plt.legend(['P','Vx','Vy','Vz'])
fig_plt.set_xlim((fmin,fmax))
fig_plt.grid(ON,axis=BOTH)
```

- Show plot: finally, the plot is shown invoking the function $draw()$ in the object "canvas."

```
canvas.draw()
```

A.3 Graphical User Interface

The graphical user interface (GUI) is composed by three panels: A, B, C. The first one, A, is where the plots and settings windows will be shown. Panel B is a menu composed for five buttons, which are used to setup the hardware and to execute, save and load the measurements. Panel C is a submenu composed for six buttons which are used to plot each kind of graph.

Next, each button of the menu (panel B) will be describe.

- Select device: In this menu (Fig.A.4) the sound cards connected to the device are shown. Here, it is possible to choose the input and output hardware (can be different), and the probe dimensions: one, two or three dimensions.

- Load Calibration: This button is used to load the calibration file of the probe (Fig.A.5).

- Excitation signal: This menu (Fig.A.6) allows to setup and choose the kind of signal to excite the field. The kind of signals are: external, single-tone, dual-tone, sweep, and white noise.

- Start measuring: This button opens the measuring menu (Fig.A.7) which allows to execute the measuring process for each spatial point. Once the measurements are made, the measurements are saved using the button "Finish".

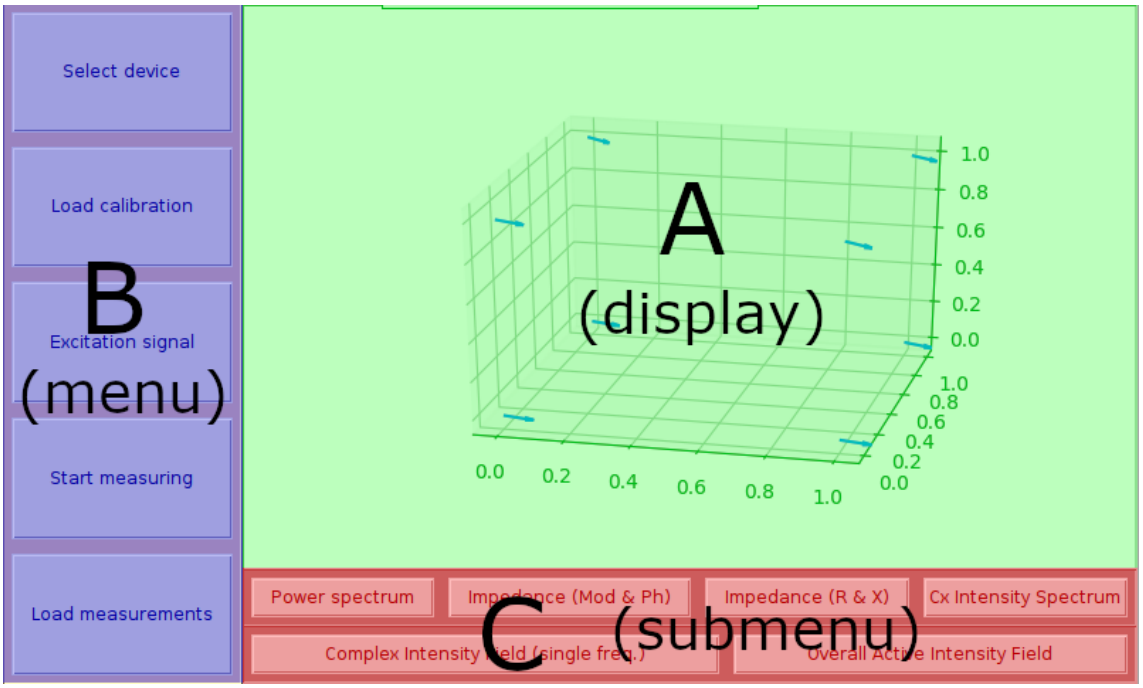

Figure A.3: Graphical User Interface.

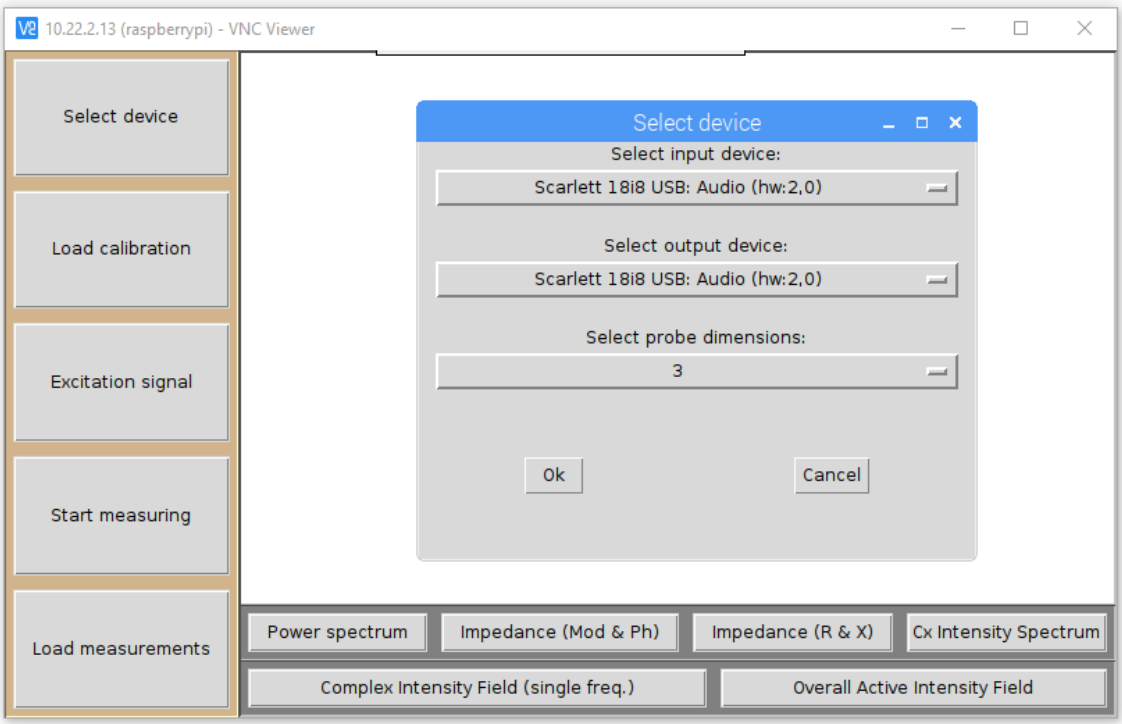

Figure A.4: Select Device Menu.

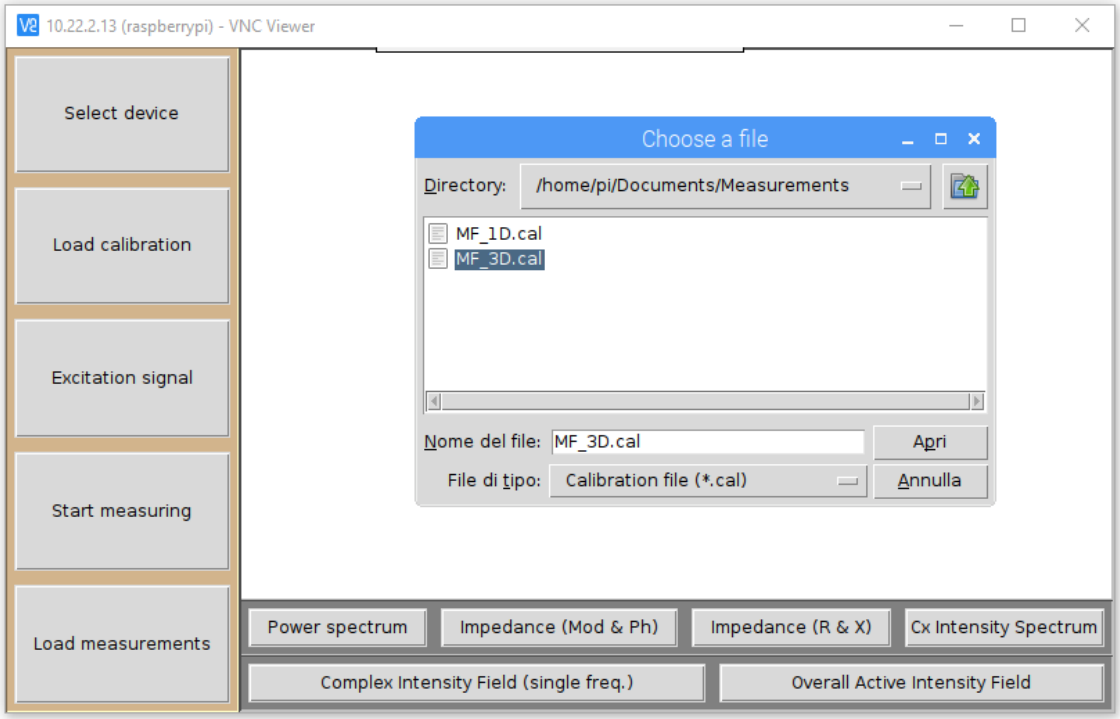

Figure A.5: Load Calibration File.

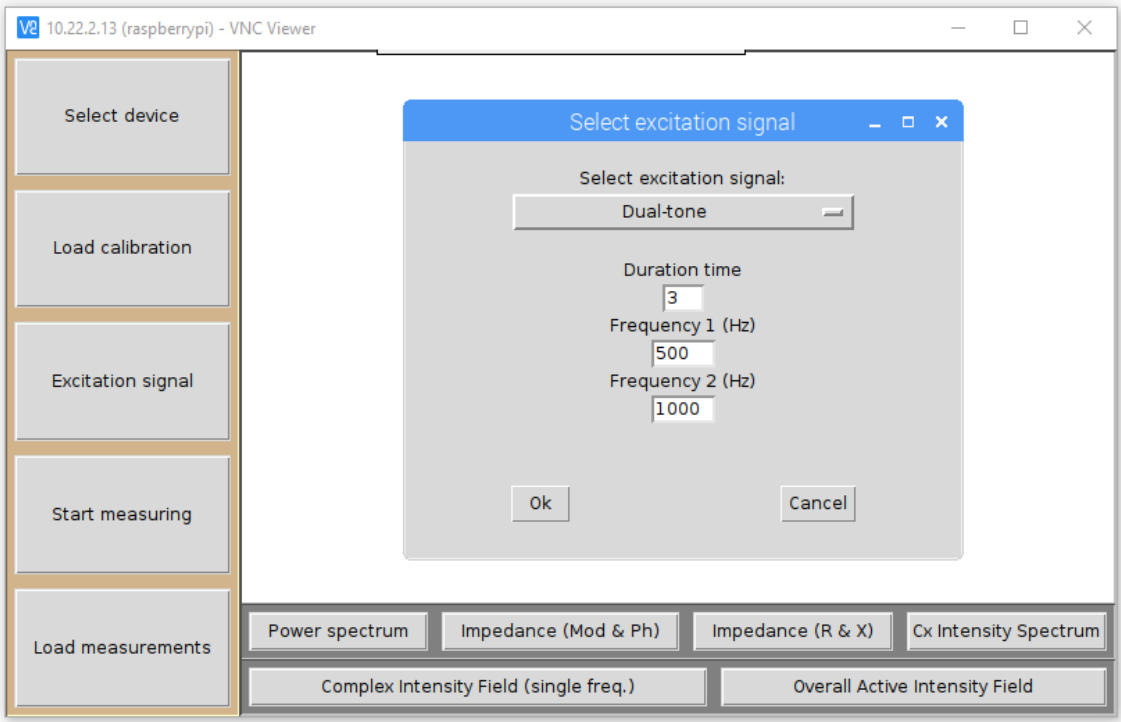

Figure A.6: Excitation Signal Menu.

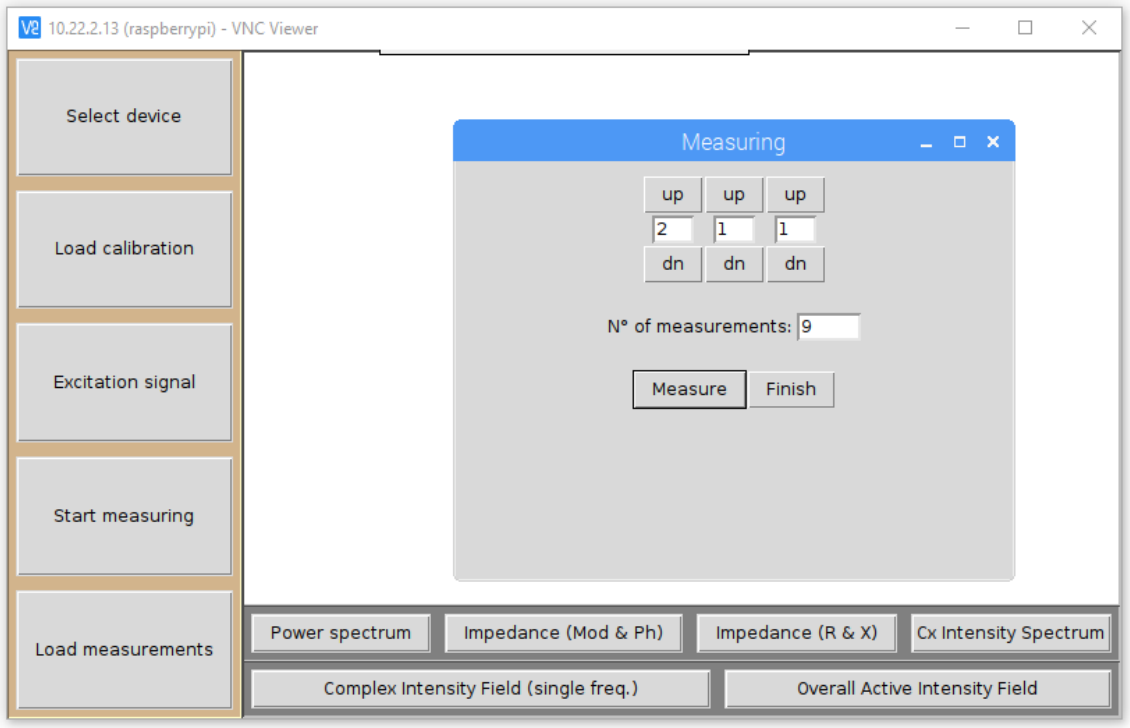

Figure A.7: Measuring Menu.

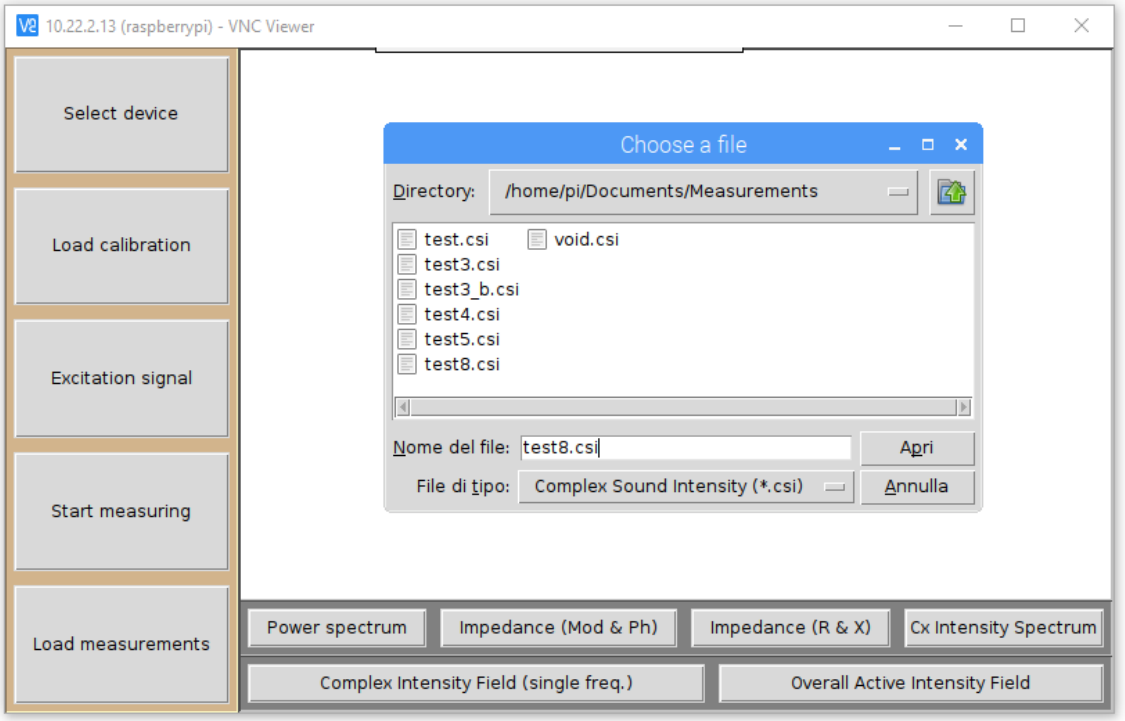

Figure A.8: Load Measurements Dialog.

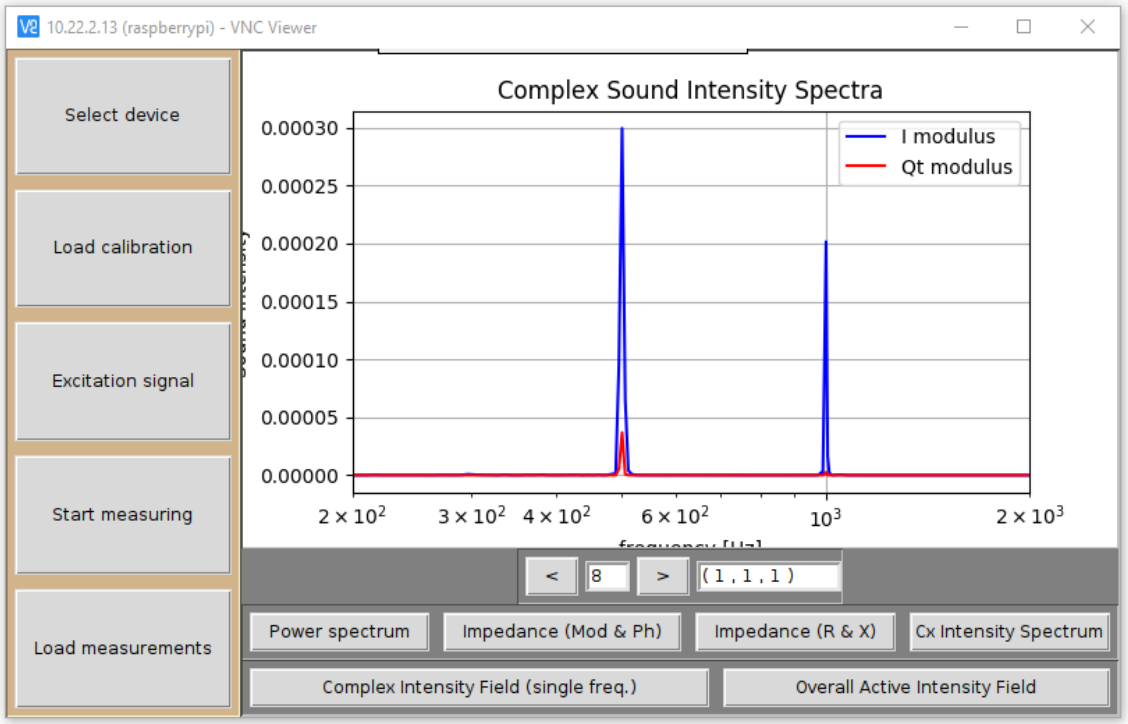

Figure A.9: Active and Reactive Intensity Spectra.

- Load measurements: This button allows saved measurements (Fig.A.8). The file extension is “csi” for “complex sound intensity”.

The six buttons in the submenu in the panel C are used to plot the graphs.

The buttons “Power spectrum”, “Impedance (Mod & Ph)”, “Impedance (R & X)”, and “Cx Intensity Spectrum” plot the power spectrum of pressure and each velocity component, impedance in module and phase, real and imaginary part of the impedance, and the spectra of the active and reactive intensity modules, respectively. Each one of these graphs are plotted for one single point in the space. Therefore, a second submenu appears to change the current spatial point (see Fig. A.9).

The buttons “Complex intensity field (single freq.)” and “Overall Active Intensity Field” plot the fields of the active and reactive intensity for a single frequency and the overall active intensity field, respectively. Also here, a second submenu appears, but now to change the current frequency (see Fig. A.10)

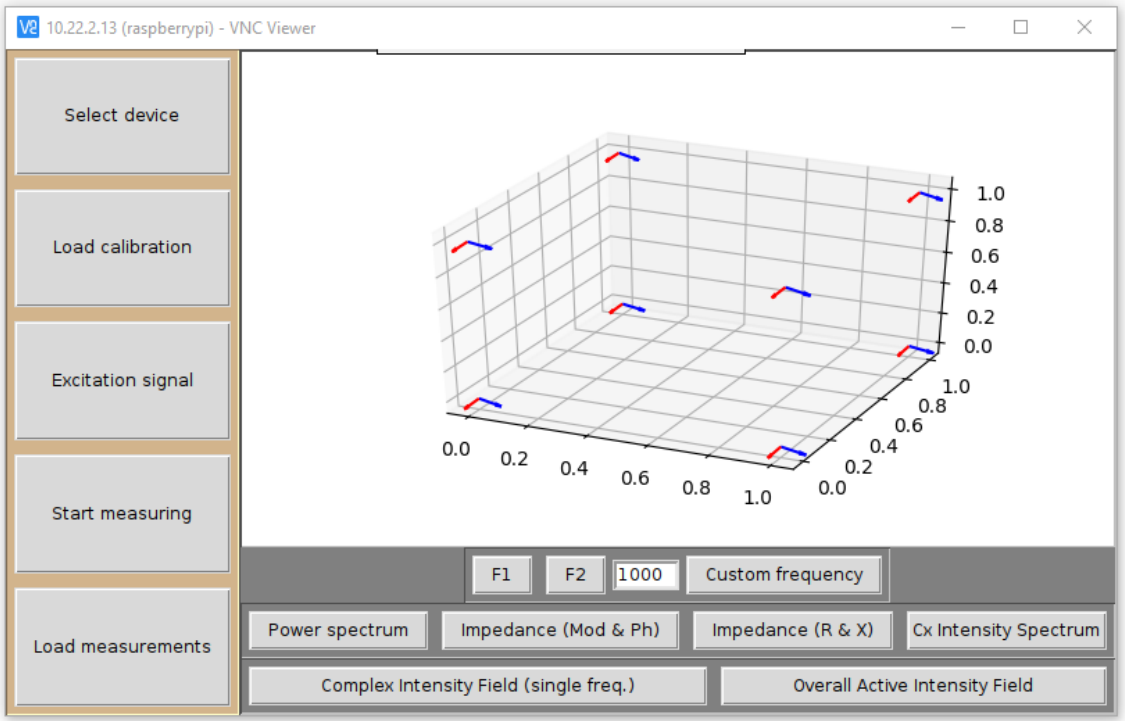

Figure A.10: Active and Reactive Intensity Field.